Effect of sediment density in bridge pier scour experiments

Dissertation

submitted to and approved by the

Department of Architecture, Civil Engineering and Environmental Sciences
University of Braunschweig – Institute of Technology

and the

Faculty of Engineering
University of Florence

in candidacy for the degree of a
Doktor-Ingenieur (Dr.-Ing.) /
Dottore di Ricerca in Mitigation of Risk due to Natural Hazards on Structures and Infrastructures *)

by
Henrich Meyering
Born 23.02.1982
from Osnabrück, Germany

Submitted on	21 March 2012
Oral examination on	7 May 2012
Professorial advisors	Prof. Andreas Dittrich
	Prof. Enio Paris

2012

*) Either the German or the Italian form of the title may be used.

Acknowledgments

I would like to take this opportunity to thank all who have supported and accompanied me during the last years, in particular:

- First of all I would like to express my gratitude to my supervisor and examiner Prof. Andreas Dittrich for giving me the opportunity for this work at his institute. He always gave me helpful recommendations and feedback throughout my time at the institute years.

  Moreover, I would like to thank Prof. Enio Paris for supervising my thesis from the Italian side. He always found the time for discussion and for letting me participate in his expertise.

- Furthermore I would like to thank Prof. Bernd Ettmer from the University of Applied Sciences Magdeburg-Stendal, I owe him deep gratitude. I appreciated very much his fruitful recommendations and great motivation during the last years.

- My gratitude goes also to my former colleagues at the Leichtweiß-Institut, especially Dr.-Ing. Katinka Koll and Prof. Jochen Aberle and to Thomas, Peter, Klaus, Ronald and Heidrun for helpful discussions, motivation and a very nice time apart from science and theory. Furthermore, I would like to thank also the team from the experimental hall, Mr. Lehmann, Mr. Neumann and Uwe, for helping me keeping my experiments running.

- In addition, I owe my thanks to Prof. Claudio Borri and Prof. Udo Peil for their effort as coordinators of the International Graduate College 802. Due to their initiative I could do my research in a beautiful country with great cultural background and wonderful people. I enjoyed many enriching conversations and discussions with people from distinct countries around the world and made great new friendships. At this point I would also like to thank Ms. Wissmann for her help.

- My deepest gratitude goes to my parents and my family for having accompanied me through all the years and for their permanent support, belief, company, and love since I can remember.

- And most especially my thank goes to my wonderful wife Anja.

Abstract

The estimation of scour depth at bridge piers is an important task in hydraulic engineering. The physical processes governing bridge scour range are highly complicated and several open questions still await clarification. This is reflected by the multitude of available approaches which yield significant differences in estimated scour depths up to several meters.

Most of the existing approaches were derived on the basis of scale model experiments carried out in the laboratory with simplified boundary conditions. However, for fine sized prototype sediments such as sand it is often not possible to downscale the sediment due to associated changes in physical and chemical properties once the scaled sediment is in the silt and clay range.

The objective of this thesis is to investigate the possibility to substitute natural sediment by artificial granulate. For this purpose, scour experiments were carried out in an 8.0 m long, 0.3 m wide and 0.6 m deep horizontal flume. A single cylindrical pier model with diameter D = 0.03 m was embedded vertically in the flume centerline. The scour experiments were carried out with natural and artificial sediments.

As a result, two points can finally be summarized. First, the material density has significant influence on the time t_e to reach the equilibrium scour depth, but not on the maximum scour depth d_{se}. Second, if artificial granulate with a lower density is used in a bridge pier model instead of natural sediment, the grain size d_{50} should be similar to get similar scour depth.

Contents

List of Figures

List of Tables

Symbols

D	[m, cm]	pier width = pier diameter for cylindric shapes
D_{eff}	[m, cm]	effective pier diameter
D^*	[1]	sedimentological diameter
d_{max}	[m, mm]	maximum grain size
d_{ch}	[m, mm]	characteristic grain diameter
d_x	[m, mm]	diameter of bed material of which x% are smaller
$d_{x,a}$	[m, mm]	diameter of armor building bed material for which x% are smaller
d_s	[m, cm]	scour depth
$d_{s,max}$	[m, cm]	maximum scour depth
d_{se}	[m, cm]	equilibrium scour depth
F	[1]	pier form
FF	[1]	form factor of a single grain
Fr	[1]	Froude number $Fr = \frac{U}{\sqrt{g\,l}}$
Fr_d	[1]	densimetric Froude number $Fr_d = \frac{U}{\sqrt{\rho'\,g\,d_{ch}}}$
$Fr_{d,crit}$	[1]	critical densimetric Froude number
g	[m/s^2]	gravity acceleration g = 9.81
H	[m]	dune hight
h_0	[m, cm]	water depth upstream of the pier
h	[m, cm]	water depth

K_{shape}	[1]	correction factor for pier nose shape
K_{angle}	[1]	correction factor including the angle of flow impact on the pier
K_{bed}	[1]	correction factor for bed form effects
K_{armor}	[1]	correction factor for armoring effects
K_{width}	[1]	correction factor for width effects
K_{size}	[1]	correction factor for sediment size effects
l	[m]	characteristic length e.g. water depth or pier diameter
Q_{flume}	[m^3/s]	discharge through the flume
R	[m]	hydraulic radius $R = \frac{A}{U}$
Re	[1]	Reynolds number $Re = \frac{U\ l}{\nu}$
Re_{flow}	[1]	approach flow Reynolds number $Re_{flow} = \frac{U\ h}{\nu}$
Re_{pier}	[1]	pier Reynolds number $Re_{pier} = \frac{U\ D}{\nu}$
Re^*	[1]	grain Reynolds number $Re^* = \frac{u_0^*\ d_{ch}}{\nu}$
t	[s, h]	operational time
t_e	[s, h]	time to develop equilibrium scour depth
t*	[s, h]	termed the equilibrium time scale, $t* = \frac{Ut_e}{D}$
t_0	[s]	time to develop the horseshoe vortex
t_r	[s]	reference time $t_r = \frac{h_0}{U}$
t_R	[s]	reference time for the scour $t_R = \frac{z_R}{\sqrt{\rho'\ d_{50}\ g}}$
T_0	[1]	relative time to develop the horseshoe vortex $T_0 = \frac{t_0}{t_R}$
T_s	[1]	dimensionless time $T_s = \frac{t}{t_r}$
U	[m/s]	depth-averaged flow velocity
U_{crit}	[m/s]	the critical depth-averaged (incipient-transport) flow velocity
U_a	[m/s]	armor peak velocity (for nonuniform sediments)
$U_{crit,a}$	[m/s]	the critical depth-averaged velocity for the armor sediment
u_*	[m/s]	shear stress velocity
$u_{*,crit}$	[m/s]	critical bed shear stress velocity
v_s	[m/s]	fall velocity of the grain
W	[m, cm]	flume width

z_R	[m]	reference length $z_R = (h\ D^2)^{\frac{1}{3}}$
δ	[mm]	thickness of the viscose sublayer
Δ	[cm]	difference between the scour depth upstream and downstream the pier
ν	[m^2/s]	kinematic viscosity
Θ	[1]	mobility Shields parameter
ρ	[kg/m^3]	fluid density
ρ_s	[kg/m^3]	material density
ρ'	[1]	relative density under buoyancy $(\rho_s - \rho)/\rho$
σ_g	[1]	particle size distribution $\sigma_g = \sqrt{\frac{d_{84}}{d_{16}}}$
τ_0	[N/m^2]	bed shear stress
τ_{crit}	[N/m^2]	critical bed shear stress

1 Introduction

1.1 Motivation

Bridges spanning watercourses are civil works that are important for our society, especially with regard to both mobility and economy. The main objectives for the design of bridges are related to stability, life expectancy, and safety during natural extreme events such as fire, earthquake and flood. The latter objective is in the focus of this work, as most bridges spanning rivers are founded in the riverbed, i.e., in alluvial sediment beds. Due to the flow conditions around piles and abutments and the associated sediment movement, large scour may develop at bridge piers and/or abutments threatening their structural integrity. This kind of scour is responsible for the majority of flood induced bridge failures and is therefore associated with a huge amount of monetary loss (Kwak, 2001; Richardson et al., 2001; Dey and Raikar, 2007a). Table 1.1 shows examples of some documented bridge damages in the United States.

Table 1.1: Number of bridges destroyed and damaged by scour between 1985 and 1995 in the United States (Müller and Wagner, 2005).

Location and Year	**Number of Bridges Damaged or Destroyed**
Pennsylvania, West Virginia, Virginia (1985)	73
New York, New England (1987)	17
Midwestern United States (1993)	>2,500
Georgia (1994)	>1,000
Virginia (1995)	74
California(1995)	45

The National Bridge Inventory (NBI) in the United States contains information on more than 580 000 bridges. Approximately 84 % of these bridges span rivers or watercourses. Accordingly, hydraulic factors like scour, ice and debris cause 60 % of the documented bridge failures in the United States (Shirole and Holt, 1991), amongst which bridge pier scour is the leading cause (Annandale, 1994; Kwak, 2001). These failures cost millions of dollars each

(a) Viaduct 1 **(b)** Viaduct 2

Figure 1.1: Damage of the railway bridge across the Elbe river due to the flood in 2002 (Reichelt and Richter, 2003).

year as a result of both the direct cost necessary to replace and restore bridges, and indirect costs related to disruption of transportation facilities. A study for the Federal Highway Administration (FHWA), Chang (1973) indicated that up to 1973, about $75 million was spent annually to repair roads and bridges that were damaged during flood events. This cost does not include the additional indirect costs to highway users for operating costs and fuel resulting from temporary closure and detours and to the public for costs associated with higher traffic, freight rates, additional labor costs and time. However, besides the monetary loss due to bridge failure, the graver consequence is loss of life.

Rhodes and Trent (1993) document that during the 1980s, $1.2 billion was spent on restoration of flood-damaged highway facilities. They emphasize that this is a conservative estimate because it only includes the amount funded by the U.S. Government, which ranges from 75 to 100 % of the total restoration costs. The funds were only for disasters related to very large floods and did not include the hundreds of smaller events that occur every year. They also demonstrate that the added cost of operating a vehicle through a detour and the time lost traveling when a bridge failed (and these are only part of the indirect costs) exceeded the direct cost of bridge replacement or repair by a large factor (Richardson et al., 2001). Thus, scour (as one of the major reasons for bridge failure), is an important issue which needs to be taken into account when designing and monitoring the foundation of bridges.

Even if the amount of bridge failures due to scour in Germany is not as high as in the United States of America or New Zealand, the impact on the economy can be very serious. Reichelt and Richter (2003) documented the damage to an important railway bridge crossing the Elbe caused by the Elbe flood in 2002 (Figure 1.1). Overall, more than 400 bridges were damaged solely on German territory as a result of this event (N.N., 2004). Figure 1.2 shows a historical drawing from the Elbe flood in 1845, which demonstrates the collapse of one bridge pier of the Augustus bridge in Dresden.

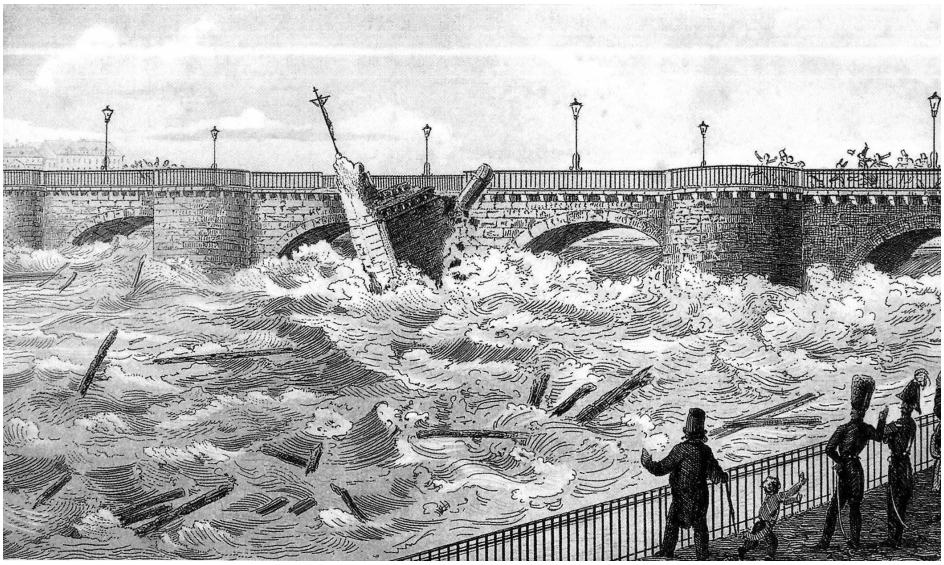

Figure 1.2: Augustus Bridge in Dresden - collapse of the "Crucifix-Pier" on the March 31, 1845 (Merz, 2007).

1.2 State of the art

Since the beginning of the last century, an abundance of studies related to scouring processes have been carried out. These studies focused on the estimation of equilibrium and/or maximum scour depth as well as time evolution of the scour. They contributed, in general, to a better understanding of the relevant physical processes. However, a number of issues still remain unsolved, which becomes apparent from the large number of published approaches.

Nearly all existing approaches have been developed on the basis of physical modeling studies carried out in the laboratory using well defined and often simplified boundary conditions. For example, a lot of experiments were carried out with uniform-sized bed material and cylindrical piers, while natural bed material is mostly characterized by a mixture of different grain sizes and complex pier geometries.

A further problem related to such experimental studies is that scale effects must be taken into account. In fact, downscaling of alluvial sediment such as sand is difficult because the physical properties of the sediment change when the downsized bed material slides into the cohesive sediment range. The forces that occur between these very fine grains cannot be scaled. In addition, the influence of the fluid viscosity, which in general can be neglected for prototype condition, increases in the model. Clark et al. (1982) for example recommended that the limiting condition for permissible sediment reduction in the model is about 0.5 mm. If the sediment size falls below this value due to the chosen model scale, a proper scaling for natural sediment is often not possible.

Thus, it is necessary to develop methods to study the scouring processes adequately in

laboratory experiments, even if the geometrical scaling for the bed material is not possible due to the mentioned reason. An interesting tool to model the sediment movement process is the substitution of natural sand by lightweight material (LWM) (Hughes, 1993). Hentschel (2007) describes this method in detail for bed-load transport process, but relatively little data concerning local scour experiments with lightweight material are available in literature, for example Dietz (1972); Zanke (1978); Whitehouse (1998); Oliveto and Hager (2002); Yu et al. (2003); Ong et al. (2004); Radice et al. (2009).

Besides the difficulties of scaling the model sediment an additional problem is to identify the time that is necessary to reach the maximum or equilibrium scour depth. Franzetti et al. (1982) noted that data for scour experiments found in literature have to be critically reviewed in relating to the testing time because experimental tests durations vary widely and are often too short to reach the equilibrium scour depth. Simarro et al. (2011) found that the criteria for equilibrium which can be found in literature, for example an increase in scour depth of less than 5 % of D/3 in 24 h (Grimaldi et al., 2009) are arbitrary and not reliable. However, in order to develop valid methods of calculation, it is important to be sure that the equilibrium scour depth is reached.

The validation of empirical as well as numerical scour estimation with field data is a difficult task because only a few sets of good field data are still available (Laursen and Toch, 1956; Müller and Wagner, 2005; Ghorbani, 2008). The main reason for this is that measurement during flood events often is a dangerous and expensive task due to high flow velocities and strong vortices around the pier, as well as the problem of floating debris, which often is transported by the river. As a result, most field data are collected after flood events. In some cases, the measured scour has again partly filled with sediment during the decreasing hydrograph of the flood. Also, the hydraulic boundary conditions around the pier are often unknown.

The numerical research is not part of this work, even though the methods and possibilities in this field are improving rapidly. However, the numerical calculation of developing three-dimensional two-phase flow around a pier is a very sophisticated problem and still needs a better understanding of the relevant processes.

1.3 Goal of research

For the use of lightweight material as a substitute for natural sediment in pier scour experiments, no systematic studies are available. Thus, LWM has been used in the previously mentioned sources without specifying and testing the transferability of results obtained in this way. This research will directly address this issue taking into account hydraulic and sedimentological model laws. Existing theories (hydraulic and sedimentological scaling laws) for the replacement of natural sediment by artificial granulates will be further improved and validated so that the relevant processes can be simulated adequately in laboratory studies (comparison of laboratory studies only, i.g. no field data).

For this purpose, experimental studies will be carried out with special regard to the substitution of natural sediment by artificial lightweight material in bridge pier models. This is an important issue for the further development of morphological numerical models and can help calculate the scouring risk at bridges. Furthermore, the experimental data set enlarges experimental scour data and therefore can help to validate empirical and numerical models.

In Chapter 2, the scour issue is embedded into the risk framework of the graduate school. The chapter gives a short introduction into the risk topic and shows the economic relevance of bridge failures. Knowing that all over the world local scour at bridge piers is a major reason for bridge collapses justifies and explains the great interest in this topic.

In Chapter 3, the scour process is explained and important parameters affecting the scouring process are pointed out. The chapter ends with the goal of this research.

The dimensional analysis, which is important for the experiments (Chapter 5), is illustrated in Chapter 4.

Chapter 5 explains the experimental setup as well as the experiments, which were carried out during the research period. The results are described and discussed in Chapter 6.

The thesis ends with the conclusion of the results and an outlook for further research.

2 Risk management

Risk management is a comprehensive approach to deal with risk, consisting of risk identification, assessment and treatment. In this context, the definition of risk is (ISDR, 2009):

" [...] the combination of the probability of an event and its negative consequences."

The objective of risk management is to identify these events and minimize the negative impact. The following chapter describes the basic steps of the risk management, focusing specifically on bridges. In addition to the presentation of each step, the particular importance and difficulty of estimating the associated economic damage is shown.

2.1 Risk management framework for bridges

Throughout the different disciplines and perils, a great variety of risk management definitions and methods can be found in literature. The risk management framework that is presented here[1] has been developed for natural hazards like floods, earthquakes, fires and so forth. The major steps of the risk management chain are briefly described and illuminated below and adapted specifically for bridge scour.

It starts with the *risk identification*, continues on with the *risk assessment* and finally leads to the *risk treatment*. These three parts are accompanied by a continuous *risk monitoring* process and a *risk review*. After giving a short introduction about the different stepts in risk management, adapted for bridges (Figure 2.1), the focus is put on the risk assessment part, especially in damage assessment. However, the knowledge acquired in the damage assessment can help to enhance the risk management treatment as well.

[1] developed and used in the Graduate College 802 in Braunschweig

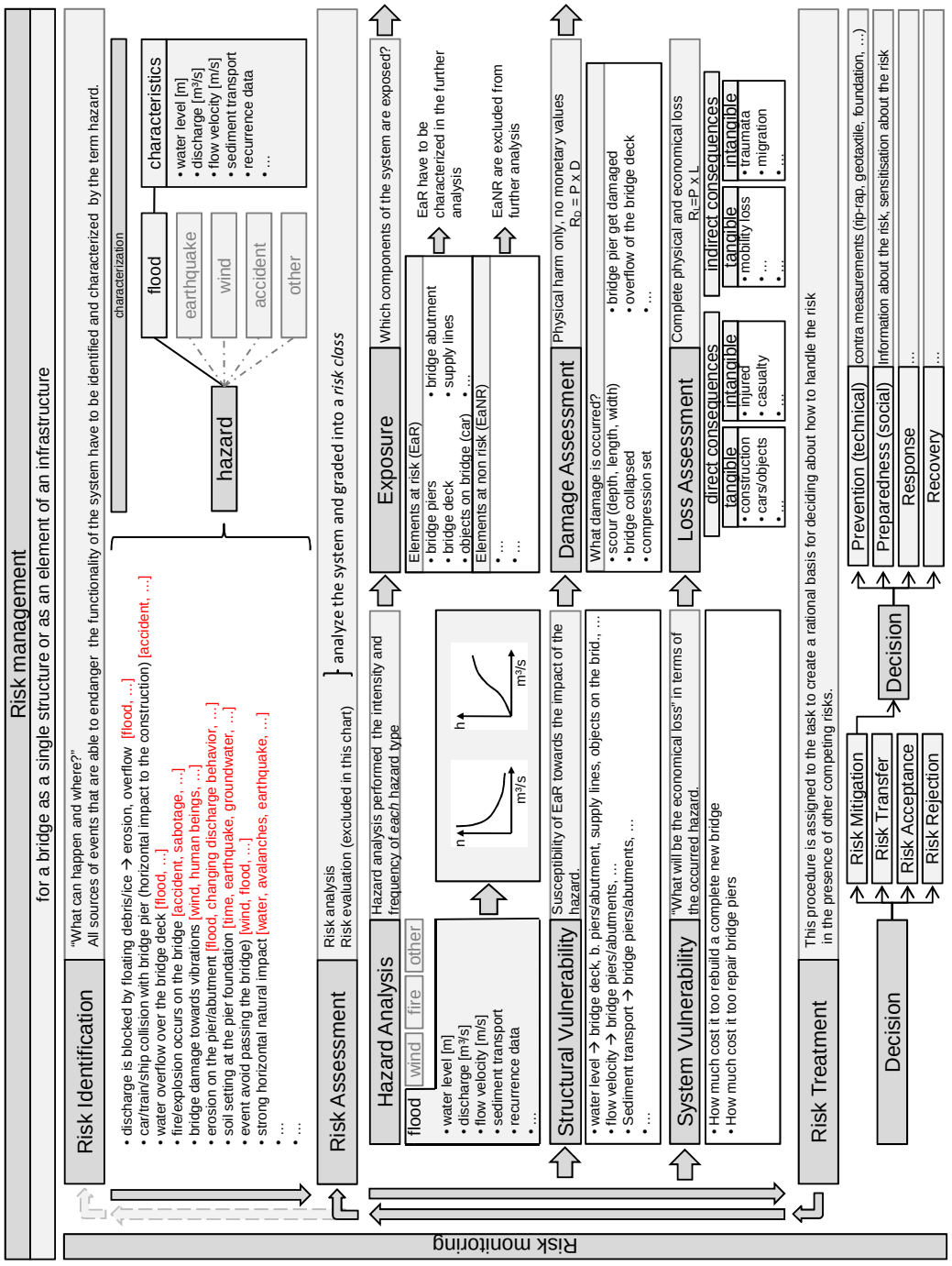

Figure 2.1: Risk management framework adapted to bridges in case of floods.

2.2 Risk identification

The risk identification process initiates the risk management chain and starts with the identification of all possible damages that could endanger the functionality of a previously defined system (e.g. bridges). The question during this step is: *What can happen and where?* The risk identification ends with the characterization of the damage inducing events using the term *hazard*. A natural hazard is defined by the United Nations as a (ISDR, 2009)

> *" [...] natural process or phenomenon that may cause loss of life, injury or other health impacts, property damage, loss of livelihoods and services, social and economic disruption, or environmental damage."*

During the initial part of the risk identification process, all of the ways that the system can be damaged should be identified. This is done without focusing in particular on a special event (mass movements, explosions, soil settings and soil erosions (scour), collisions, ...). Thereby the same damage can be induced by various hazards. For example, bridge collapse due to vibrations can happen due to wind, earthquakes and also due to human beings. The characterization of these hazards leads into the second step of the risk identification. Regarding the inducing event, the hazards can be assigned to different extreme events like floods, wind, earthquakes, accidents and others, which are characterized by different parameters.

This thesis focuses on local scour at bridge piers as a result of floods. The hazards associated with the occurrence of extreme floods play a dominant role, and can be categorized into (Annandale, 1994):

- river instability
- morphological changes due to extraneous factors
- fluvial hydraulics near the river crossing
- structural integrity of the bridge

For the risk identification process as well as for the following steps of the risk management process, detailed and accurate data are necessary. The following itemization shows the variety of data that should be collected in order to estimate and identify the hazards:

- aerial images of the river and river crossing
- maps of the catchment
- survey data of the river crossing site
- geological information of both river and catchment
- hydro meteorological and hydrological data
- vegetation maps
- land use plans
- design and maintenance reports
- construction drawings of the bridge

2.3 Risk assessment

The risk assessment represents the second step of the risk management chain. From this step onwards a periodical evaluation is very important because changes in the environment and in knowledge can influence the following procedure eminently. In itself the risk assessment is divided into the *risk analysis* and the *risk evaluation*. The goal of the risk analysis is to quantify the risk, preferably in monetary units per time, while the risk evaluation compares, for example, the scour risk of different bridge foundations, assisting in coming to an objective decision.

Annandale (1994) developed a risk assessment procedure consisting of two parts: the so-called Level I and Level II risk assessment. While the Level I risk assessment can mostly be conducted as a desk study, the Level II risk assessment requires more effort and should preferably be conducted by experts in the field (see itemization mentioned below). This is additionally necessary when insufficient information for Level I is available, and/or when the result of the Level I analysis points out the need for the more comprehensive risk analysis. Beyond that, for the identification of the exposed elements, the Level I approach only takes into account the elements that may suffer losses due to river crossing failure. The Level II approach is more detailed and includes, in contrast to the Level I approach, the identification of pathways that represent the relationship between elements that are consequently subject to losses.

2.3.1 Risk Analysis

The risk analysis starts with a so-called hazard assessment, considering the hydrology, stream stability, potential for morphological change due to extraneous factors, fluvial hydraulics and the structural integrity of the river crossing (Figure 2.2). It culminates in a structure-based hazard rating. The goal of this step is to estimate the endangerment of the structure by taking into account the significance of different flood associated hazards (Annandale, 1994).

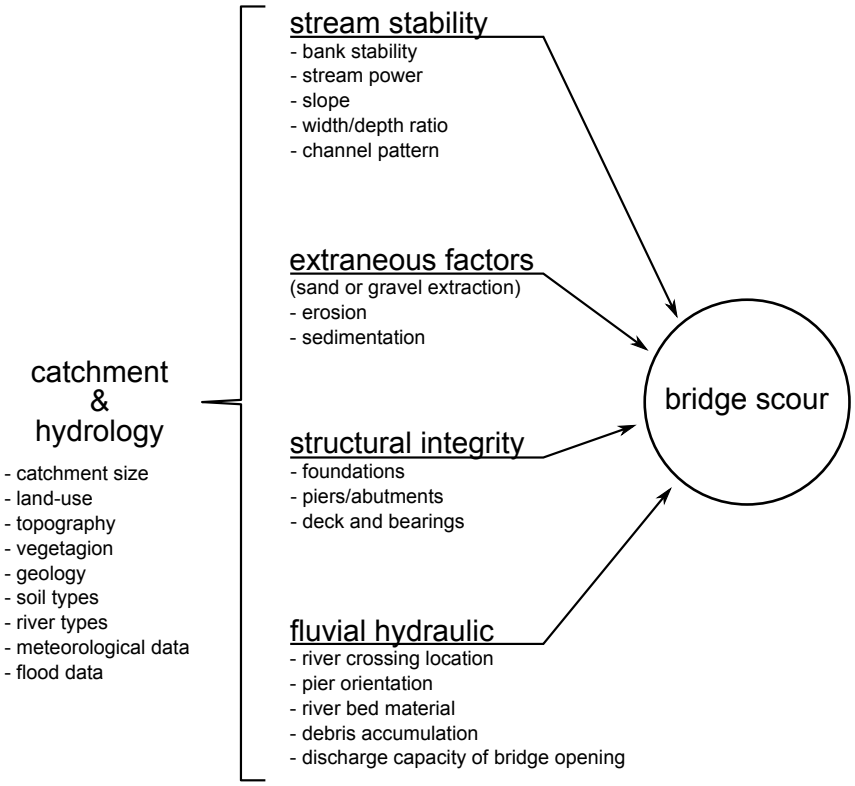

Figure 2.2: Categories of hazards influencing bridge scour.

Catchment and Hydrology: The hydrology of the hazard event has to be characterized in terms of intensity and frequency. The catchment characteristics include size, topography, land-use, soil types, river and stream types, geology and vegetation. With all of this information it is possible to conduct the hydrological analysis in order to determine the flood peak and the frequency of occurrence of significant flood events. Also combined with this information are the erodibility and stability of the rivers and streams, the debris accumulation, and the potential of morphological changes during flood events.

Stream stability: The stream stability is related to the river channel and depends on the combination of parameters such as sediment load (sediment size, bedload/suspended load ratio), bank stability, stream power, slope, width to depth ratio, and channel pattern.

Extraneous factors: Extraneous factors for morphological changes are, for example, sand and gravel extraction from a river bed, or alternatively, sediment depositions, which can induce significant morphological changes and therefore influence the safety of bridges. In this context, morphological changes are defined as erosion and/or deposition of sediment. Man-made activities can influence the river system in an unexpected and also relatively fast way.

Fluvial hydraulics: The local effects of fluvial hydraulics in the vicinity of a river crossing depend on various aspects. The potential for lateral erosion depends highly on the location of the river crossing. For example, bridges located on a straight river (low), between river bends (low to moderate) or on a river bend (high). The local scour depth highly depends on the pier orientation and the induced turbulences. Furthermore, the riverbed material and the potential for debris accumulation (overtopping and influence on local turbulence inducing scour) and the maximum discharge capacity of the bridge opening play an important role.

Structural integrity: The structural integrity of bridges can be determined by evaluating design and construction drawings, maintenance reports and field investigations. The objective is to evaluate the status of the structural integrity such as the foundation, piers, abutments and the bridge deck. Due to the age of many bridge constructions, reliable information is often not available.

Hazard rating

Considering the above-mentioned categories, a hazard rating (R_{Hazard}) can be calculated. This result provides the user an initial indication of whether or not the combinations of hazards endanger the structure (Table 2.1).

Table 2.1: Rating classification for the hazard assessment according to Annandale (1994).

composite rating	endangerment
$R_{Hazard} \geq 70$	significant
$20 < R_{Hazard} < 70$	moderate
$R_{Hazard} \leq 20$	low

R_{Hazard} is calculated by taking the individual hazard rating parameters into account (Equation 2.1). The required parameters can be obtained from Tables 2.5-2.2. In order to be conservative, the upper value should be used. Thus, the composite rating is calculated as follows (Annandale, 1994):

$$R_{Hazard} = f_1 \times f_2 \times f_3 \times f_4 \tag{2.1}$$

where f_1 is the factor for the river stability (Table 2.5), f_2 the factor for extraneous morphological changes in the river (Table 2.4), f_3 the product of the four hydraulic aspects taken from Table 2.3 and f_4 is the product of the four factors concerning the structural integrity taken from Table 2.2.

Table 2.2: Rating of the structural integrity (f_4) for the hazard assessment according to Annandale (1994).

component	integrity		
	intact	minor problems	major problems
foundations	1.189 – 1.433	1.434 – 1.550	1.551 – 1.586
piers	1.189 – 1.433	1.434 – 1.550	1.551 – 1.586
abutments	1.189 – 1.433	1.434 – 1.550	1.551 – 1.586
deck and bearings	0.595 – 0.716	0.717 – 0.774	0.775 – 0.793

Table 2.3: Hydraulic aspects for the hazard assessment (f_3) according to Annandale (1994).

hydraulic aspect	potential for damage		
	low	moderate	high
location of river crossing	2.115 – 2.549	2.550 – 2.757	2.758 – 2.820
contraction scour	1.057 – 1.274	1.275 – 1.378	1.379 – 1.410
local scour	1.057 – 1.274	1.275 – 1.378	1.379 – 1.410
debris accumulation	0.423 – 0.509	0.510 – 0.551	0.552 – 0.564

Table 2.4: Morphological changes due to extraneous factors (f_2) for the hazard assessment according to Annandale (1994).

type of morphologic change	potential for change		
	low	moderate	high
erosion			
degradation			
nickpoint migration	1.000 – 2.114	2.115 – 2.892	2.893 – 3.162
bank erosion			
deposition			
aggradation and fill			
down- and backfilling	1.000 – 2.114	2.115 – 2.892	2.893 – 3.162
berming			

Table 2.5: River stability factor f_1 for different channel types for the hazard assessment according to Annandale (1994).

parameters	Type 1	Type 2	Type 3a	Type 3b
sediment load	small	moderate	small to moderate	height
bed/susp load ratio	low (suspended load)	moderate (mixed load)	low (suspended load)	moderate (mixed load)
bank stability	cohesive soil, high stability	moderate to high	moderate	low
stream power	low	moderate	low to moderate	moderate to high
slope	low	low	moderate to low	moderate
width/depth ratio	low	low	low to moderate	moderate
sediment size	small	moderate	small to moderate	moderate (coarse)
channel pattern	naturally straight	straight, sinuous thalweg	meandering, high sinuosity	meandering, wide bends
factor	1.000	2.105	2.205	2.447

parameters	Type 4	Type 5	Type 6
sediment load	high	high	moderate to high
bed/susp load ratio	moderate to high	high	moderate to high
bank stability	low	low	low to moderate
stream power	high	high	moderate to high
slope	high	high	high
width/depth ratio	high and variable	high	high to moderate
sediment size	large (sand, gravel)	large	large to moderate
channel pattern	meander braided	bar braided	anabranched
factor	2.893	3.162	3.028

Exposure

After the estimation of the hazard parameters and the hazard rating, all elements that are exposed to the hazards have to be identified and estimated, in concern of their relative importance. Possible pathways, in which the combination of single effects results in failure and important losses, must also be determined (Annandale, 1994). Depending on the hazard, specifically the hazard intensity, the system can be divided into elements at risk (EaR) or elements at no risk (EaNR). The EaNR are excluded from further analysis because they are not exposed to the risk. For example, bridge piers are always EaR, whereas supply lines and objects on the bridge are only exposed in situations with relatively high water level or total bridge collapse.

Structural vulnerability

The behavior of all EaR has to be analyzed, with particular attention to their susceptibility of dependence on a certain hazard impact. This step is called *structural vulnerability*. Each EaR has to be opposed to the accordant impact. For example, the impact on a bridge pier is dependent on the water level, the flow velocity, the angle of flow attack, and floating debris. The resistance of a bridge foundation against the hazard impacts depends on the pier construction itself as well as on the footing in the riverbed. The footing depth, construction and the soil characteristics can characterize this. If the structure resists the impact forces and connected consequences, for example local scour, the pier is not vulnerable.

Damage assessment

The next step is the *damage assessment*, in which the structural risk [damage/year] can be calculated by Equation 2.2. It is the result of the annual probability of occurrence for the particular event which may exceed the structural resistance multiplied by the damage itself (e.g. local scour). In the case of local scour, the annual probability of flood (P_{flood}), which may increase the structural resistance, is characterized by certain hydraulic parameters, which, in combination with the structural parameters, can cause a critical local scour depth (damage). The damage range depends on the ratio of scour depth to the maximum acceptable scour depth (or foundation depth) and varies between total collapse and no physical harm at all of the bridge structure.

$$R_{damage} = P_{flood} \times \text{damage} \qquad \text{[damage/year]} \tag{2.2}$$

System vulnerability

A further part of the risk assessment is the *system vulnerability*. Contrary to the structural vulnerability, the economical loss induced by the occurred hazard has to be found out [loss/year]. The challenge is to find out the costs that emerge from the direct and indirect costs. The loss which occurs due to non-use is particularly difficult to evaluate. Although the scenario of overflow over the bridge does not necessarily lead to physical harm, it could lead to an economical loss. In Section 2.6 and 2.7, detailed direct and indirect costs are given.

Loss assessment

The final step in the risk analysis is the *loss assessment*. The loss assessment takes the complete physical and economical loss into account and can be calculated by Equation 2.3. The total risk (R_{loss}) is the annual probability of the occurrence of the loss inducing event (P_{event}) multiplied by the loss itself.

$$R_{loss} = P_{event} \times loss \qquad [loss/year] \tag{2.3}$$

The loss assessment is separated into *direct* and *indirect* consequences (Figure 2.1). In contrast to the indirect consequences, which are not directly time connected with the hazard associated event, the direct consequences occur during the event. Furthermore, consequences can be divided into *tangible* consequences that are monetarily assessable (construction damage, loss of capital, ...), and *intangible* consequences which are not monetarily assessable (e.g. casualties, injured, migration, ...) (Merz (2006)).

Direct consequences for river crossing failure are:

- loss of capital investment due to damages at the bridge
- loss and damage in the vicinity of the river crossing
  - commercial property
  - residential property
  - public property
  - personal property
  - industrial property
- other losses (loss of lives, loss of environment)

The losses in the vicinity of a river crossing mainly occur due to flooding upstream or downstream of the river crossing, caused by debris accumulation blocking the bridge opening. In case of sudden fail, the surge may cause damage downstream from the river crossing.

Additionally, there are various indirect consequences affecting the economy due to the disruption of the transportation system

- loss of time
- disruption of communications
- loss of production
- loss of salary
- loss of revenue (taxes, utility income, business revenue)
- loss of utilities (transport, water, energy)

2.3.2 Risk evaluation

A very important procedure in the risk assessment phase is the *risk evaluation*. In this step for example, the entire risk to different bridges can be compared (Section 2.7). In this connection, so called exceedance probability curves are a useful tool to visualize the risk graphically (Figure 2.3). These curves plot the probability that losses will exceed different loss or damage

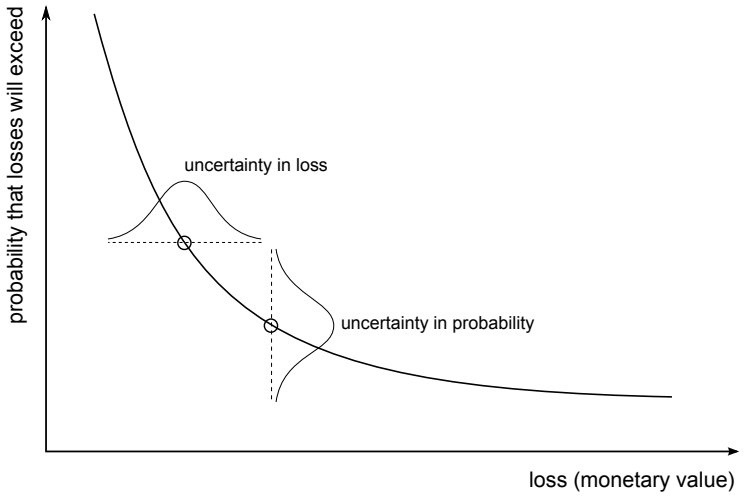

Figure 2.3: Example of an exceedance probability curve.

levels, whereas the loss level can be specified in terms of monetary loss, in terms of fatalities or in terms of other suitable impact measures like scour depth. Even if the estimation in these curves would be not very exact, using a similar-based procedure provides the possibility of comparing different scenarios and structures, in order to come to an objective decision.

Annandale (1994) developed a basic procedure to interpret the findings of the investigations by determining the acceptability of risk and relating it to the Level I composite hazard rating (Figure 2.4). The upper part indicates the function of the annual probability of occurrence

(i.e. a 100 year event), whether the risk for a certain loss (e.g. monetary loss, loss of life) is low, moderate, high or unacceptable. The lower part of the figure makes use of the hazard rating and indicates to the user what action should be taken. In combination with the risk acceptability for a certain probability of occurrence, three different actions are distinguishable:

- the common occurrence of a significant hazard and an unacceptable risk requires a more comprehensive risk analysis and a detailed risk management plan
- the common occurrence of a significant hazard and high risk, and the common occurrence of moderate and low hazard ratings and moderate, high or unacceptable risk, requires a detailed risk management plan
- the common occurrence of low risk and significant, moderate or low hazard ratings require casual maintenance only

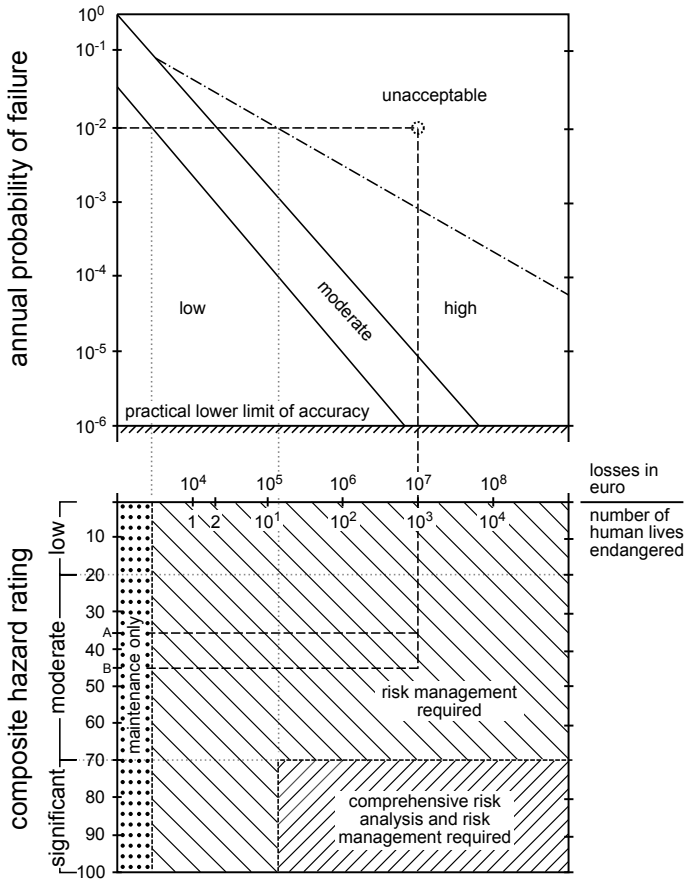

Figure 2.4: Level I risk characterization for an annual failure probability of 10^{-2} according to Annandale (1994).

2.4 Risk treatment

This procedure is assigned the task of creating a rational basis for deciding how to handle the risk in the presence of other competing risks. There are four basic issues: the *risk mitigation*, the *risk transfer*, the *risk acceptance* and the *risk rejection*. In this case, a critical issue might be seen in the wide variety of different individual risk perceptions. Individuals, or groups of individuals, often have varied preferences as how to deal with different risk scenarios. As there are only limited resources for risk mitigation, the public risk reduction often cannot focus on a particular group of individuals. The main goal should be the maximum benefit for the whole society, taking ethical aspects into consideration.

Regarding the bridge scour risk, several solutions are imaginable, while the main focus is certainly put on risk mitigation. This step is divided into *pre-disaster* interventions, for example prevention and preparedness and *post-disaster* activities, like response and recovery.

Prevention activities are, for instance, all kinds of technical counter measurements like rip-rap, geo-textile and so on, which force the resistance of the bridge pier against scouring.

The preparedness involves all social activities to sensibilize the people to the risk. Often they are killed because they are not aware of the consequences of standing on a bridge during a flood. It also includes the elaboration of contingency plans for the failure of existing bridges.

The response covers all activities that are undertaken immediately after or during the disaster, such as the organization of help and the communication between the different emergency forces. For instance, they must decide which bridge can indeed be used during a flood, so as to discover the best route for the emergency services.

The recovery phase includes all activities until the pre-disaster status of the system is obtained again. That involves the identification of damages and the process of repairing them.

2.5 Risk monitoring

By means of *risk monitoring*, the information of all actively or passively involved or participating persons in the risk management process is captured. This exchange of information is required to guarantee a trouble-free collaboration between interdisciplinary researchers and also to discover new hazards due to the ever-changing environment (Pliefke et al., 2007).

Therefore, the risk review, as part of the *risk monitoring*, is assigned to the task of including all new information and experiences about the risk event, in order to indicate its evolution within the process over time. This warrants that the risk management system be updated on a regular basis. The risk review can only be performed for events that have already run at least once through the whole process. Consequently, each risk review shows the effectiveness of possibly implemented risk reduction arrangements.

2.6 Important economic data for the risk evaluation

Calculating the economic loss of bridge failures is very difficult and an exact calculated value cannot be given due to the high variety of parameters and the fact that each bridge has its own unique situation. Annandale et al. (2002) gives an example of a bridge failure having a significant impact on the local economy. The socioeconomic costs linked to a bridge collapse in New Zealand in 1988 have been estimated. This was at least as much as the expense of the bridge replacement, which cost NZ$ 4 200 000.

There are a lot of parameters that often influence the economic loss of bridge failure. This can be separated into two aspects according to the aforementioned nomenclature.

- direct monetary loss (rebuilding or repairing the bridge)
- indirect monetary loss (mainly induced by obstruction of traffic and supply lines)

While the direct losses are relatively easy to calculate, the indirect economic loss is much more complicated to estimate, however it is often of prime importance. One of the most important aspects for the indirect loss is the obstruction of traffic, which on its own is very sophisticated. It is mainly a combination of time, effort and both personal and operational costs.

A very detailed work on this subject is written by Maibach et al. (2007). In this report, a detailed overview of external costs is given, as well as a summarization of the major studies of the last decades. In Germany, the Federal Transport Infrastructure Plan includes an approach to estimate the incurred costs related to traffic. The following itemization gives an overview of the variety of parameters that have to be taken into account in order to estimate the economic impact of different infrastructure scenarios. To calculate the impact of a bridge failure on the economy, both scenarios (with the bridge and without the bridge) must be calculated to see the differences and therewith the emerging costs related to traffic obstruction.

- route length and the respective alternative route length
- traffic volume and constitution as a function of time

  personal or commercial traffic

  origin and destination

  changing time requirement due to traffic jams and alternative route lengths
- number of people using the vehicle

  labor costs
- costs of accidents as a function of traffic density

- cost of air pollution and climate change
- noise costs

Regarding the fact that the indirect monetary losses can achieve very high values, it must be pointed out that they can occur without direct loss (bridge collapse). This can happen in cases such as bridge overtopping due to very high water levels or preventive bridge blocking to prevent fatal casualties.

Table 2.6 shows an assortment of the main traffic costs for different countries (estimation). The costs are related to time (hour, year), compared to distance (kilometer) or event (accident), and also compared to the emission per weight (tonnes) and the noise (decibels). It shows a high variance between the different countries for the same parameters. In particular, the cost of labor differs between industrialized countries and non-industrialized countries, therefore having a varied influence on the economy. To simplify the approach for indirect loss, the author assumes that they basically depend on the time effect.

The estimation of costs for damage caused to the environment due to harmful substances (noise, NO_x, CO_2) is hard to determine. This is because these substances often have no direct measurable impact on the environment, or, furthermore, this impact is still not clear due to the long time that often is needed before the impact can be attributed to a specific emission. The question of how to evaluate injuries, especially fatal injuries, is afflicted with the ethics question "What is the monetary value of a human life?". Both aspects, even if they have a large influence on indirect loss, will not be discussed in detail in this work.

In case of an extraordinary bridge failure, the indirect loss highly depends on the regional situation of the economy. A local failure in an intact environment will result in a different situation than when there is a bridge failure in an unstable environment after an regional destroying event. Therefore, the indirect loss is related particularly to the regional economy and time.

Table 2.6: Monetary values of selected traffic parameters (Alston et al., 2004).

	VOT (car) €/(car×h)*		VOT (truck) €/(car×h)	VOC (car) €/(car×km)	VOC (truck) €/(car×km)	fatal injury €	non-fatal injury €	noise €/(person×a)	NO_x €/t	CO_2 €/t
	work	non-work								
Australia	16.5	5.2	17.0 −27.0	0.10	0.37 −0.60	728 000	7700 −184 000			
Canada	8.6		14.0	variable	variable	1 660 000				
Czech Rep.	8.2	2.8	6.6	0.15	0.60 −0.68	231 000	8600 −85 100			
Denmark	31.5	6.6	38.2	0.11	0.16 −0.28	1 124 000	31 700 −116 000	7200 /SBT **	3273	41
France	35.0	10.0	40.0	0.11	0.36	1 061 000	23 000 −155 000	variable ***	variable	28
Germany	30.9	6.5	25.3 −30.9	0.13	0.28 −0.36	1 250 000	3790 −86 700	58/dB	387	217
Hungary	5.2	4.0	4.9			136 000	2000 −9300			
Japan	31.8		28.8 −44.4	0.10	0.21 −0.31	284 000	5500 −98 000	22 000 /dB/km	27 200	21
Netherlands	23.0	6.6	26.0							
New Zealand	12.0	3.5	3.5 −10.0	0.08	0.14 −0.45	1 320 000	6000 −137 000	33 /dB		13
Norway	22.3	9.6	42.6	0.12	0.37	2 850 000	36 000 −459 000	1320	1930	13
Slovenia	14.6	5.1	4.3 −8.6	0.04	0.14 −0.25	590 000	6100 −49 300			
South Africa	6.7	2.5	1.6 −4.8	0.20	0.51 −1.27	46 500	1800 −8000			
Sweden	9.3		25.2	variable	variable	1 900 000	22 600 −346 000		2700 −8000	226
Swiss	4.5 −23		26.0							
UK	37.2	10.9	13.3	0.10	0.14 −0.48	1 775 000	15 300 −199 000			
USA	20.8		28.3	0.15	0.15 −0.49	3 641 000	16 200 −280 900		1120 −2580	

VOT = value of time

VOC = value of operating costs

* per occupant

** Noise pollution index - change in noise pollution (number of dwellings affected and noise level)

*** Value calculated by square meter of dwelling, variable according to noise level, example: 6.91 €/m^2/year for 70dB(A)

2.7 HYRISK approach of calculating the cost of bridge failure

The Federal Highway Administration (FHWA) have developed a risk-based model called HYRISK in order to evaluate and compare the scour risk of bridges. The program estimates the failures related to the scour risk using figures from the database of the National Bridge Inventory (NBI)[2]. Thereby, the product of the probability of scour failure and the economic consequence associated with these failures, result in the annual risk of scour failure of a bridge or series of bridges in monetary values. Thus, comparing the results can help the decision maker to improve the safety of infrastructural systems. Such a model is therefore helpful in order to categorize a series of scour-critical bridges according to degree of deficiency and is additionally helpful in ranking those bridges so that priority is given to the most vulnerable ones. The following key parameters extracted from NBI data are used in the HYRISK method (Stein and Sedmera, 2006):

- bypass length
- functional classification
- year of construction
- average daily traffic (ADT)
- type of service
- type of span
- structure length
- deck width
- waterway adequacy
- average daily truck traffic
- scour critical bridges

To clarify the HYRISK approach, the terms used in the model are briefly commented on. In case of a bridge failure, the bridge is closed and traffic must follow a detour. The bypass length is the additional distance traveled while detouring. The functional classification of a bridge is determined according to its location and character, for example if it is a major road or a local one. The aging effects of bridge construction are taken into account by looking at the year of construction, thus using the age of the bridge as a reality check. The annual average daily

[2]Due to the interaction of HYRISK with the NBI database, the use of HYRISK outside the USA needs special care about the definitions and default and/or characteristic parameters used in the model.

traffic load on the inventory route is termed average daily traffic (ADT). The type of service is determined both for under the bridge and over the bridge, whether the bridges are highway, railroad, waterway, or another service type. The type of span describes both the material used for the bridge construction and for the design. The structure length is the length of the roadway supported on the bridge sub-structure. The out to out width of the bridge slab is taken into account by the NBI item 49. Waterway adequacy is related to whether the waterway opening under the bridge is sufficient for overtopping or not. The average daily truck traffic (ADTT) is the annual average daily truck traffic load on the inventory route. Based on the scour field inspection or scour evaluation study, if either are available, the scour vulnerability of a bridge is indicated (Pearson et al., 2002; Apaydin, 2010).

The simple form of the risk equation used in the HYRISK methodology (Equation 2.4) is the product of the estimated probability of failure and the total cost of failure.

$$\text{Risk} = \text{KP}\,[(\text{Rebuilding Cost}) + (\text{Running Cost}) + (\text{Time Cost})] \tag{2.4}$$

Here, Risk is the annual scour failure risk (money/year), K the risk adjustment factor split into the bridge type factor (K_1) and the foundation type factor (K_2) and P is the annual probability of scour failure (1/year). The rebuilding cost is the cost of replacing the bridge, the running cost is the additional cost associated with vehicles running while detouring during the rebuilding period and the time cost is the financial loss of trucks and people in vehicles while detouring (Apaydin, 2010).

More detailed Equation 2.4 can be written:

$$\begin{aligned}\text{Risk} = \text{C}_1\text{eWL} &+ \left[\text{C}_2\left(1 - \frac{\text{T}}{100}\right) + \text{C}_3\frac{\text{T}}{100}\right]\text{D A d} \\ &+ \left[\text{C}_4\ \text{O}\left(1 - \frac{\text{T}}{100}\right) + \text{C}_5\frac{\text{T}}{100}\right]\frac{\text{D A d}}{S} \\ &+ \text{C}_6\text{X}\end{aligned} \tag{2.5}$$

in which, Risk = the total cost of bridge failure (money), C_1 = rebuilding cost i.e. taken from Table A.2 or local data (money/area), e = cost multiplier for early replacement based on average daily traffic taken from Table 2.7, W = bridge width i.e. taken from NBI item 52 (length), L = bridge length from NBI item 49 (length), C_2 = cost of running vehicle i.e. Table A.3 or local data (money/distance), C_3 = cost of running truck i.e. Table A.3 or local data (money/distance), D = detour length from NBI item 19 (length), A = average daily traffic (ADT) from NBI item 29, d = duration of detour based on ADT from Table 2.7 (days), C_4 = value of time per adult in passenger car i.e. from Table A.4 or local data (money/time), O = average occupancy rate i.e. Table A.1 or local data, T = average daily truck traffic (ADTT) from NBI item 109 (percent of ADT), C_5 = value of time for truck i.e. Table A.6 or local data (money/time), S = average detour speed, C_6 = cost for each life lost (i.e. \$500 000 or

local data), and X = number of fatalities resulting from failure i.e. Table A.5 or local data (Stein and Sedmera, 2006).

Equation 2.5 is the sum of three basic parts: the C_1 term specifies the cost of bridge reconstruction, the detour related consumer costs are expressed by the terms C_2, C_3, C_4, and C_5. In addition to the basic Equation 2.4 the C_6 term tries to estimate the potential cost of fatalities. Thus, this equation provides a template that is easily adjusted for local data and other concerns. Certain general economic assumptions are necessary for the risk computation (Stein and Sedmera, 2006). These are:

- commercial and non-commercial vehicle operating costs
- passenger vehicle occupancy rates
- the value of lost productivity and life
- bridge replacement costs

This itemization clearly shows that the total cost in the case of bridge failure is more than the costs of constructing a new bridge.

The HYRISK approach estimates the average time that a road user spends on a detour. Depending on the road importance, for example classified by the ADT, the duration of the average detour route varies from 183 to 1095 days. Table 2.7 shows the time variation according to the ADT. The cost of wear, which is generated on the detour, must be accurately weighed against the reduced wear on the closed section of road. If the wear on the detour will be significantly higher in comparison to the wear on the original road, then this cost may also be added to the bridge failure (Stein and Sedmera, 2006). In Appendix A additional important parameters used in the HYRISK approach are illustrated.

Table 2.7: ADT versus duration of the detour route and cost multiplier (Pearson et al., 2002).

Average Daily Traffic (ADT)	detour duration (days)	multiplier
ADT $<$ 100	1095	1.00
100 $\leq$ ADT $<$ 500	730	1.10
500 $\leq$ ADT $<$ 1000	548	1.25
1000 $\leq$ ADT $<$ 5000	365	1.50
5000 $\leq$ ADT	183	2.00

2.8 Risk management conclusion

Taking a detailed look at bridge structures shows that they are not only important for traffic but also for supply infrastructures like cables and pipes and provide a cultural value. The overall picture shows the enormous economic importance of bridges and also the difficulty of accurately estimating the economic loss when a bridge is damaged.

The aforementioned chapter shows the complexity of a detailed risk management chain with the focus on river crossing structures, and gives an example of how a risk-management chain is structured and the way to estimate the impact on the society and economy. Thus, the risk management framework developed in the Graduate College 802 was adapted with the help of subject-related literature.

Risk management can be divided into two main aspects. One is to calculate the probability of occurrence of a certain amount of damage, the other part is the estimation of the consequences for a given event. There are a lot of different hazards influencing and interacting with each other, treating the structural integrity of the bridge and even more variables influencing the often enormous economical loss for society. In this work, only the hazards induced by floods were taken into account and the focus is put on one of the most important damages due to this hazard, the local bridge pier scour.

This work is focusing on the occurrence of local bridge pier scour because, in case of a precise estimation of the maximum scour depth, the risk of bridge collapse could decrease relevantly. The fact that bridges still collapse due to local bridge scour shows that there is a lack of related knowledge. The following chapter tackles this issue summarizing the local scour research of the last decades, and also by explaining the basic process of bridge scour.

3 Literature review

This chapter summarizes the major points of scour research of the last decades. It starts with a short section on the basics of particle motion and goes on to state the general definitions of various scour types. It follows the description of the vortex system around the pier and the various parameters that influence the scour depth development. Based on this compilation and related information, at the end of this chapter the goal of research is formulated.

3.1 Basics of particle motion

Before taking a closer look at the scour phenomenon and the parameters that have effects on this process, the basics of particle motion are described shortly. Due to the fact that scouring around an obstacle (for example a bridge pier) is a special case of sediment transport, the next section considers the basics of sediment transport relevant to unidirectional boundary layer flow. Because of the fact that the basics of particle motion is a very complex topic in itself, the author recommends further reading. This includes the recent book by García (2008).

The process of moving and removing particles from their original source or resting place (for example from a riverbed or riverbank) occurs due to the two-phase interaction between water and sediment, also known as erosion. In a river, the water (fluid phase) erodes the available material (solid phase) in the stream bed and/or banks. Usually there are three modes to describe this way of particle motion.

- rolling and/or sliding
- saltating or hopping
- suspended

The aforementioned principals of movement can be divided into *bed load* transport (rolling, sliding and saltating) and *suspended load* transport. While the bed load transport only includes material taken out of the river bed, the suspended load may also include fine particles brought into suspension from the catchment area, which is called *wash load*. Both the bed load and the suspended load may occur simultaneously (van Rijn, 1993).

3.1.1 Initiation of motion in unidirectional currents

When the instantaneous fluid force acting on a particle exceeds the instantaneous resisting force related to the submerged particle weight and friction coefficient, particle movement will occur. If the riverbed consists of appreciable amounts of clay and silt, cohesive forces occur and increase the resisting forces of the particle.

The driving forces are strongly related to the local near bed velocities and, in turbulent flows, they are fluctuating in space and time. Together with the randomness of both particle size, shape and position that initiation of motion is not merely a deterministic phenomenon but a stochastic process as well (van Rijn, 1993). Nevertheless, van Rijn (1993) and Wang and Dittrich (1999) found that the influence of the particle shape on the initiation of motion of individual grains is negligible.

Critical bed shear stress

Fluid forces acting on a sediment particle on a horizontal bed consist of skin friction forces and pressure forces (Figure 3.1). The skin friction force acts on the particle surface by viscous shear, while pressure forces, consisting of a drag F_D and a lift force F_L, are generated due to pressure differences along the particle surface (van Rijn, 1993).

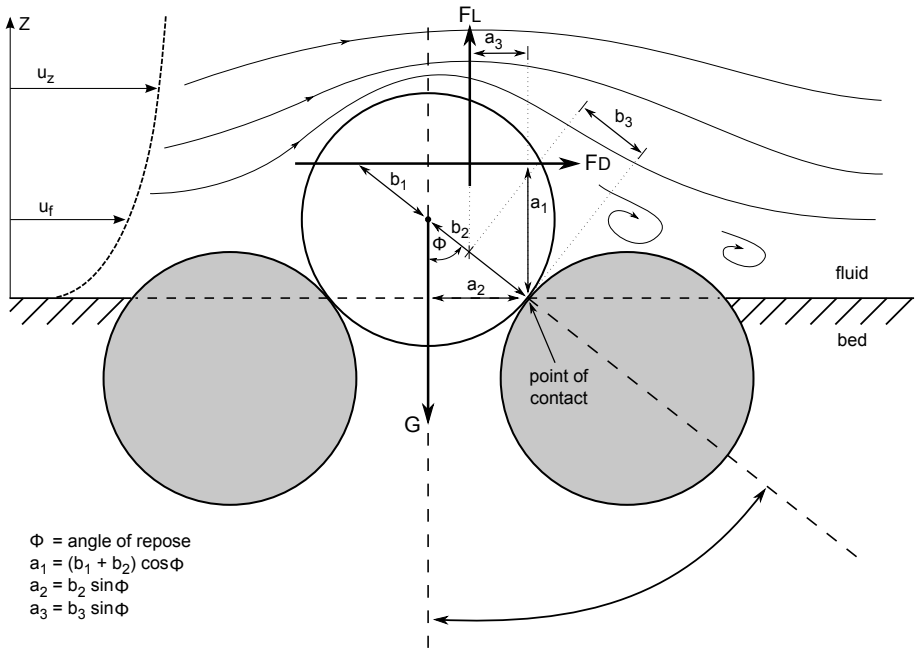

Figure 3.1: Forces acting on a sediment particle (horizontal bed) according to van Rijn (1993).

The angle of repose ϕ is the angle between the line through the particle center and the point of contact, and the line through the particle center normal to the bed surface. Particle movement occurs when the moments of the instantaneous fluid forces F_D and F_L, with respect to the point of contact, to exceed the stabilizing moment of the submerged particle weight G.

$$F_D \; a_1 + F_L \; a_3 \geq G \; a_2 \tag{3.1}$$

or

$$F_D \; ((b_1 + b_2) \; \cos\phi) + F_L(b_3 \; \sin\phi) \geq G(b_2 \; \sin\phi) \tag{3.2}$$

or

$$\frac{(b_1 + b_2) \; F_D}{b_2 - b_3 \; \frac{F_L}{G}} \geq G \; \tan\phi \tag{3.3}$$

For simplicity reasons, the ratio of the lift force and the submerged particle weight is assumed to be relatively small ($F_L/G << 1$), even if this is physically not necessarily true. Due to the fact that the lift force depends on the same variables as the drag force, the effect of the lift force is automatically taken into account by the empirical coefficient $\alpha_1 = b_2/(b_1 + b_2)$ (van Rijn, 1993).

$$F_D \geq \alpha_1 \; G \; \tan\phi \tag{3.4}$$

The value α_1 depends on the grain Reynolds number. At high grain Reynolds number, the pressure force will be much larger than skin the friction force. This is due to the viscosity and the resulting fluid force F_D acting through the particle center ($b_1 = 0$ and thus $\alpha_1 = 1$). In the case of a low grain Reynolds number, the viscous friction force at the top of the particle will dominate and thus $b_1 > 0$ and $\alpha_1 < 1$. The expression (G $\tan\phi$) in Equation 3.4 can be seen as a stabilizing friction force with $\mu = \tan\phi$ as the friction coefficient (van Rijn, 1993).

The effect of both the pressure force and the viscous skin friction, usually can be expressed as

$$F_D = \frac{1}{2} \; \rho \; C_D \; \left(\frac{1}{4} \; \pi \; d^2\right) \; u_f^2 \tag{3.5}$$

where F_D is the drag force, C_D the drag coefficient, d the particle diameter, ρ the fluid density and u_f the fluid velocity at the center of the particle. The drag coefficient C_D is a function of the grain Reynolds number and the fluid velocity u_f at the center of the particle can be expressed as

$$u_f = \alpha_2 \; u_* \tag{3.6}$$

where the α_2-coefficient depends on the grain Reynolds number when the flow regime is hydraulically smooth. u_* is the shear velocity, which can be defined as

$$u_* = \sqrt{\frac{\tau_0}{\rho}} \tag{3.7}$$

The fluid force can now be expressed as

$$F_D = \alpha_3 \, \rho \, d^2 \, u_*^2 \tag{3.8}$$

where the coefficient $\alpha_3 = \alpha_2^2 \, \pi \, C_D/8$ depends on the grain Reynolds number.

The weight of the submerged particle G, depending on the shape of the particle that is taken into account by $\alpha_4 \approx \pi/6$, can be expressed as

$$G = \alpha_4 \, (\rho_s - \rho) \, g \, d^3 \tag{3.9}$$

The substitution of Equations 3.8 and 3.9 into Equation 3.4 yields

$$\frac{u_*^2}{\left(\frac{\rho_s - \rho}{\rho}\right) \, g \, d} \geq \alpha_5 \tan \phi \tag{3.10}$$

or

$$\Theta \geq \Theta_{crit} \tag{3.11}$$

in which

$$\Theta = \frac{u_*^2}{\left(\frac{\rho_s - \rho}{\rho}\right) \, g \, d} = \frac{\tau_0}{(\rho_s - \rho) \, g \, d} = \text{mobility Shields parameter}$$

$$\Theta_{crit} = \alpha_5 \tan \phi = \frac{4 \, \alpha_1 \tan \phi}{3 \, \alpha_2^2 \, C_D} = \text{critical Shields parameter}$$

The Θ_{crit} factor depends on the particle shape, its position relative to the other particles, and on the hydraulic conditions near the bed, expressed by the grain Reynolds number. Thus $\Theta_{\text{crit}} = \text{f}(\text{Re}^*)$.

To determine Θ_{crit} as a function of Re*, a lot of experiments have been performed based on the work of Shields (1936). A detailed overview on the development of the Shields curve by various researchers in the past few decades is given by Buffington (1999). The Shields curve can be roughly separated into the following ranges

		Θ_{crit}	$\geq$	0.035	for		Re*	$\leq$	5	hydraulic smooth regime
0.03	$\leq$	Θ_{crit}	$\leq$	0.04	for	5	$\leq$ Re*	$\leq$	70	transitional regime
0.04	$<$	Θ_{crit}	$\leq$	0.06	for		Re*	$\geq$	70	hydraulic rough regime

For a Reynolds number smaller than approximately 5, the particle diameter of the grain is smaller than the thickness of the viscous sublayer (Figure 3.2). The Shields curve in terms of Θ and Re* is not practical because the τ_{crit} value can only be obtained by iteration (van Rijn, 1993).

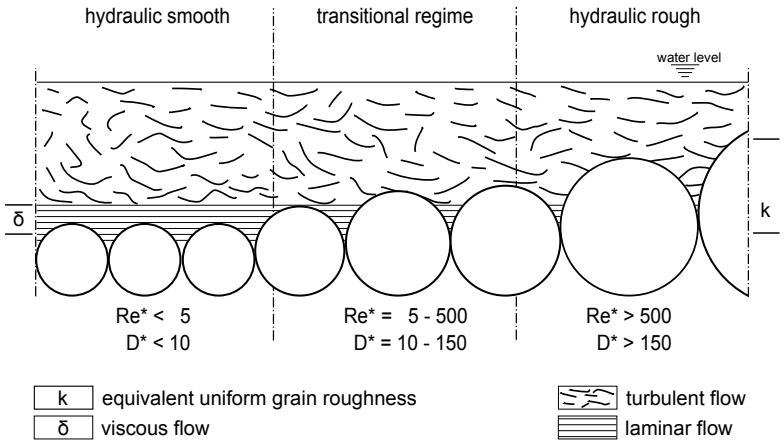

Figure 3.2: Schematic plot of hydraulic flow condition (smooth - transition regime - rough) close to the river bed.

Bonnefille (1963) and Yalin (1972) showed that the Shields curve can be expressed in terms of the mobility parameter Θ and the dimensionless sedimentological diameter D* (Equation 3.12). By applying these parameters, the Shields curve can be represented as shown in Figure 3.3. Therefore the bed-load is not significantly dependent on the grain size (van Rijn, 2007).

$$
\begin{aligned}
\Theta_{crit} &= 0.24D^{*-1} && \text{for} && 1 < D^* \leq 4 \\
\Theta_{crit} &= 0.14D^{*-0.64} && \text{for} && 4 < D^* \leq 10 \\
\Theta_{crit} &= 0.04D^{*-0.1} && \text{for} && 10 < D^* \leq 20 \\
\Theta_{crit} &= 0.013D^{*0.29} && \text{for} && 20 < D^* \leq 150 \\
\Theta_{crit} &= 0.055 && \text{for} && 150 < D^*
\end{aligned}
\tag{3.12}
$$

Dittrich et al. (1992) found, that the parameter combination of Θ and Re* does not satisfactorily describe the initiation of particle movement, in particular for material that has a different density than sand. Therefore, special attention is required when using the Shields curve with lightweight material.

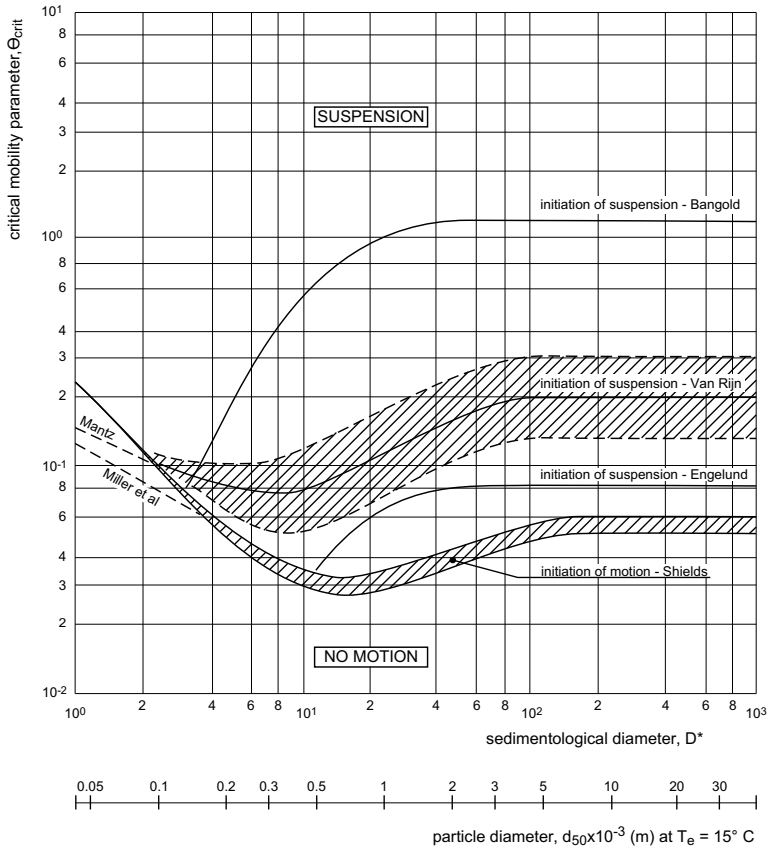

Figure 3.3: Initiation of motion and suspension for a current over a plane bed according to van Rijn (1993).

3.1.2 Equations calculating the critical flow velocity U_{crit}

The critical flow velocity U_{crit} defines the threshold between no motion (clear-water) and motion (live-bed) of the bed material (Section 3.3.1), and can be identified by using experiments, different equations (Appendix B) or diagrams (e.g. Shields, Hjulström). One of the most important and famous researches related to this topic was done by Shields (1936). The equations in Appendix B are used in Section 5.3.1 to calculate the critical velocities for the sediments used in the experiments.

The majority of pier scour equations include the ratio of flow velocity U to critical velocity U_{crit} as a major factor for the hydraulic impact on the pier-sediment interaction, either directly as the mean velocity or indirectly using the Froude and/or Reynolds number. Hence, the reliable prediction of this value is a central task of great significance. The reader should be aware, that even if the equations for the critical velocity give back a single value, the transition between motion and no-motion cannot be determined with just a single value and are therefore better describe using a velocity range. This is due to the range of sediment size, forms and transport mechanisms (turbulences).

Most equations for calculating the critical flow velocity can be applied for any unvegetated channel or overbank area, in order to determine threshold velocity between clear-water or live-bed. However, this procedure should be undertaken cautiously with regards to assessing whether or not scour will be clear-water or live-bed, especially for overbank flow (Richardson and Davis, 2001).

The use of the critical velocity as a criterion for the threshold of sediment motion has been criticized by many researchers (Dey and Papanicolaou, 2008). Nevertheless, the flow velocity, particularly the ratio of flow velocity to the critical flow velocity U/U_{crit} or the Froude number, has a great influence on the scour development and is often used in hydraulic modelling practice and, therefore also in scour equation.

The uncertainties in the determination of the critical flow velocity can also be held responsible for the different estimations of local scour depth in the field.

Besides the mean flow velocity, precisely the bed shear velocity, different parameters influence the erodibility of the bed material around the pier. This is particularly evident from the fact that scour occurs even in clear-water conditions in which no sediment motion can be observed ($U/U_{crit} < 1$).

3.2 Scour definitions

Scour is the result of a natural transportation phenomenon that can occur due to natural flow changes or as part of morphological changes to the river. However there are also man-made reasons for scour, for instance any kind of structures placed inside a stream. In river beds, granular alluvial materials are more susceptible to erode than, for example, coarse gravel. Nevertheless, nearly every material is vulnerable. Finally, it is merely a matter of time.

In literature, a lot of scour definitions are used and different scour types are distinguished. In order to give an overview of the various types of scour and to avoid misconceptions it is useful to define the different meanings at the beginning. The following description is taken out of the *manual on scour at bridges and other hydraulic structures* (May et al., 2002) and gives an overview about frequently used scour definitions, starting with those that are the most widespread and moving on to those that are the most local.

Natural scour: This group is comprised mainly of phenomena associated with the characteristic of the overall form of the river and the whole catchment. These phenomena include the degradation and aggradation of the channel, the lateral channel migration, the bend scour, and the confluence scour. It is known that some of them could also be man induced, for example due to changes in the catchment of the river.

Contraction scour: Contraction scour is in comparison to the natural scour a local phenomena. It is the result of flow restriction, for example between bridge abutments and piers. Due to this restriction, the flow velocity and shear stress increases and the bed material remove from all or most of the stream bed width. The contraction scour can be estimated from considerations of the resistance of the bed material in relation to the flow conditions. Contraction scour can occur in both clear-water and live-bed conditions.

Local scour: Local scour is directly connected with local features that obstruct and split the flow (bridge piers, abutments, dykes). This type of scour occurs in their immediate vicinity due to the fact that the structures increase the complexity of the local flow conditions (velocity and turbulence). The flow conditions close to the structures and the interaction between fluid and bed material are very complicated. To find out the local phenomena that are responsible for the scour process, a lot of research was, and still is being carried out in conjunction with physical model experiments. For this reason a huge number of formulae are available to predict the equilibrium scour depth for clear-water as well as for live-bed scour and also to characterize the scour depth during the development phase.

Total scour: The total scour depth is the sum of all applicable scour processes at a given place. To calculate the probable equilibrium scour depth, all possible scour has to be calculated before adding the results (superposition).

Marine scour: Scour in marine environments is generally subject to the same processes that affect fluvial scour. However, there are additional considerations like tidal flows, littoral drift, interaction of tidal and fluvial streams in estuaries, and normally a greater influence by wave action.

Boat scour: This kind of scour occurs due to the effects of navigation, especially by the vessel's propeller, which can increase the local velocity relevantly. This effect is important to have in mind for cases particularly close to quay walls in harbors.

3.3 Local scour at bridge piers

Figure 3.4 gives a good overview of the scour types that can occur close to bridge crossings. It clearly shows that different kinds of scour can overlap and influence each other, and therefore be part of the total scour. Nevertheless, from this point onwards, the focus is put on local scour induced by a single cylindrical pier.

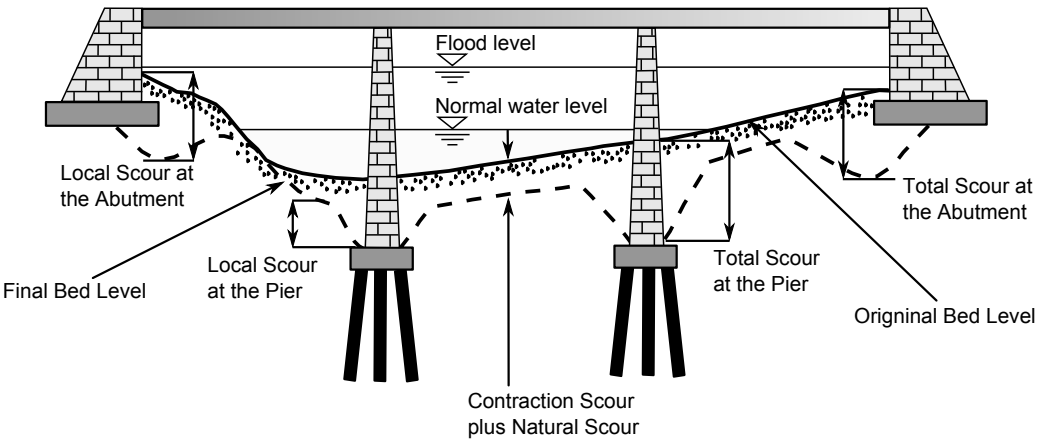

Figure 3.4: The types of scour that can occur on bridges modified according to Melville and Coleman (2000).

3.3.1 Live-bed and clear-water scour

The flow conditions in which scour can occur are divided into *live-bed* and *clear-water*. According to Yanmaz and Köse (2007), Chabert and Engeldinger (1956) were probably some of the first researchers to investigate the temporal variation in scour depth at bridge piers in clear-water and live-bed conditions. Clear-water scour occurs when the mean flow velocity U is less than the critical mean velocity U_{crit} and there is no transport of bed material on the river bed. In contrast, during live-bed conditions bed material is transported from upstream of the bridge cross-section and then flows into it. Nevertheless, clear-water scour may occur if the upstream material is transported in suspension through the bridge cross-section (Richardson and Richardson, 2008).

Typical situations for clear-water scour include (1) flat gradient streams during low flow, (2) streams with coarse bed material, (3) local deposits of bed materials that are larger than the biggest sediment fraction transported by the flow, (4) armored stream beds where the only locations with tractive forces adequate to move the armor layer are at the piers and (5) vegetated channels where, similar to the aforementioned point, the cover is penetrated only at the piers and/or abutments (Richardson and Richardson, 2008).

During a flood event, the flow conditions can change, especially for coarse bed material from clear water scour to live-bed scour at higher discharges and then again for clear-water scour in the falling stages. In Figure 3.5, the development of clear-water scour is plotted in contrast to live-bed scour.

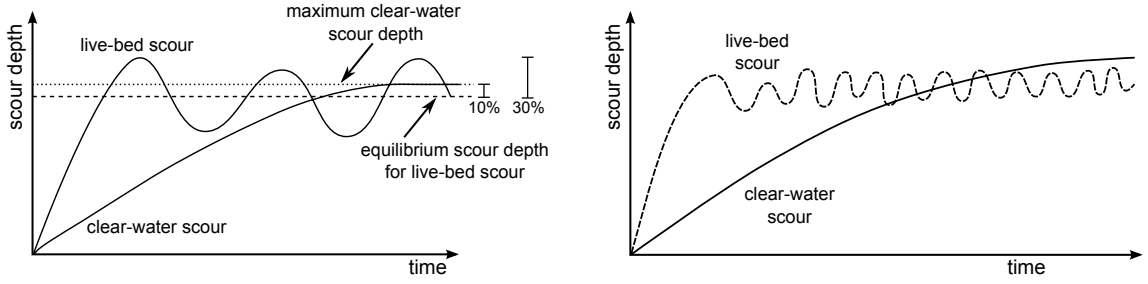

(a) Richardson and Davis (2001)

(b) Ettema et al. (2011)

Figure 3.5: Pier scour depth in a sand-bed stream as a function of time modified after Richardson and Davis (2001) and Ettema et al. (2011).

In general, clear-water scour needs a longer time (or infinity) to reach the equilibrium depth. In contrast, pier scour in live-bed conditions fluctuates due to the variability of the sediment transport in the approach flow around the equilibrium scour depth. In case of dune bed configuration in the channel, the maximum scour depth can be about 30 % larger than the equilibrium scour (Richardson and Davis, 2001). However, with the exception of large river crossings (for example the Mississippi), the bed configuration in sand-bed streams will

plane out during flood events due to the increase in velocity and bed shear stress. In general practice, the maximum scour depth is approximately 10 % greater than the equilibrium scour (Shen et al., 1969; Richardson and Davis, 2001).

3.3.2 Scour development at a single cylindric pier

The main physical processes that are responsible for the scour process at a cylindrical bridge pier in uniform bed material are well known. In this subsection, the main phases of the scour development are briefly summarized.

The scour process is time dependent and can be separated, according to Zanke (1978), into four different phases (Figure 3.6). Link (2006) defines the phases as:

Initial phase: During this phase the scouring process starts with the lateral erosion at the pier under an acute angle of 40° to 55°. The flow pattern is characterized by two main vortices, the horseshoe vortex and the wake vortex.

Beginning phase: This phase is characterized by the conjunction of the two initial scours at the front of the pier. In the following, the deepest point of scour is directly in front of the pier. Behind the pier the eroded material is settled in the form of dunes (live-bed conditions) or a barchan (clear-water conditions). The scour depth development goes on very fast.

Developing phase: After reaching the maximum depth in front of the pier, the scour development slows down.

Equilibrium phase: Here, the erosion inside the scour is negligible. The scour also reaches the maximum depth and expansion.

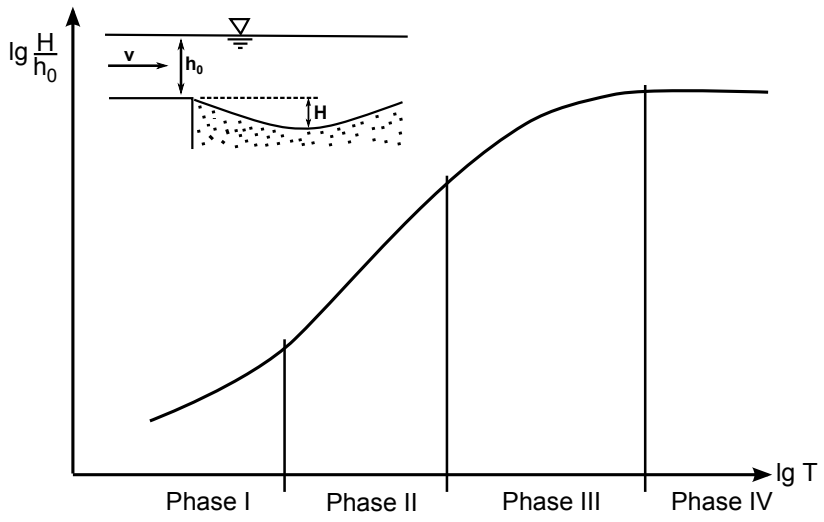

Figure 3.6: Four different phases of scour depth development according to Zanke (1978).

3.3.3 Flow pattern around cylindric piers

The flow pattern around a cylindric bridge pier is illustrated in Figure 3.7. The most important flow features are the down-flow and the surface roller ahead of the pier, the horseshoe vortex along the pier base, and the wake vortices downstream from the pier.

The down-flow, as well as the surface roller, are consequences of flow deceleration ahead of the pier. The stagnation pressures on the pier face are highest near the surface and decrease downwards. Due to this pressure gradient, the down-flow develops and hits the riverbed like a vertical jet before the flow redirects around the pier. At the beginning of the scour process the down-flow immediately erodes a groove adjacent to the pier front, which initiates the horseshoe vortex (Melville and Coleman, 2000). For Melville and Coleman (2000), the horseshoe vortex is, together with the down-flow, the major reason for scouring. The wake vortices arise at the sides of the pier because of the flow separation. All vortices together are responsible for mobilizing and transporting the sediment downstream from the bridge pier.

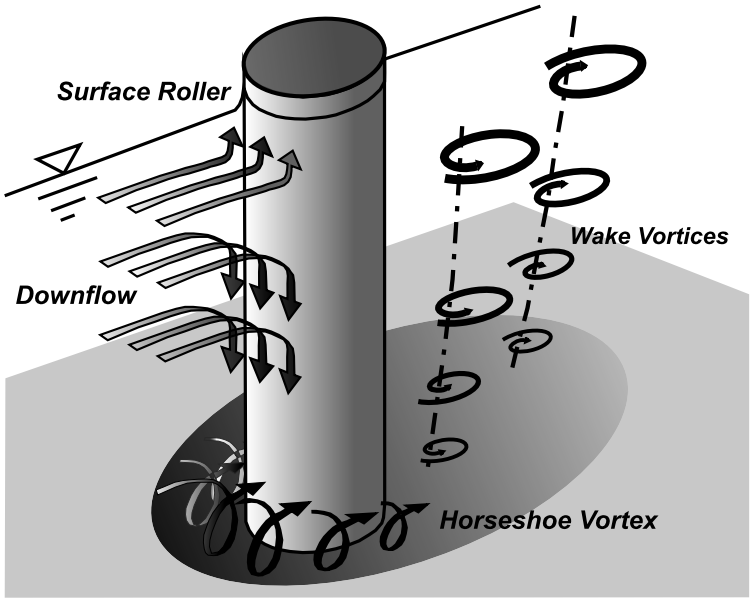

Figure 3.7: Flow pattern around a cylindric bridge pier according to Melville and Coleman (2000).

Surface roller

The surface roller occurs ahead of the pier between the stagnation point and water surface. The vortex has no influence on the scouring process as long as the water is deep enough. Otherwise, the surface roller interferes with the horseshoe vortex. This is because the two have the opposite sense of rotation, which can lead to a scour depth reduction (Melville and Sutherland, 1988). Different threshold conditions are outlined in Subsection 3.4.5.

Flow contraction

If the streamlines of the flow are separated by an obstacle and reduce their cross sectional area, then (assuming a non-compressible fluid) the preservation of the mass flux will lead to an increase in flow velocity at the flow contraction point (Sigloch, 2008). Pier diameter greater than 10 % of the flume or river width can affect the flow patter around the pier (Subsection 3.4.4).

Primary and horseshoe vortices

When the approach flow hits the upstream face of an object, a stagnation pressure is induced. The concept of a stagnation pressure (Figure 3.8) can be shown by applying the *Bernoulli*-Equation to two points along the stagnation streamline (P_1 and P_2).

$$P_1 + \frac{\rho\, U_1^2}{2} = P_2 + \frac{\rho\, U_2^2}{2} \tag{3.13}$$

where P is the pressure energy, ρ the density of the fluid and U the horizontal component of the fluid velocity.

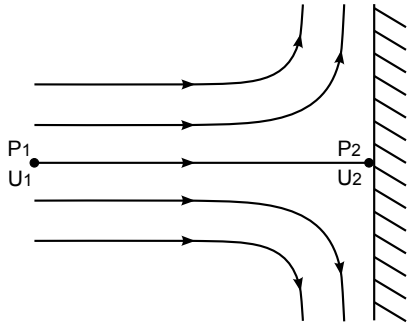

Figure 3.8: Schematic of the stagnation point in the flow impinging a plate according to Saunders (2004).

Because of the zero velocity at the stagnation point ($U_2 = 0\,m\,s^{-1}$), the stagnation pressure P_2 is the sum of the pressure energy and the kinetic energy at P_1. Assuming no energy losses, at any level, the pressure is proportional to the square of the free stream velocity at that level. Due to the logarithmic flow field, a strong vertical pressure gradient forms at the upstream face of the object, with high pressure at the higher flow and low pressure at the base of the object. This in turn causes a down-flow of the fluid along the upstream face, which is impinging on the bed and induces a recirculation flow pattern (Figure 3.9). As the oncoming flow is drawn into the primary vortex, flow line contraction occurs within the vortex and increases the local velocities (Saunders, 2004).

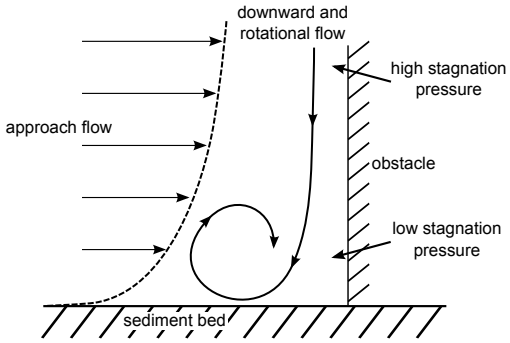

Figure 3.9: A schematic depiction of the formation of the primary vortex according to Saunders (2004).

The primary vortex separates to both sides of the object (Figure 3.10). In the case of breaking objects, this extended primary vortex separates around the object and is swept downstream by the approaching flow. Viewed from above, this vortex system looks like a horseshoe and is therefore termed as a horseshoe vortex. Where the recirculation of the primary and horseshoe vortices contacted the oncoming flow, a flow separation occurs, dividing the vortex system and the approach flow (Figure 3.11) (Saunders, 2004; Unger, 2006). This vortex system is practically independent on the wake vortices (Dargahi, 1989).

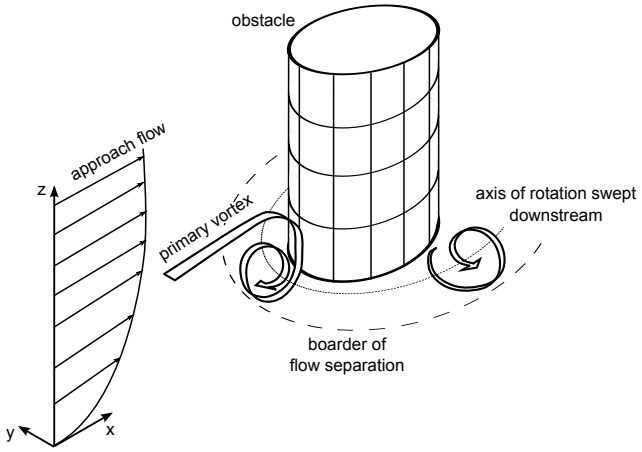

Figure 3.10: A schematic depiction of the formation of the characteristic horseshoe vortex according to Saunders (2004).

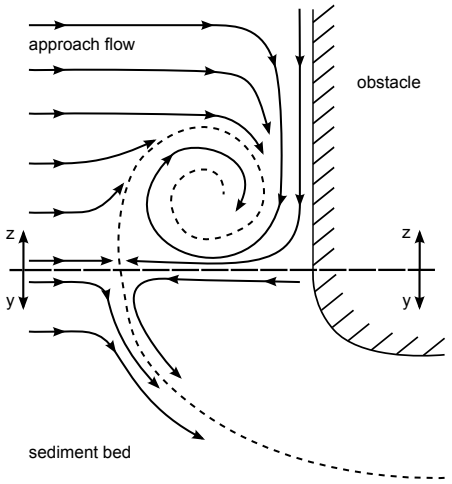

Figure 3.11: Upstream flow separation according to Saunders (2004), the dashed line represents a separation border in the flow.

Lee wake vortices

Lee wake vortices, also known as *Von Kármán* vortices, are relatively small, regular fluid rotations that are shed periodically from alternative sides of the object at a frequency which, in the case of a cylinder, is dependent on the pier Reynolds number (3.12).

The flow regimes experienced with increasing pier Reynolds numbers are summarized in Figure 3.13. For further reading on this topic, and a detailed analysis of the different conditions, see Chapter 1 of the recent book written by Sumer and Fredsøe (2006).

$$Re_{pier} = \frac{UD}{\nu} \tag{3.14}$$

where U is the depth averaged mean flow velocity [$\mathrm{m\,s^{-1}}$], D the pier diameter [m] and ν the kinematic viscosity of the fluid [$\mathrm{m^2\,s^{-1}}$].

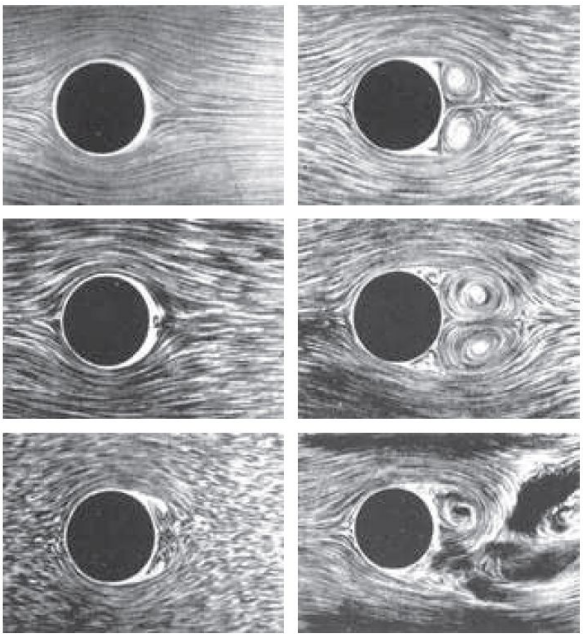

Figure 3.12: Formation of the Kármán vortex street for increasing pier Reynolds number Oertel et al. (2009).

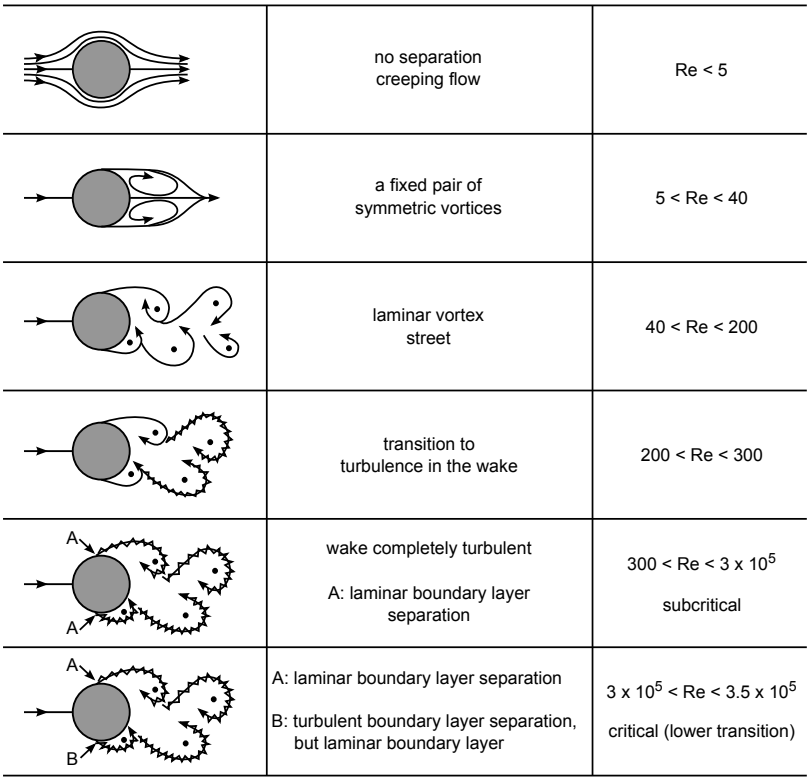

Figure 3.13: Regimes of flow around a circular cylinder in a steady current according to Sumer and Fredsøe (2006).

3.3.4 Development of the vortex system

Unger (2006) has investigated the vortex system around a cylindrical pier. He defines four phases for the scour depth development in accordance with the aforementioned phases. However, he puts the focus on the development of the horizontal and vertical flow patterns around the pier. First, the four phases for the vertical flow field are described:

Phase 1: The scouring process starts with the lateral erosion at the pier under an acute angle of 75°. The flow pattern is characterized by a relatively undisturbed logarithmic flow upstream of the pier. Directly at the front of the pier, at the stagnation point, the flow is divided into two vertical streams. The up-flow reaches the water level and builds the surface roller, while the down-flow builds the initial vortex on the riverbed surface. The stagnation point, the up-flow, the surface roller, as well as the down-flow, exist in all phases. The lateral erosion at the pier occurs because of the acceleration of the flow around the pier, while the initial vortex has no erosive impact.

Phase 2: In this phase the two initial lateral scours join together at the front of the pier. The initial vortex disappears and the flow goes around the pier, inducing a strong acceleration of the flow. Thus, the scour depth increases to the side of the pier and the increasing scour depth in front of the pier happens due to material slides caused by the lateral erosion.

Phase 3: The horseshoe vortex occurs. At the beginning of Phase 3, only one main vortex exists and it induces the critical shear velocity at the bottom of the scour. The maximum scour depth shifts to the pier symmetry axis in front of the pier. In the following, the velocity of the scour development decreases due to the growth of the cross section.

Phase 4: The influence of the horseshoe vortex on the scouring process increases and, with the enlargement of the scour, the diameter of the horseshoe vortex also enlarges. Besides the main horseshoe vortex, additional sub-vortices occur.

Parallel to the four phases for the vertical flow, the horizontal flow field develops:

Phase 1: The main flow reaches the pier and deflects into the channel cross section. In this connection the flow accelerates and the erosion of the bed material starts at an acute angle of 75°. The break off point of the flow is in between the angle of 75° and 110°, and marks the point in which the wake vortices start. The scour has no influence on the flow pattern during this phase.

Phase 2: The erosion around the pier influences the horizontal flow pattern. While, near the water surface, the stream lines have the same characteristics as in Phase 1. Here, the breaking point close to the bed level (inside the scour) moves to the downstream part of the pier up to an angle of 125°. Due to this fact, the wake vortices get smaller. Because of the sedimentation area downstream of the pier, the flow will be partly deflected around this area into the channel cross section.

Phase 3: The horseshoe vortex occurs. The stream lines close to the bed level around the scour are similar to the *Coanda*-flow and butt against the pier. The breaking point is close to the downstream end of the pier. Unger (2006) presents two reasons for this: (1) Due to the increasing hydraulic pressure inside the scour, the comprehensive gradient at the outside wall of the pier decreases and (2) the geometry of the scour is like a guide wall for the stream.

Phase 4: The horseshoe vortex is completely developed and there is no flow separation at the pier close to the bed level. Because of the advanced scour geometry and the increased cross section, the velocity of the accelerated flow around the pier, like in Phase 1 and 2, is noticeably decreased.

Dimension of the horseshoe vortex

Unger (2006) carried out extensive laboratory tests to characterize the vortex system. The main limitations of this model, which was based on the work of Oliveto and Hager (2005), are: (1) sediment size $d_{50} \geq 0.8\,mm$ in order to exclude viscous effects; (2) rectangular channel geometry; (3) relative flow depth to exclude macro roughness effects; and (4) approach flows producing clear water scour $0.6 < U/U_{crit} < 1.2$.

He developed a set of parameters and equations to calculate the dimensions of the different vortices. Identifying the horseshoe vortex as one of the essential mechanisms responsible for scour depth development, the dimension $d_{vortex} = (a_v + b_v)/2$, where a_v is the long axis of the ellipse and b_v is the short axis, of the main horseshoe vortex is

$$\frac{d_{vortex}}{z_R} = 0.03\ \sigma^{-\frac{1}{2}}\ \left(\frac{U}{U_{crit}}\right)^{-\frac{1}{8}}\ Fr_d^{\frac{3}{2}}\ log(T_s) \tag{3.15}$$

The Equation 3.15 shows, that the diameter of the horseshoe vortex d_{vortex} depends on the grain size distribution $\sigma = (d_{84}/d_{16})^{0.5})$, the flow intensity U/U_{crit}, the reference length z_R, which is defined as

$$z_R = (h\ D^2)^{\frac{1}{3}} \tag{3.16}$$

and the densimetric Froude number Fr_d,

$$Fr_d = \frac{U}{\sqrt{\rho'\ g\ d_{50}}} \tag{3.17}$$

which includes the approach flow velocity U, the sediment properties d_{50} as well as the relative sediment density ρ' and gravity g.

The dimensionless time T_s ($T_s = t/t_r$) is also taken into account in which t is the operational time and $t_r = h/U$ the reference time. Equation 3.15 is only valid for $T_s > T_0$. The relative time T_0 to develop the horseshoe vortex can be calculated with the following equation.

$$T_0 = 0.25 \left(\frac{U}{U_{crit}}\right)^{-\frac{3}{2}}\ \frac{z_R}{d_{50}} \tag{3.18}$$

Regarding the focus of this thesis, it can be said that the characteristics of the horseshoe vortex strongly depend on the densimetric Froude number and the time. Thus, the characteristics of the sediment are included in σ and the Fr_d.

3.3.5 Equations calculating local bridge scour

Many scour equations can be found in the related literature. Most scour prediction formulas, such as the equation of the Colorado State University (CSU-Equation), which is currently used in the U.S. Federal Highway Administration (FHWA) Hydraulic Engineering Circular Number 18 (HEC-18), as well as those published by Breusers et al. (1977), Melville and Coleman (2000) and Sheppard et al. (2004), are empirical and based on laboratory data. Many of these equations yield similar results for laboratory-scale cylindrical structures, but differ significantly in their predictions for prototype scale structures (Florida Department of Transportation, 2005).

In general, the majority of these equations estimate the equilibrium scour depth d_{se} according to the special importance for the stability of the pier foundations. In the following section a selection of the most important scour equations are briefly described and compared by means of literature data for clear water conditions and round pier shapes. Time dependent scour equations are excluded.

Laursen and Toch (1956)

Laursen and Toch (1956) investigated the influence of the pier shape, angle of attack, water depth, velocity and sediment size. The authors presented a graphic design curve, which Neill (1964) expressed for the cylindric pier as the following.

$$d_{se} = 1.35 \left(\frac{h}{D}\right)^{0.3} D \tag{3.19}$$

Shen (1969)

Shen et al. (1969) investigated a scour equation that depends on the pier Reynolds number. According to Breusers et al. (1977) the Reynolds number is an unsuitable parameter to characterize the scour depth. The given equation is the only one that includes only the pier Reynolds number.

$$d_{se} = 0.000223 \, Re_{pier}^{0.615} \tag{3.20}$$

Breusers (1977)

Breusers (1977) made a detailed literature analysis and give the following equation for scour depth estimation. For circular piers K_{shape} and K_{angle} become 1.0.

$$d_{se} = f_1\left(\frac{U}{U_{crit}}\right)\ \left[2.0\tanh\left(\frac{h}{D}\right)\right]\ K_{shape}\ K_{angle}\ D \tag{3.21}$$

with

$$f_1\left(\frac{U}{U_{crit}}\right) = \begin{cases} 0 & \text{if} \quad \frac{U}{U_{crit}} \leq 0.5 \\ \frac{U}{U_{crit}} - 1 & \text{if} \quad 0.5 < \frac{U}{U_{crit}} < 1.0 \\ 1 & \text{if} \quad 1.0 < \frac{U}{U_{crit}} \end{cases} \tag{3.22}$$

Jain (1981)

Jain (1981) studied the local pier scour for large Froude numbers in the laboratory, and gives the following equation for clear water conditions. In case of different pier shapes from circular piers, as well as pier alignment other than parallel with the stream flow direction, the result of the Jain equations should be multiplied by the coefficients given in Table 3.2 and Table 3.4 (Richardson and Richardson, 2008).

$$d_{se} = 1.84\ Fr_{crit}^{0.25}\ \left(\frac{h}{D}\right)^{0.3}\ D \quad \text{if} \quad (Fr - Fr_{crit}) \leq 0.2 \tag{3.23}$$

Melville and Sutherland(1988)

Melville and Sutherland (1988) developed a K-factor based equation. For threshold flow conditions $U = U_{crit}$, K_{flow} becomes 2.4, K_{depth} becomes 1.0 if $h/D > 2.6$, K_{size} becomes 1.0 if $D/d > 25$ for $D/d < 25$ $K_{size} = 0.57 \log (2.24\ D/d)$. The influence of K_σ is included in K_{flow}. K_{shape} as well as K_{angle} become 1.0 for circular piers.

$$d_{se} = K_{flow}\ K_{depth}\ K_{size}\ K_\sigma\ K_{shape}\ K_{angle}\ D \tag{3.24}$$

CSU-Equation (1988)

The so called CSU-Equation (1988) was constantly developed over the last few decades and new K-factors are included (Johnson, 1992). This modified equation (see Richardson and Richardson (2008))is recommended by the Federal Highway Administration in the United States of America. K_{shape} and K_{angle} become 1.0 for circular piers.

$$d_{se} = 2.0\ K_{shape}\ K_{angle}\ \left(\frac{h}{D}\right)^{0.35}\ Fr^{0.43}\ D \tag{3.25}$$

Breusers and Raudkivi (1991)

Breusers and Raudkivi (1991) calculated the scour depth with different K-factors that can be determined by corresponding figures and tables. In uniform sediments K_σ becomes 1.0, furthermore K_{depth} becomes 1.0 for fine uniform sediment if $h/D > 2.0$ whereas K_{depth} for relative coarse sediment becomes 1.0 if $h/D > 6.0$. K_{size} becomes 1.0 if $D/d_{50} > 50$. K_{shape}, as well as K_{angle}, become 1.0 for circular piers.

$$d_{se} = 2.4\ K_{depth}\ K_{size}\ K_{shape}\ K_{angle}\ K_\sigma\ D \tag{3.26}$$

Johnson (1992)

Johnson (1992) developed a probabilistic pier scour approach, because hydraulic variables such as discharge, flow depth, and velocity are generally stochastic in nature. Because these parameters are significant for the scour process, the scour depth itself is also a stochastic variable.

$$d_{se} = 2.02\ h\ \left(\frac{D}{h}\right)^{0.98}\ Fr^{0.21}\ \sigma^{-0.24} \tag{3.27}$$

Gao (1993)

Gao (1993) presented and validated the Chinese-Equation which has been used by highway and railway engineers in China for more than 20 years. This equation, based on laboratory studies and a great number of field data, and is valid for both live-bed and clear water scour Gao et al. (1999).

$$d_{se} = 0.46\ K_{shape}\ D^{0.6}\ h^{0.15}\ d^{-0.07}\ \left(\frac{U - U'_{crit}}{U_{crit} - U'_{crit}}\right)^{\eta} \tag{3.28}$$

$\eta = 1.0$ for clear-water condition, $K_{shape} = 1.0$ for circular piers and $U'_{crit} = 0.645\ (d_{ch}/D)^{0.053}\ U_{crit}$.

CSU-Equation (1995)

The CSU-Equation (1995) includes two new K-factors K_{bed} and $K_{armoring}$. K_{shape}, K_{angle} and $K_{armoring}$ become 1.0 for circular piers in uniform material, $K_{bed} = 1.1$ for clear-water scour without dunes (Table 3.5). This equation is still in use in the United States of America with an additional K-factor for the pier width K_{width} which is considered important if $h/D < 0.8$ (Richardson and Richardson, 2008).

$$d_{se} = 2.0\ K_{shape}\ K_{angle}\ K_{bed}\ K_{armoring}\ \left(\frac{h}{D}\right)^{0.35}\ Fr^{0.43}\ D \tag{3.29}$$

Melville (1997)

Melville (1997) gave the following equation for calculating the equilibrium local scour depth at bridge piers. For circular piers K_{shape} and K_{angle} become 1.0.

$$d_{se} = K_{depth}\ K_{flow}\ K_{size}\ K_{shape}\ K_{angle} \tag{3.30}$$

The correction factor K_{depth} takes into account the ratio of the flow depth to the pier width. For deep water flows $D/h < 0.7$ the scour depth is connected linearly to the pier width, in shallow water $D/h > 5$ the scour depth increases linearly with the flow depth. Regarding these values, the development of the scour is dependent on the water depth h as well as on the pier width D.

$$K_{depth} = \begin{cases} 2.4\ D & \text{if} \quad \frac{D}{h} < 0.7 \\ 2.0\sqrt{h\ D} & \text{if} \quad 0.7 < \frac{D}{h} < 5 \\ 4.5\ h & \text{if} \quad 5 < \frac{D}{h} \end{cases} \tag{3.31}$$

The correction factor K_{flow} is divided into clear water and live-bed conditions. For uniform material $\sigma < 1.3$ the armor peak velocity becomes equal to the critical velocity $U_a = U_{crit}$. U_a is the mean approach velocity at the armor peak ($0.8\ U_{crit,a}$)

$$K_{flow} = \begin{cases} \frac{U-(U_a-U_{crit})}{U_{crit}} & \text{if} \quad \frac{U-(U_a-U_{crit})}{U_{crit}} < 1.0 \quad \text{clear-water} \\ 1.0 & \text{if} \quad \frac{U-(U_a-U_{crit})}{U_{crit}} \geq 1.0 \quad \text{live-bed} \end{cases} \tag{3.32}$$

The sediment size is considered by using the factor K_{size}. The scour depth decreases with the ratio $D/d_{50} \leq 25$ and becomes independent for higher values of D/d_{50} (Equation 3.41).

May (2002)

May et al. (2002) combines the main results of the approaches developed by different authors (for example Breusers et al. (1977); Melville and Sutherland (1988); Breusers and Raudkivi (1991)), and gives the following K-factor based equation to estimate the equilibrium scour depth.

$$d_{se} = S_F\ K_{depth}\ K_{flow}\ K_{shape}\ K_{angle}\ D \tag{3.33}$$

S_F is a safety factor that takes into account random variation in scour development and uncertainties about the flow conditions. Suitable values are given in Table 3.1, recommended by Johnson (1992). For laboratory studies it has been found that $S_F = 1.6$ corresponds to the maximum observed scour depth.

Table 3.1: Values of factors of safety S_F

Percentage number of cases in which predicted scour depth might be expected to be exceeded	S_F
50	1.00
10	1.20
1	1.40
0.1	1.60
0.01	1.75
0.001	1.85

The factor K_{depth} takes into account the effect of the relative water depth on the scour depth and can be calculated with the following formula.

$$K_{depth} = \begin{cases} 0.55 \frac{h}{D}^{0.6} & \text{if} \quad \frac{h}{D} \leq 2.7 \\ 1.0 & \text{if} \quad \frac{h}{D} > 2.7 \end{cases} \tag{3.34}$$

The influence of flow velocity is described by the factor K_{flow}. Uniform graded sediments may overestimate the scour depth for widely graded sediments, if the value of U/U_{crit} exceeds 3 to 4, the flow intensity factor is likely to reach an upper limit of $K_{flow} \approx 0.9$ for widely graded sediments.

$$K_{flow} = \begin{cases} 0 & \text{if} \quad \frac{U}{U_{crit}} \leq 0.375 \\ 1.6 \frac{U}{U_{crit}} - 0.6 & \text{if} \quad 0.375 \leq \frac{U}{U_{crit}} \leq 1.0 \\ 1.0 & \text{if} \quad 1.0 < \frac{U}{U_{crit}} \end{cases} \tag{3.35}$$

The effect of the pier shape on the local scour depth is taken into account by K_{shape}. Table 3.3 gives values of K_{shape} for different pier shapes based on information collected by Hoffmans, G. J. C. M. and Verheij (1997). Complex pier structures need to be determined with physical hydraulic models.

The factor K_{angle} describes the influence of the angle of attack of the flow on the scour depth. This value can be calculated by the Equation 3.38 and becomes 1.0 for circular piers..

Sheppard (2004)

Sheppard et al. (2004) carried out large clear water experiments with different cylindric pier width D and different sediment sizes d_{50}. Sheppard et al. (2004) specifically investigated the dependence of d_{se}/D on D/d_{50} on the scour depth d_{se}. In comparison with the dimensionless quantities of the flow velocity U/U_{crit} (mean velocity upstream of the pier divided by the critical sediment velocity), and the aspect ratio h/D (water depth upstream of the pier divided by the pier diameter), they noticed that the ratio of the pier diameter divided by the median sediment size D/d_{50} is not taken accurately into account in many studies. For non circular piers, D is changed to an effective structure diameter D_{eff} (pier width times coefficient).

$$d_{se} = 2.5\ tanh\left[\left(\frac{h}{D}\right)^{0.4}\right]\ \left(1 - 1.75\left[ln\left(\frac{U}{U_{crit}}\right)\right]^2\right)\ \frac{D/d}{0.4(D/d)^{1.2} + 10.6(D/d)^{-0.13}}\ D \tag{3.36}$$

Comparison of the scour equations

Figure 3.14 and Figure 3.15 show scatter plots of computed versus measured scour depth data taken from literature (clear water and round piers). The black dots are laboratory data taken from literature (Chabert and Engeldinger, 1956; Ettema, 1980; Melville and Chiew, 1999; Molinas, 2003; Mia and Nago, 2003; Yu et al., 2003; Sheppard et al., 2004; Dey and Raikar, 2007b) and the red dots are field data taken from Müller and Wagner (2005). Altogether, the data of 266 scour depths are available including 63 field measurements. For a better comparison, the data in Figure 3.15 are normalized with the pier diameter D.

Figure 3.14 and Figure 3.15 clearly show that the prototype scour depth (field data) will be overestimated in most cases by the scour equations, this goes in line with the observation of for example May et al. (2002). This leads to the assumption that either the field data are not corresponding with the maximum scour depth, or that the transfer between the physical model and prototype is not correct. Due to the high number of bridge failures and the complex task of in-situ scour measurements during flood events, it seems likely that the measured field data are not equal to the maximum scour depth. Different reasons can be responsible for this.

- the flood may not have lasted long enough for the equilibrium scour depth
- the flow conditions may not have corresponded exactly
- the scour may have partly filled in again by the time before the measurements were carried out

However, the smaller scour depths in the field also correspond with the research carried out by Sheppard et al. (2004) for high values of D/d_{50}, which in general leads to a scour depth reduction for values $D/d_{50} \geq 50$.

Based on various studies, for example Melville and Sutherland (1988), the maximum scour depth for round nose piers aligned with the flow can be calculated with Equation 3.37 (Richardson and Davis, 1995; Melville and Coleman, 2000; García, 2008). Scour depths larger than those given by Equation 3.37 for round nose piers aligned with the flow should be questioned and carefully evaluated.

$$d_{se} \leq \begin{cases} 2.4\ D & \text{for} \quad Fr \leq 0.8 \\ 3.0\ D & \text{for} \quad Fr > 0.8 \end{cases} \tag{3.37}$$

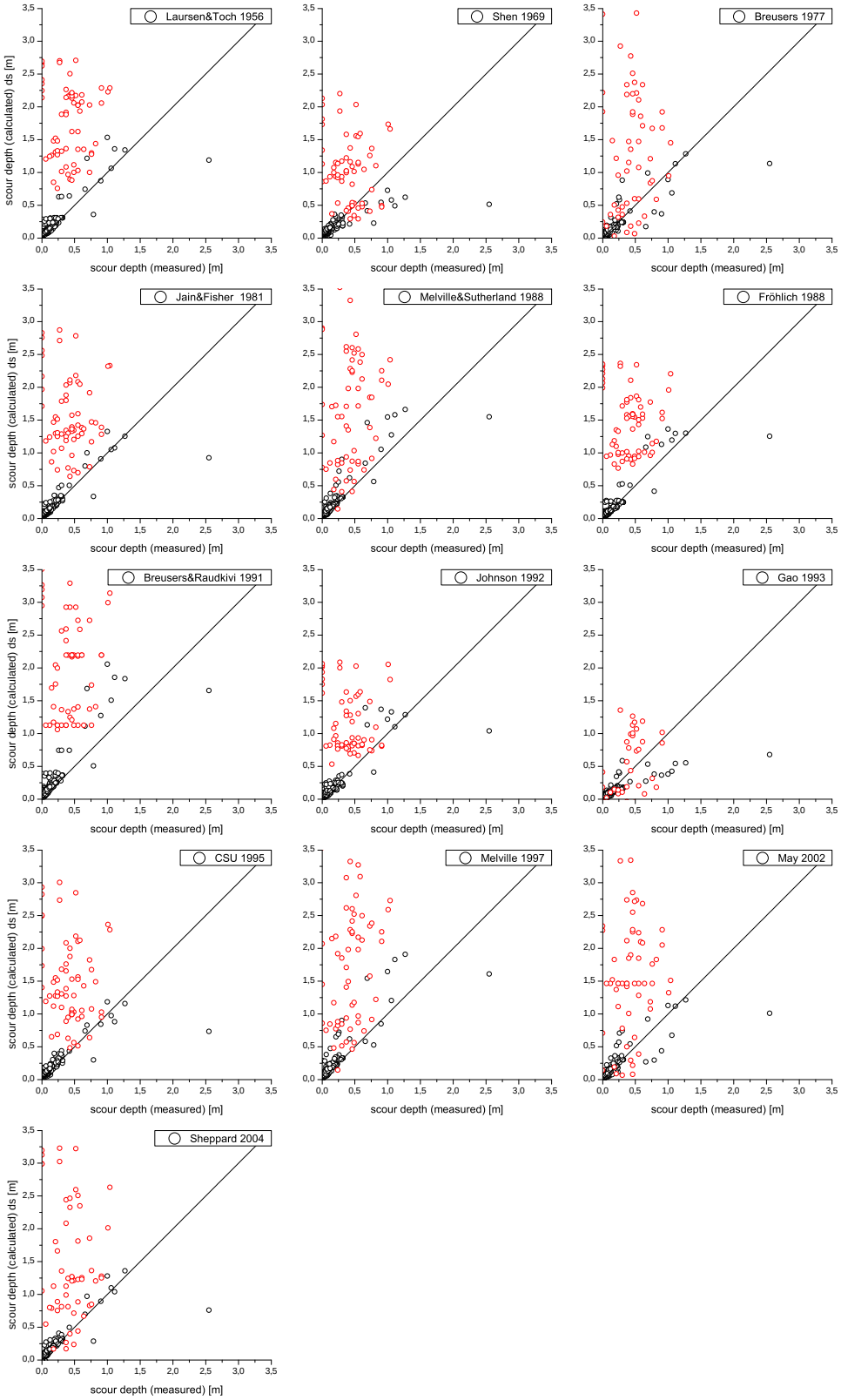

Figure 3.14: Scatter-plots of computed versus observed scour depth, in meters [m], for selected pier scour equations.

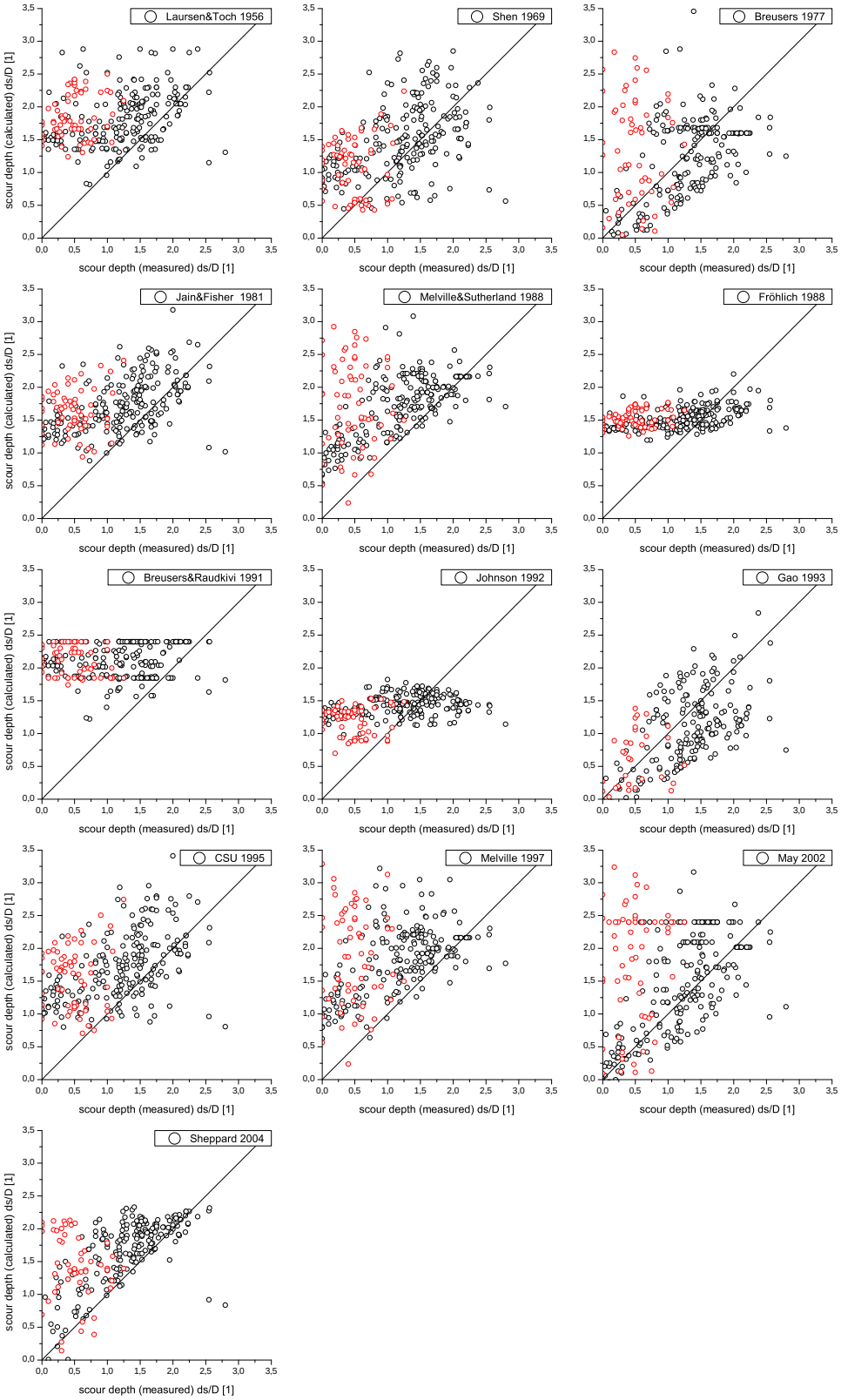

Figure 3.15: Scatter-plots of computed versus observed scour depth, dimensionless [1], for selected pier scour equations.

The review of the current scour research by Ettema et al. (2011) indicates that the scour depth development for simple single-column pier forms can be reliably estimated by semi-empirical methods like the current HEC-18 method or the modified Sheppard-Approach. For boundary conditions that differ from those previously mentioned, which are quite common in the field (e.g. pile cap, debris or ice accumulation, abutment interaction, ...), a reliable scour depth estimation is not possible and results taken from semi-empirical or empirical methods should be validated with hydraulic models. In case of complex or unusual pier situations where reliable information on parameter influences does not exist (e.g. scour for wide-piers), hydraulic modeling possibly aided by numerical modeling is recommended.

In general, scour depth estimation calculated with laboratory-based formulas should provide an upper limit estimation of the maximum scour depth that can be expected to occur in full size structures, due to the high number of uncertain parameters affecting the scour in the field.

3.4 Characteristic parameters for the scour process

Scour is a local transport phenomenon induced by an obstacle being placed in the stream, thereby various parameters influence riverbed erosion. The influence of each parameter on the scour process, as well as the interaction between these parameters with each other, is still not clear.

3.4.1 Effect of pier size

The equilibrium local scour depth is directly proportional to D (Ettema, 1980). As easily can be seen from the above mentioned scour equation, the pier diameter D, respectively the pier surface that is hit by the flow, is one of the most important parameters. Breusers and Raudkivi (1991) found that pier size affects the time t_e required for the maximum local clear-water scour. The larger the pier diameters the longer the requirement to scour. The relative scour depth magnitude d_{se}/D is not affected if the relative depth h/D and the relative grain size D/d_{50} are excluded. The volume of the local scour hole formed around the upstream half of the pier is proportional to the cube of the projected pier width or diameter (Raudkivi, 1998).

As will become clear below, for example the effect of flow depth h and sediment size d_{50}, the pier diameter has an important role in combination with other the parameters.

3.4.2 Effect of pier shape

Commonly used pier shapes are shown in Figure 3.16. The pier shape has a significant influence on the scour depth. Breusers et al. (1977) summarized several approaches from

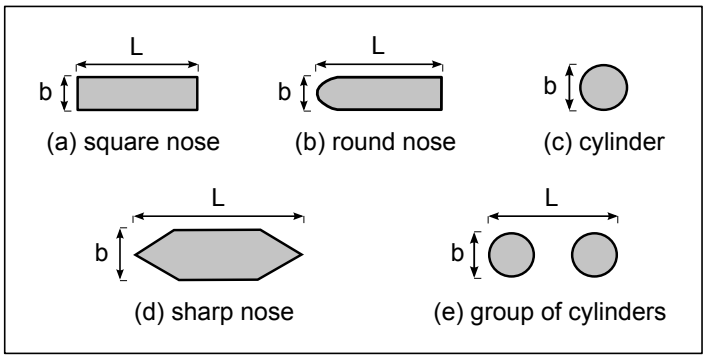

Figure 3.16: Commonly used pier shapes (Richardson and Davis, 2001).

different authors and concluded that if a circular or round-nosed pier is taken as a reference, a scour depth reduction of 25 % can be obtained by streamlining the pier. This positive effect disappears in cases of angles of attack larger than 10° to 15°. On the other hand, rectangular piers can increase the scour depth up to 40 % compared with the reference pier. Ettema (1980)

concludes that the blunter the pier, the deeper the local scour depth. The influence of the downstream end of the pier is of little significance to the maximum local scour depth.

The correction factor K_{shape} for the CSU-Equation (Equation 3.29), should be determined by using Table 3.2 for angles of attack of up to 5°. In case of greater angles, the K_{angle} dominates and the K_{shape} should be considered as 1.0.

Table 3.2: Correction factor for pier nose shape K_{shape} (García, 2008).

shape of pier nose	K_{shape}
(a) square nose	1.1
(b) round nose	1.0
(c) circular cylinder	1.0
(d) group of cylinders	1.0
(e) sharp nose	0.9

The correction factor K_{shape} for the equation recommended by May et al. (2002) differs significantly from the one used for the CSU-Equation (Table 3.3).

Table 3.3: Shape factor values K_{shape} for different structures May et al. (2002).

type of structure	K_{shape}
cross-sectional shape in plan	
circular	1.5
lenticular	1.0-1.2
elliptic	0.9-1.2
square	2.0
rectangular	1.5-1.8
cross-sectional shape in elevation	
pyramid (widest at base)	1.15
inverted pyramid (narrowest at base)	1.8

Neill (1978), as well as Müller and Wagner (2005), found that the pier shape does not affect the scour depth in the field as much as in the laboratory. The effect of variable flow directions, depth variating pier shapes and submerged debris in the field particulary reduce the effect of the pier shape on the scour depth. Neill (1978) stated that sharp-nosed piers tend to catch and accumulate debris, whereas the bow wave induced by blunt piers tends to throw debris clear.

3.4.3 Effect of angle of attack

The influence of the angle of attack has been intensively studied during the past few decades. By using a single circular pier, this effect has no influence on the scour process. Therefore a lot of hydraulic scour experiments have been carried out for single circular piers in order to reduce the number of influencing factors. Figure 3.17 shows the chart of multiplying factors developed by Laursen and Toch (1956). Neill (1978) and Ettema et al. (1998) noted that the use of these curves is not without complications, however, these curves can still be found in actual literature (Richardson and Davis, 2001; Ettema et al., 2011).

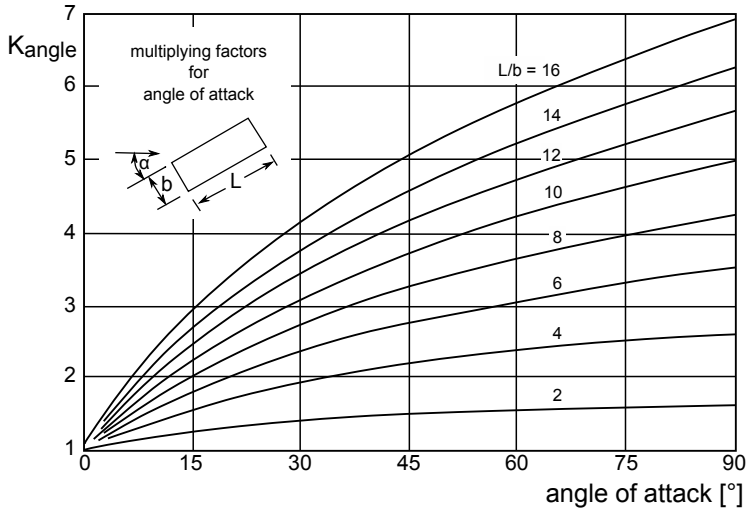

Figure 3.17: Design factors for piers not aligned with flow according to Laursen and Toch (1956).

The correction factor K_{angle} takes the angle of attack α of the flow into account and can be calculated by using Equation 3.38 and Table 3.4 (Richardson and Davis, 2001). If the ratio L/b is larger than 12, then L/b = 12 is used as a maximum value in Table 3.4 and Equation 3.38.

$$K_{angle} = \left(\cos\alpha + \frac{L}{b}\sin\alpha\right)^{0.65} \tag{3.38}$$

The values calculated for K_{angle} should only be applied when the entire length of the pier is exposed to the angle of attack of the flow. As can be seen in Table 3.4, the influence of these factors can be really important and could, in fact, produce a significant over-prediction of the scour if (a) a part of the pier is shielded from the direct flow impact due to another pier or abutment; or (b) the flow is redirected in a parallel way to the pier by another pier or abutment. For such cases the K_{angle} factor must be reduced by selecting the effective length of the pier.

Table 3.4: Correction Factor K_{angle} depending on the angle of attack of the flow (Richardson and Davis, 2001).

α	L/b= 4	L/b= 8	L/b= 12
0	1.0	1.0	1.0
15	1.5	2.0	2.5
30	2.0	2.75	3.5
45	2.3	3.3	4.3
90	2.5	3.9	5.0

α = skew angle of flow

L = length of pier [m]

b = width of the pier [m]

3.4.4 Influence of constriction

Clark et al. (1982) determine on the basis of their experimental results the limiting ratio of the flume width to pile diameter as W/D $\cong$ 5. Scour results obtained with values up to a ratio of W/D = 7 have to be treated with caution. Whitehouse (1998) recommends that the ratio of object area to flume area should be less than 1/6. Chiew and Ettema (2003) recommend a value smaller then 8 to 10 % of the flume width to neglect blockage effects. Mia and Nago (2004) note that a pier diameter greater than 10 to 12 % of the flume width would affect the flow near the pier due to the flow constriction. The primary vortex inside the scour will interfere with the reverse eddies from the wall in the same way that the interference of the surface roller will interfere with the primary vortex for shallow flows.

3.4.5 Effect of flow depth

The water depth h in relation to the pier width D have a great influence on the scour depth (Figure 3.18). With decreasing flow depth, the influence of the surface roller on the riverbed increase and damp the base vortex in front of the pier. Thus, the local scour depth is reduced for shallow flows (Melville and Sutherland, 1988; Melville and Coleman, 2000). Dietz (1972) finds that the influence of the water depth can be neglected if the ratio h/D $>$ 2 to 2.5. Breusers et al. (1977) conclude after an intensive literature and experimental data review that the influence of water depth in relation to pier width can be neglected for h/D $>$ 3. Ettema (1980) concludes that the local scour depth around piers is independent of the flow depth for values of h/D $>$ 3 and is almost independent of flow depth for h/D $>$ 1. He shows that the relationship between scour depth and water depth is a family of curves at different D/d_{50} values. Clark et al. (1982) find that the limiting condition for the depth to pile diameter

classification	ratio	dependency
narrow	$D/h < 0.7$	$d_{se} \propto D$
intermediate width	$0.7 < D/h < 5.0$	$d_{se} \propto (D\ h)^{0.5}$
wide	$D/h > 5.0$	$d_{se} \propto h$

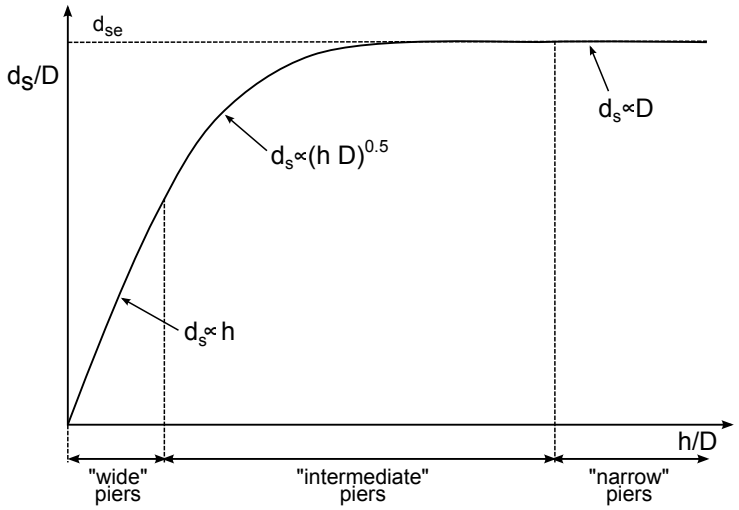

Figure 3.18: Local scour depth variation due to flow shallowness (Melville and Coleman, 2000).

ratio is $h/D > 2$. In case of smaller values, the scour mechanism and the flow pattern around the pile are disturbed. Melville and Sutherland (1988) recommend for the design purpose (Figure 3.19) that the scour depth is independent of the water depth if $h/D > 2.6$. Breusers and Raudkivi (1991) find that the finer the sediment relative to pier size, the smaller the influence of flow depth. While for fine sediments the scour depth may be almost independent of flow depth when $h/D \geq 2$, this ratio may be closer to six for relatively coarse sediments. Whitehouse (1998) recommends $h/D \geq 4$ to avoid water depth effects on the scour. Raikar and Dey (2009) analyze the influence of water depth in armor building river beds. They also find a connection between the ratio h/D and different armor grades[1] of the river bed. The water depth h for nearly uniform bed material can be neglected for $h/D > 3$, whereas in a totally armor covered river bed the water depth can be neglected for $h/D > 5$.

In contrast to the aforementioned authors, Link (2006) observes in his experiments that the scour depth is increases with decreasing water depth.

[1] see Dey and Raikar (2007b) for detailed information

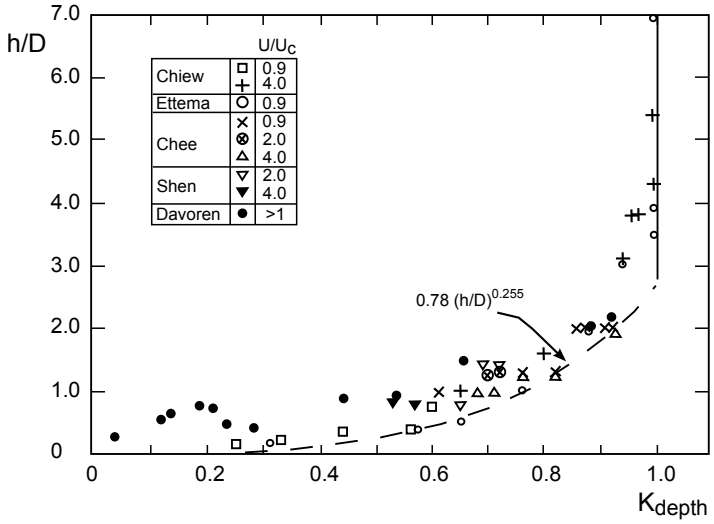

Figure 3.19: Influence of flow depth on scour depth. Data compiled by Melville and Sutherland (1988).

K_{width} is the correction factor for wide piers in shallow flows and should be applied when the ratio flow depth h to pier width D is less than 0.8 ($h/D < 0.8$) and the ratio of pier width D to the median diameter of the bed material d_{50} is greater than 50 ($D/d_{50} > 50$). Besides, the flow Froude number has to be subcritical. Flume studies as well as field observation indicate that existing equations, including the CSU-Equation, overestimate scour depth in shallow flows. Taking this issue into account, the modified CSU-Equation includes the K_{width} factor, which can be calculated by Equation 3.39 (García, 2008).

$$K_{width} = \begin{cases} 2.58 \left(\frac{h}{D}\right)^{0.34} Fr^{0.65} & \text{if} \quad \frac{U}{U_{crit}} < 1 \\ 1.0 \left(\frac{h}{D}\right)^{0.13} Fr^{0.25} & \text{if} \quad \frac{U}{U_{crit}} \geq 1 \end{cases} \tag{3.39}$$

It has to be noted that the K_{width} factor is based on limited data from flume experiments. Hence engineering judgments should use K_{width} cautiously. Due to the fact that K_{width} reduces the scour depth, engineering decisions should take into consideration the volume of traffic, the importance of the highway, the cost of a failure (potential loss of lives and dollars), and the change in cost that would occur if the K_{width} factor is used.

3.4.6 Flow intensity

A central parameter in scour research, used to describe the hydraulic forces acting on the riverbed, is the flow intensity parameter U/U_{crit}. Thus U is the mean flow velocity of the undisturbed approach flow and U_{crit} the critical mean flow velocity for the bed material with d_{50}. By summarizing the results of various investigations (Breusers et al., 1977; Ettema, 1980; Zanke, 1982b; Chiew, 1995; Melville and Coleman, 2000; Dey and Raikar, 2007b), the influence of this parameter can be obtained.

$\mathbf{\frac{U}{U_{crit}} < 0.3 - 0.5}$

No scour occurs; the approach flow velocity is not sufficient to start the erosive process at the bridge pier. In the literature, the value 0.5 U_{crit} (Zanke, 1982a) is more popular than 0.3 U_{crit} found by Chiew (1995) and Mia and Nago (2003) or 0.4 U_{crit} found by Jones and Sheppard (2000).

$\mathbf{0.5 < \frac{U}{U_{crit}} \leq 1.0}$

Clear-water scour can occur, but no riverbed material is transported from upstream into the scour zone. The scour depth increases almost linearly with U. The maximum equilibrium scour depth in a uniform material occurs.

$\mathbf{1.0 < \frac{U}{U_{crit}}}$

Live-bed scour occurs under conditions of general sediment transport. The scour depth does not further increase with U, and is fluctuating with time due to the influence of the moving bed material. Sometimes a slight decrease of d_{se} with increasing U can be observed.

Using the flow intensity parameter U/U_{crit} in physical hydraulic models can violate the Froude similarity between model and prototype because of the larger critical velocities associated with the model sediment sizes that are necessarily too large (Lee and Sturm, 2009). Simarro et al. (2007) investigate the use of the flow intensity factor in hydraulic models for pier scour experiments under clear-water conditions, and recommend adapting the flow intensity parameter to the approach flow roughness.

Unger (2006) uses $Fr_d/Fr_{d,crit}$ instead of U/U_{crit} to define the hydraulic conditions of the flow. The densimetric particle Froude number at the beginning of motion $Fr_{d,crit}$ is related to the sedimentological diameter D* and can be calculated according to Hager and Oliveto (2002) (Equation 3.40). $Fr_{d,crit}$ includes when the bed material is inside the transition area between smooth and turbulent flow conditions, the viscous influence on the beginning of particle motion, as well as the material density.

$$Fr_{d,crit} = 1.08 D^{*1/12} \left(\frac{R}{d_{50}}\right)^{1/6} \quad \text{for} \quad 10 \leq D^* \leq 150 \tag{3.40}$$

The time taken to reach the equilibrium scour depth is strongly dependent on the ratio of flow velocity to critical flow velocity. Comparisons can only be made for the same values of this ratio (Breusers and Raudkivi, 1991). The equilibrium scour depth d_{se} occurs at $U = U_{crit}$ (Melville, 1997). Consequently the equilibrium scour depth is not equal to the probably reachable maximum scour depth $d_{s,max}$, which can occur during strong floods when $U > U_{crit}$. Ballio et al. (2010) notice that clear-water scour has been most frequently considered for estimating the maximum scour depth, even though the majority of bridge failures due to scour occur during floods where a significant sediment flux is carried by the flow.

The correction factor K_{bed} results from the fact that for plane bed conditions the maximum scour may be 10 % greater than calculated. In the uncommon situation that a dune bed configuration with large dunes exists at a site during flood flow, the maximum pier scour may be 30 % greater than the calculated value. This can occur only in large rivers, such as the Mississippi. For smaller streams that have a dune bed configuration at flood flow, the dunes will be smaller and the maximum scour may be only 10 % to 20 % larger (Richardson et al., 2002). In Table 3.5 the correction factor K_{bed} is pointed out in relation to the bed condition.

Table 3.5: Increase of the equilibrium scour depth due to different bed conditions K_{bed}

bed condition	dune height H [m]	K_{bed}
clear water scour	not applicable	1.1
plane bed and antidune flow	not applicable	1.1
small dunes	$0.6 \leq H < 3$	1.1
medium dunes	$3 \leq H < 9$	1.1 to 1.2
large dunes	$9 \leq H$	1.3

3.4.7 Sediment coarseness

While realistic values of flow intensity U/U_{crit} and relative flow depth h/D usually can be reproduced in the laboratory, the relative sediment size (sediment coarseness D/d_{50}), due to limitations of laboratory flume dimensions, can not be reproduced. Experimental studies have typically been performed with values of D/d_{50} smaller than those found in field situations.

Sheppard et al. (2004) and Lee and Sturm (2009) note that this parameter can represent one of the most important differences between field and laboratory results, and that it can have a significant influence on the scour depth prediction of prototype scale structures. This might be one reason for the spread depending on which available predictors of equilibrium scour depth tend to over-predict field scour. The influence of the D/d_{50} parameter on the scouring process is still in discussion.

While the initial phase of scouring develops similarly for most values of D/d_{50}, the erosion and equilibrium phase are both affected by the ratio D/d_{50} (Breusers and Raudkivi, 1991). Ettema (1980) identifies four regions of the relative size parameter D/d_{50} in which either the development or the equilibrium scour depth diminished with increasing values of D/d_{50}.

$D/d_{50} \geq 130$

The sediment is fine in comparison with the pier width. While the down-flow impinges, the horseshoe vortex entrains sediment from the scour.

$130 < D/d_{50} \leq 30$

The sediment is of an intermediate size. The zone of sediment entrainment is limited to a groove formed around the upstream part of the pier by the impinging downflow.

$30 < D/d_{50} \leq 8$

The sediment is coarse, which is relative to the pier width. The roughness of the bed surface inside the scour causes a reduction in the equilibrium scour depth.

$D/d_{50} < 8$

The sediment is very coarse in comparison to the pier width. The principal erosion phase does not occur. The erosion mainly occurs due to the acceleration of the flow at the sides of the pier.

According to Ettema (1980), Breusers and Raudkivi (1991), Melville and Chiew (1999) and Melville and Coleman (2000), the maximum scour depth for clear-water scour is unaffected by particle size, as long as the value of D/d_{50} is larger than 25. Melville and Chiew (1999) put this limit at 50.

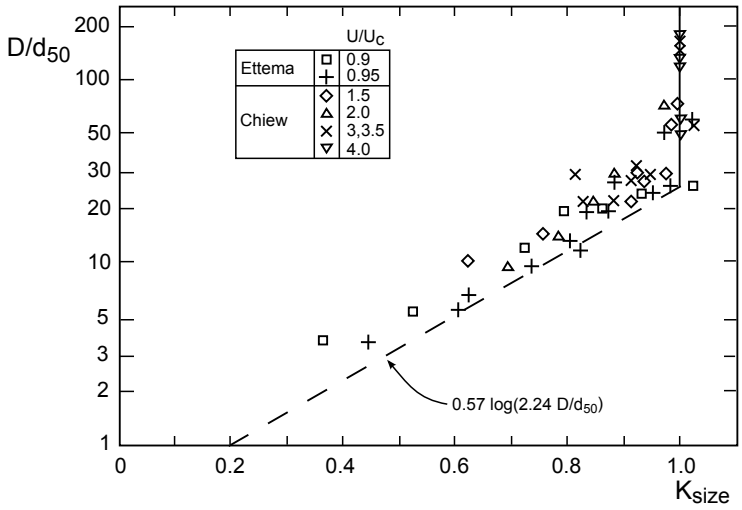

Figure 3.20: Influence of sediment coarseness on scour depth. Data compiled by Melville and Sutherland (1988).

The correction factor K_{size} (Equation 3.41) is recommended by Melville and Sutherland (1988) for different D/d_{50}.

$$K_{size} = \begin{cases} 1 & \text{if} \quad \frac{D}{d_{50}} > 25 \\ 0.57 \log\left(2.24 \frac{D}{d_{50}}\right) & \text{if} \quad \frac{D}{d_{50}} < 25 \end{cases} \tag{3.41}$$

Chiew (1984) (cited in Baker (1986)) observed that the effect of the size of the pier in relation to the sediment decreases with increasing velocity

However, Sheppard et al. (2004) found that d_{se}/D may decrease for large values D/d_{50}. He finds that the dependence of d_{se}/D on D/d_{50} decrease with increasing values of D/d_{50} beyond $D/d_{50} \sim 45$. In his experiments, Sheppard et al. (2004) variate the D/d_{50}-range from 143 to 4155. By the wide variation of different pier diameters in the laboratory and especially in the prototype structures, this relation can have a significant influence on the scour depth prediction for prototype scale structures (Sheppard et al., 2004; Lee and Sturm, 2009; Lança et al., 2011).

Lança et al. (2011) note that further research is needed to characterize the influence of D/d_{50} on the equilibrium scour depth for values of $D/d_{50} > 100$.

3.4.8 Effect of bed material density

Lightweight materials can be used in hydraulic models. For example, when the experimental grain size becomes very fine due to the geometrical scaling factor. Therefore, several researchers investigate the properties of lightweight sediments for hydraulic experiments. Besides the work of Shields (1936), several authors study the beginning of motion, including lightweight material (Eustis, 1936; Hager and Oliveto, 2002).

Besides the experiments concerning the initiation of motion, different authors also used lightweight material for their pier scour experiments (Dietz, 1972; Clark et al., 1982; Franzetti et al., 1982; Zanke, 1982b; Oliveto and Hager, 2002; Yu et al., 2003; Saunders, 2004; Radice et al., 2009). Neill (1978) recommends using low-density material in laboratory experiments, in order to reproduce sediment suspension, whilst preserving sufficient grain roughness.

Breusers et al. (1977) conclude, based on the studies of Nicollet and Ramette (1971) and Dietz (1972), that the density influences the maximum scour depth. A tendency for scour depth to increase with decreasing bed material density for identical U/U_{crit} can be observed in these experiments (Figure 3.21). The use of low material densities in model experiments seems to be possible in cases where reproduction of the Froude number is necessary.

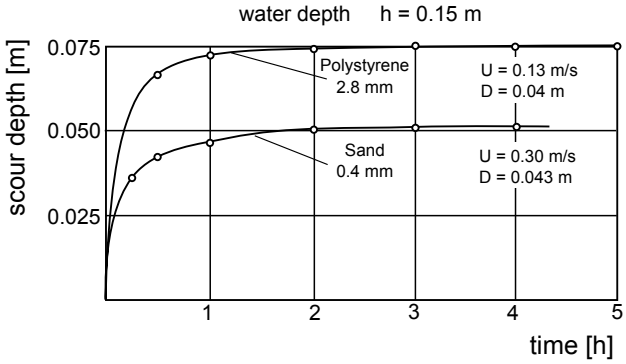

Figure 3.21: Comparison of scour depth development for Sand and Polystyrene (Dietz, 1972).

Clark et al. (1982) find that when using lightweight material in physical models (for example bakelite), in clear-water scour experiments, the flow velocity is possibly too low for a turbulent structure and a horseshoe vortex to develop. In contrast, Saunders (2004) observes that even at a lower experimental flow, velocities adopted for clear water scour over a bakelite bed, the horseshoe vortex does exist. Raudkivi (1998) notes that lightweight particles in a laboratory flume induce deeper scour depth because of the high turbulences in the interface and wake region. As a result the bed is lowered at the rear of the pier, which in turn eases the removal of material from the front of the pier. Yu et al. (2003) evaluate four bridge scour equations (Modified 65-1 Equation, Gao-Equation, Melville-Equation 1997, HEC-18 Equation)

comparing them with the experimental data of lightweight experiments. They found that none of the methods are applicable for experiments with lightweight bed material because the effect of density is mainly, but not sufficiently, considered in these equations. Ettmer (2004) investigates the influence of lightweight sediment on scour behind a sliding lock-gate. He successfully scaled natural sediment into lightweight material using the sedimentological diameter D*.

Nevertheless, little data can be found regarding the use of lightweight material in hydraulic pier scour models, and a detailed description of the effects is often missing. Saunders (2004) identifies scale effects which arise from using lightweight material as a model bed material. In scour experiments with a round pier using lightweight material, it is seen that scour depths from the model will be less than in the prototype and that, where scarping is seen to occur in the model, scour extents in these areas will be less than in the prototype.

3.4.9 Effect of grain size distribution

Nicollet and Ramette (1971) were two of the first to investigate the influence of sediment grain size distribution on the local scour depth at cylindrical piers. A test series with uniform material (sand a, b, c), as well as a sediment mixture were conducted with the same hydraulic conditions and the same pier. The bed material was a mixture of 33 % of the previously used uniform sands, giving a rather straight grading curve of between 0.8 mm and 3.2 mm. Figure 3.22 illustrates the results of these experiments. Nicollet and Ramette (1971) found that the maximum scour of the mixture occurs in the vicinity of the critical flow velocity of the middle grain size, and that the depth is about 25 % less than those taken out with uniform material. Furthermore, the scour depth for the experiment with sediment nourishment is less compared to the clear-water scour depth.

The influence of sediment gradation on pier scour for clear-water conditions has been investigated by several authors (Ettema, 1976; Dey and Raikar, 2007b; Raikar and Dey, 2009). The basic observations are that there is a dramatical reduction of scour depth with increasing non-uniformity σ due to the formation of an armor layer. A further finding was that in the vicinity of $\sigma = 1.5$, the scour behavior for ripple-forming sediments differs from non-ripple-forming sediments. The results are plotted in Figure 3.23.

The reason for the scour depth reduction is the presence of an armor layer on the approach bed as well as inside the scour hole. Baker (1986) found that for live bed conditions, at high flow velocities ($U/U_{crit} > 4$), scour depth becomes almost independent of σ. The results of Baker (1986) are replotted by Melville and Coleman (2000). Figure 3.24 shows the development of the local scour depth for an increasing flow intensity and increasing non-uniformity..

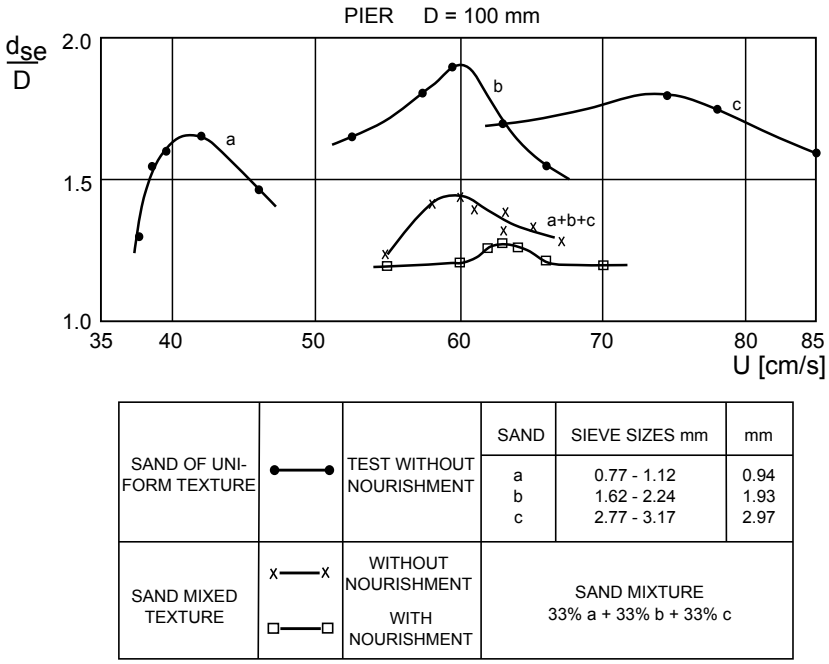

Figure 3.22: Relative scour depth d_{se}/D as a function of undisturbed approach velocity for different particle sizes and the mixture of the different sizes according to Nicollet and Ramette (1971).

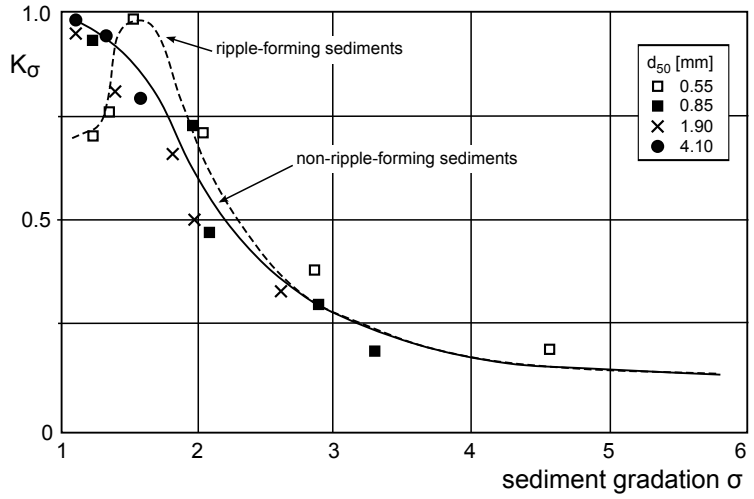

Figure 3.23: Influence of sediment gradation on the maximum scour depth in clear water conditions according to Ettema (1976).

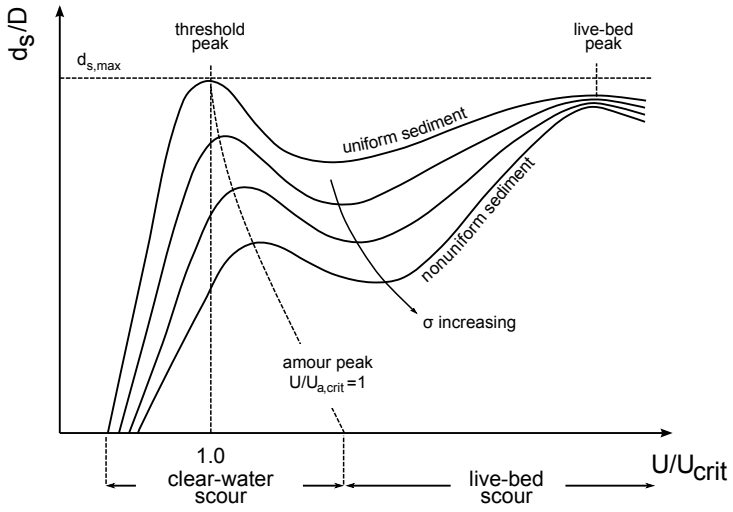

Figure 3.24: Local scour depth variation with flow intensity and increasing non-uniformity Melville and Coleman (2000).

If the sediment tends to build an armor layer (non-uniform material $\sigma > 1.3$), live-bed scour occurs when $U/U_a > 1.0$, in which U_a marks the transition velocity between clear-water and live-bed conditions for non-uniform sediments and is equivalent to U_{crit} used for uniform sediments.

To calculate the armor peak velocity U_a, the knowledge of the largest grain sizes in the non-uniform sediment is required. In practice, d_{90} can be used instead of d_{max} which is unlikely to be known. In such a case, $d_{50,a} = d_{max}/1.8$ can be used to calculate the critical velocity for the armor sediment $U_{crit,a}$, when knowing $U_{crit,a}$ the armor peak velocity is $U_a = 0.8\ U_{crit,a}$ (Melville and Coleman, 2000).

K_{armor} is the correction factor for armoring of the bed material size recommended by Müller and Jones (1999). For bed materials that have a d_{50} equal or larger than 2.0 mm and d_{95} equal to or larger than 20 mm, the scour depth decreases and K_{armor} should be calculated by Equation 3.42. If the sediment d_{50} is smaller than 2.0 mm and d_{95} smaller than 20 mm $K_{armor} = 1$. The minimum value of K_{armor} is 0.4 and it should only be used if $U < U_{ic,d_{50}}$.

$$K_{armor} = \begin{cases} 1.0 & \text{if} \quad d_{50} < 2\text{mm} \quad \text{and} \quad d_{95} < 20\text{mm} \\ 0.4\ U_R^{0.15} & \text{if} \quad d_{50} \geq 2\text{mm} \quad \text{and} \quad d_{95} \geq 20\text{mm} \end{cases} \tag{3.42}$$

with

$$U_R = \frac{U - U_{ic,d_{50}}}{U_{c,d_{50}} - U_{ic,d_{95}}} > 0$$
$$U_{ic,d_x} = 0.645 \left(\frac{d_x}{D}\right)^{0.053} U_{c,d_x}$$
$$U_{c,d_x} = K_u h^{(1/6)} d_x^{(1/3)}$$

where:

U_{ic,d_x} = flow velocity required to initiate scour at the pier for the grain size d_x [m/s]
U_{c,d_x} = critical velocity for incipient motion for the grain size d_x [m/s]
D = pier width [m]
d_x = grain size for which x% of the bed material is finer [m]
U = velocity of the approach flow just upstream of the pier [m/s]
h = average depth of flow upstream of the bridge, excluding local scour [m]
K_u = 11.17 (English units)[1]

In the actual review of scour research carried out by Ettema et al. (2011), the authors mentioned that the effects of sediment non-uniformity are mostly accounted for in the flow intensity factor U/U_{crit}.

3.4.10 Influence of the wash load on the equilibrium scour depth

Sheppard et al. (2004) observe that there seems to be a high sensitivity of equilibrium scour depth due to the suspended fine sediment concentration in the flow. They note that this might help to explain the scatter in the published data and also help to explain why laboratory data often result in an over prediction of clear water scour depth observed in the field. The probably high influence of the sediment concentration can be seen in Figure 3.25, where Experiment A and Experiment B (and the adapted Experiment B) are plotted. Experiment A and B have nearly the same flow condition ($D = 0.914\,m$, $D_{50} = 0.22\,mm$, $h_A = 1.20\,m$, $h_B = 1.80\,m$, $U = 0.30\,m\,s^{-1}$, $U_{crit} = 0.32\,m\,s^{-1}$), and only the water depth in experiment B was 0.60 m higher than in Experiment A. In the Experiment $B_{adjusted}$-plot, the data from Experiment B have been adjusted to the water depth and flow velocity of Experiment A using Sheppard's-Equation. The noticeable difference between Experiment A and B is the sudden increase of turbidity after 10 h in experiment A, and thus the noticeable reduction in scour depth development, which was, up to this moment, similar to Experiment B.

Sheppard et al. (2004) suspect that scour depth reduction is due to the suspended fine sediment induced reduction in bed shear stress reported by researchers working in the field of drag reduction. Additional observation concerning the influence of wash load on the scour process is not known.

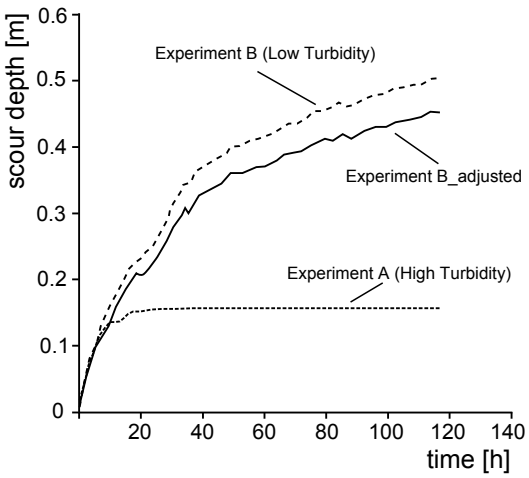

Figure 3.25: Scour depth development affected by high sediment concentration in comparison to scour development by low sediment concentration according to Sheppard et al. (2004).

3.4.11 Time effect

Due to the fact that the equilibrium clear-water scour depth d_{se} is reached asymptotically with time, it can take a very long (perhaps infinite) time for the equilibrium scour hole to form (Melville and Chiew, 1999). Before reaching the equilibrium scour depth, the depth of scour depends, especially at the beginning, on the time. That means, if scour experiments are stopped too early, the maximum depth is not reached. Franzetti et al. (1982) noted that data for scour experiments found in literature have to be critically reviewed (in regards to the testing time) because the duration of experimental tests is often from 2 to 8 hours. Melville and Chiew (1999) note that data obtained after lesser times (10 to 12 h), can exhibit scour depths of less than 50 % of the equilibrium depth. However, due to the decreasing scour rate within this time, it is very hard to identify the equilibrium scour depth and the time t_e at which the equilibrium scour depth is reached. Figure 3.26 shows this problem.

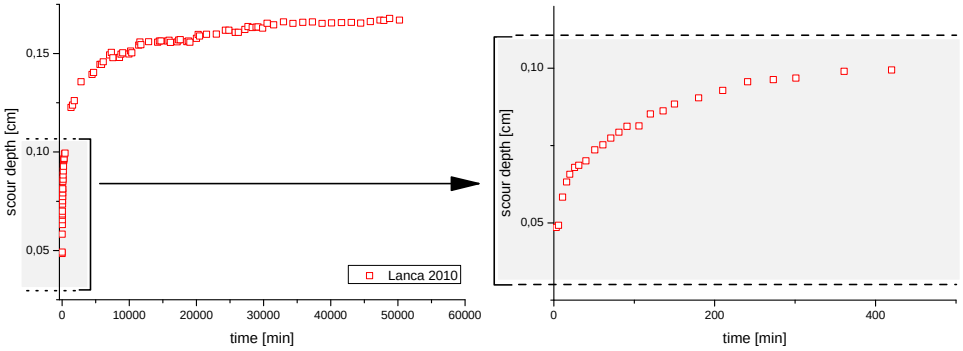

Figure 3.26: Comparison of the scour depth for the same experiment after different time steps, data taken from Lança et al. (2010). Left hand side 50 253 min (837.5 h); Right hand side 420 min (7.0 h)

Melville and Chiew (1999) define equilibrium scour as a depth at which the increase in scour depth is less than 5 % of the pier diameter D in 24 h (Equation 3.43). Grimaldi et al. (2009) characterize the equilibrium scour when the increase in scour depth is less than 5 % of D/3 in 24 h.

$$\delta d_{s,24} \leq \frac{0.05D}{24h} \tag{3.43}$$

Melville and Chiew (1999) analyze the influence of different parameters in determining the time t_e for the development of d_{se} for a given pier, sediment, and approach flow velocity. They confirm, that because t_e and d_{se} are inherently interdependent, both should have similar dependence on the same set of parameters. For example, t_e should depend on flow shallowness for low values of h/D, but becomes independent for high values of h/D (narrow piers).

The apparent limit to the influence of flow shallowness on the equilibrium time scale t* (t* = U t_e/D) occurs at h/D $\geq$ 6, although there is a minimal effect of flow shallowness for h/D $\geq$ 3. The limit to sediment coarseness influences on t* occurs at D/d_{50} $\approx$ 100. For clear-water scour conditions, the relation between the equilibrium time scale and the flow intensity is similar to that of equilibrium scour depth. The equilibrium time scale t* increases rapidly with the flow intensity 0.4 < U/U_{crit} > 1 for clear-water conditions and also attains the maximum value at the threshold condition U/U_{crit} = 1. For higher values (live-bed conditions) t* is expected to decrease rapidly.

Melville and Chiew (1999) developed the Equation 3.44 to estimate the time that is needed to reach the equilibrium scour depth, depending on the ratio h/D.

$$t_e = \begin{cases} 48.26 \frac{D}{U} \left(\frac{U}{U_{crit}} - 0.4 \right) & \text{[days]} \quad \text{if} \quad \frac{h}{D} > 6 \\ 30.89 \frac{D}{U} \left(\frac{U}{U_{crit}} - 0.4 \right) \left(\frac{h}{D} \right)^{0.25} & \text{[days]} \quad \text{if} \quad \frac{h}{D} \leq 6 \end{cases} \tag{3.44}$$

Simarro et al. (2011) analyze six long-lasting experiments and come to the conclusion that adequate equilibrium scour depth can only be provided as long as the experiments last for at least 1-2 weeks. For shorter experiments, there seems not to be any possibility of guaranteeing that the equilibrium scour depth can be obtained by extrapolation. They find that the equilibrium-criteria (Equation 3.43) is not reliable.

3.5 Results of literature

The bridge scour process in general is a well known process and much research has been done on it during the last few decades, starting in the middle of the last century. Consequently, many studies have been published concerning scour depth development. The main results of this research is summarized in the preceding chapter concerning the hydraulics around the pier and the parameters that influence the scour depth.

Recently, the focus was put more and more on the development of numerical models and, due to better measurement equipment, on detailed vortex development and visualization, for example Unger (2006). Despite this, the combination of physical processes that are responsible for the scour development are still not identified in an adequate way. Complex pier structures and foundations still have to be carried out by using physical hydraulic models (Ettema et al., 2011), which in themselves have strong application limits.

3.5.1 Need for research

Physical models are often geometrically downscaled from the prototype size to the model size. The subsequent transfer and interpretation of the results taken from the model back to the prototype is a central task in hydraulic modeling. In general, hydraulic models that are dealing with sediment transport have the problem that the prototype sediment is often not geometrically scalable in a proper way due to the change in properties when cohesive forces appear for small grain sizes. Some authors give the critical diameter d_{50} for sediment used in pier scour experiments to 0.5 mm (Clark et al., 1982), 0.8 mm (Unger, 2006) or 1.5 mm (Novák, 2010). For this reason, physical bridge pier models often are not scalable without geometric and hydraulic distortions. That means that the sediment grain size, and therefore the associated flow velocity, is no longer scaled correctly and therefore the interpretation of the results requires a high degree of experience.

In connection with the previously mentioned point, the ratio pier width in relation to the sediment diameter D/d_{50} cannot, in general, be scaled in a proper way. A growing number of recent studies (Sheppard et al., 2004; Lee and Sturm, 2009; Lança et al., 2011) show a great effect of these parameter that differs from previous studies and former assumptions (Melville and Sutherland, 1988; Breusers and Raudkivi, 1991; Melville and Coleman, 2000).

An additional task of importance is to define the hydraulic condition for which the maximum scour depths occur. In literature this is mainly the equilibrium scour depth under clear water conditions for uniform material. This refers to the time when the scour depth stops increasing, and no more material is transported from upstream into the scour. Often scour experiments last (1) only a couple of hours while long term model experiments also show that, after several days, the scour depth is still increasing and (2) the experiments are often run under simplified

boundary conditions (uniform flow, uniform grain size, ...). Contrastingly, the scour process at the prototype stage (1) can last much longer than the experimental time in the laboratory and (2) the boundary conditions often change during flood events (live-bed conditions, debris accumulation at the pier, change of flow direction, wash load concentration, ...). Therefore scour results taken from literature and experiments, which are declared to be the maximum (equilibrium) scour, must be used cautiously.

It is known that it is not possible for hydraulic physical scour models to represent the prototype condition, but that instead they are an important tool for identifying the basic physical processes and combination that can lead to the maximum scour. Until now, it has been more or less the only way to measure and visualize the scour process because in-situ prototype measurements, especially during flood events, are infrequent due to the sophisticated and often dangerous measurement procedure.

3.5.2 Goal of research

In the aforementioned subsection, it becomes clear that hydraulic models still are an important tool for the scour depth estimation. The fact that, for a single cylindrical pier in uniform sediment, the influence of most parameters concerning the scour depth seem to be quite clear, leads this thesis to take a closer look at the influence of material density on the scour process. The results of this thesis should help to improve hydraulic scour models.

While the substitution of natural sediment by artificial lightweight material is a well known technique in hydraulic bed-load modelling with several advantages, only few clearly defined pier scour experiments were carried out with this kind of material. Moreover, in these studies accurate information about the reasons for the application and its scalability often are missing.

The focus of this thesis is the influence of lightweight material in physical pier scour models with the aim of finding substitution criteria to substitute natural sediment with artificial lightweight granular. Existing theories for the replacement of natural sediments with artificial granulates will be further developed and validated so that the relevant processes can be better simulated in laboratory studies. The following aspects are part of the work.

- Extensive laboratory test with the focus on the influence of different material densities ρ on the local bridge pier scour process.
- Influence of the material density on the time t_e which is necessary to achieve the equilibrium scour depth d_{se} .
- Description and interpretation of the influence of D/d_{50} in combination with lightweight material on the scour process.

4 Dimensional analysis

It may be argued that scour measurements around prototype bridge piers would be the best way to investigate the scour process. However, the cost limitations in time and money rules out such an approach. Therefore, a hydraulic physical model is the precision device of choice for the experimental investigation of a hydro-mechanical phenomenon and can give reliable information if its scale is determined correctly according to certain rules (Yalin, 1971; Hughes, 1993; Novák, 2010).

The initial part of starting physical models is the selection of the physical variables which may have a dominant effect on the process. This step is called **dimensional analysis**. Dimensional analysis is a fundamental step before physical experiments can begin. It helps to optimize the experimental setup to get the maximum information with a minimal amount of time and effort (Kobus, 1974).

4.1 Important variables influencing the bridge pier scour

Many researchers use the physical modeling approach to investigate different aspects of the scour process. A major interest in scour research is the interaction of the fluid (flow) with the sediment of the river bed (sediment) caused by the vortices building up around the solid structure (object) and time. The most important variables are summarized in Table 4.1.

Equation 4.1 brings together the findings of an extensive literature review (Ettema et al., 2011). Thus, the functional relation between local scour depth d_s and the relevant variables (Table 4.1) can be stated as

$$d_s = f\left[\text{flow}(\rho, \nu, U, h, g), \text{sediment}(d_{50}, \sigma, \rho_s, U_{crit}), \text{object}(D, F, \alpha), \text{time}(t)\right] \tag{4.1}$$

Sometimes it is useful to take the shear stress velocity u_* instead of the depth averaged velocity U. The shear stress velocity u_* relates to the depth averaged velocity U, as $U = u_* (8/f)^{0.5}$, where f = function (d_{ch}/h) is the Darcy-Weisbach resistance coefficient for fully developed turbulent flow. With this relationship the critical bed shear stress velocity for the beginning of sediment motion $u_{*,crit}$ can also be expressed in terms of the critical mean approach flow velocity for entrainment of bed sediment, U_{crit}. Thus, in Equation 4.1, U and U_{crit} could be replaced with u_* and $u_{*,crit}$. However, the use of U instead of u_* provides greater clarity in

Table 4.1: Important parameter for the pier scour process.

symbol	dimension	unit	description
d_s	m	L	scour depth
D	m	L	pier diameter
h	m	L	water depth
d_{50}	m	L	sediment size
ρ	$kg\,m^{-3}$	$M\,L^{-3}$	fluid density
ρ_s	$kg\,m^{-3}$	$M\,L^{-3}$	sediment density
ν	$m^2\,s^{-1}$	$L^2\,T^{-1}$	kinematic viscosity
t	s	T	time
g	$m\,s^{-2}$	$L\,T^{-2}$	gravity
U	$m\,s^{-1}$	$L\,T^{-1}$	flow velocity
U_{crit}	$m\,s^{-1}$	$L\,T^{-1}$	critical flow velocity
F	–	–	pier form shape
σ	–	–	grain size distribution
α	–	–	flow angle relative to the pier alignment

describing the relationship between the flow field around the pier and the scour depth (Ettema et al., 2011).

Using the Π-Theorem, developed by Buckingham (1914), the functional dependence with n dimensional parameters can be reduced by the number of fundamental physical units. In this case there are three, the mass [M], the length [L] and the time [T].

Thus, the dimensional functional dependence with 14 variables (Equation 4.1) turns into a non-dimensional functional dependence (Equation 4.2) with 11 parameters:

$$\frac{d_s}{D} = f\left(\frac{h}{D}, \frac{D}{d_{50}}, \frac{U}{U_{crit}}, \frac{\rho_s - \rho}{\rho}, \frac{U}{\sqrt{\rho' g d}}, \frac{UD}{\nu}, \frac{Ut_e}{D}, F, \alpha, \sigma\right) \tag{4.2}$$

Equation 4.2 can be simplified using the relative density under buoyancy ρ', the densimetric Froude number Fr_d, the pier Reynolds number Re_{pier} and the equilibrium time scale t*.

$$\frac{d_s}{D} = f\left(\frac{h}{D}, \frac{D}{d_{50}}, \frac{U}{U_{crit}}, \rho', Fr_d, Re_{pier}, t*, F, \alpha, \sigma\right) \tag{4.3}$$

It must be pointed out that some variables appear in several parameters, and complicate the parameter framework. In particular the pier diameter D appears in several of the parameters influencing the pier flow field; (1) the relative flow depth h/D of the flow field; (2) the sediment coarseness D/d_{50} of the scour hole base, and the possibility of bedforms developing in a sufficiently large scour hole; (3) the pier Reynolds number Re_{pier} and therefore the intensity

of circulation in the pier flow field; (4) the variation of the effective pier shape and, (5) the equilibrium time scale, (t U)/D.

In the following, a short explanation of the parameters influencing the dimensionless sour depth d_s/D (Equation 4.2) is given.

The **relative flow depth** h/D, indicates the geometric scale of the pier flow field. A detailed description of the influence of this parameter can be found in Section 3.4.5.

The **relative sediment size** (or sediment coarseness D/d_{50}) relates the length scales of pier width to the median diameter of bed particle. The influence of this parameter is described in Section 3.4.7.

The **flow intensity parameter** U/U_{crit} expresses the extent or stage of sediment transport on the river/sediment bed (Section 3.4.6). While the approach flow velocity U can change depending on the boundary conditions (unsteady flow) the critical flow velocity U_{crit} remains in dependence of the respective sediment constant. This parameter distinguishes whether clear-water ($U/U_{crit} \leq 1$) or live-bed ($U/U_{crit} > 1$) scour occur.

The **relative density** under buoyancy ρ' (Equation 4.4) takes the different densities between the fluid and the sediment into account, thereby also accounts for the inertia of the submerged sediment grains. Often it is assumed that it is sufficient to include the relative density ρ' in the densimetric Froude number Fr_d or the critical flow velocity U_{crit}. Different studies (Bonnefille, 1963; Dietz, 1969; van Rijn, 1984) come to the conclusion, that the influence of ρ' is better taken into account by the sedimentological diameter D*.

$$\rho' = \frac{\rho_s - \rho}{\rho} \tag{4.4}$$

where ρ_s [kg m^{-3}] is the material density and ρ [kg m^{-3}] the density of the fluid. The influence of this parameter is described in Section 3.4.8.

The **sedimentological diameter** D* is a dimensionless parameter which can be calculated by Equation 4.5. This parameter is independent from the hydraulic boundary conditions and includes only material properties like the relative density under buoyancy ρ' [1], the gravity acceleration g [m s^{-2}], the kinematic viscosity of the fluid ν [m^2 s^{-1}] and the characteristic sediment diameter d_{ch} [m].

$$D^* = \sqrt[3]{\frac{Re^{*2}}{Fr^*}} = \sqrt[3]{\frac{\frac{u_*^2\, d_{ch}^2}{\nu^2}}{\frac{u_*^2}{\rho'\, g\, d_{ch}}}} = \sqrt[3]{\frac{\rho'\, g\, d_{ch}^3}{\nu^2}} = \left(\frac{\rho'\, g}{\nu^2}\right)^{\frac{1}{3}}\, d_{ch} \tag{4.5}$$

Sediments with the same sedimentological diameter D* are 'moving' on the same line as can be seen in Figure 4.1. This means that theoretically they should have a similar

sediment behavior (e.g. motion and no motion, dunes) for the same grain Reynolds number as well as the same Shields parameter.

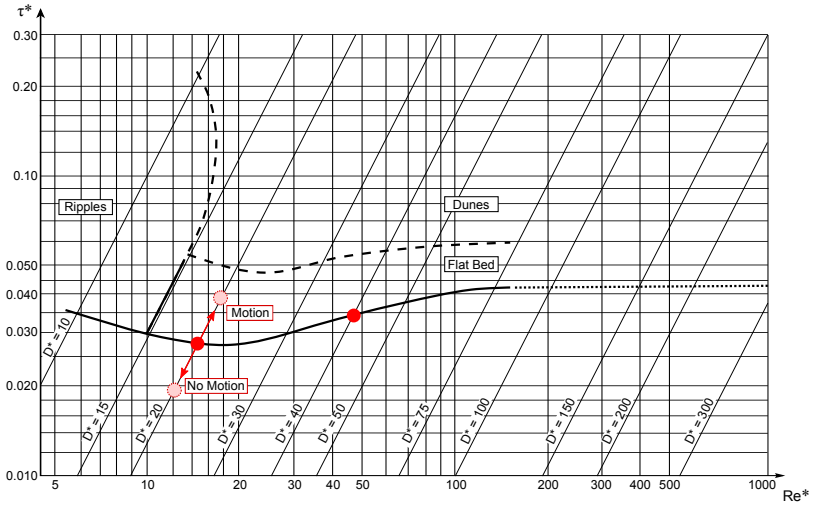

Figure 4.1: Bedform characteristics depending on sedimentological diameter D* according to García (2008).

The **densimetric Froude number** $\mathrm{Fr_d}$ is the ratio of the impact forces of the water flow and the resistant forces of the grain among buoyancy (Equation 4.6). This parameter includes the relative sediment density and, in contrast to the sedimentological diameter, also the hydraulic impact represented by the approach flow velocity U.

$$Fr_d = \frac{U}{\sqrt{\rho' \; g \; d_{ch}}} \tag{4.6}$$

where U is the flow velocity [$\mathrm{m\,s^{-1}}$], rho' the relative density [1], g the gravity acceleration [$\mathrm{m\,s^{-2}}$] and $\mathrm{d_{ch}}$ the characteristic grain size of the sediment [m].

The **pier Reynolds number** $\mathrm{Re_{pier}}$ takes the viscous effect into account (Equation 4.7). However, viscous effects are unlikely to have an effect on the scour depth at the pier because fully turbulent flow occurs around bridge piers.

$$Re_{pier} = \frac{U \; D}{\nu} \tag{4.7}$$

where U is the flow velocity [$\mathrm{m\,s^{-1}}$], D the pier diameter [m] and ν the kinematic viscosity [$\mathrm{m^2\,s^{-1}}$].

The **equilibrium time scale** t* relates scour duration to pier width D, and approach velocity U (4.8). Many studies focus on the time-development of scour at piers of simple cylindrical form (Section 3.4.11).

$$t* = \frac{U \; t_e}{D} \tag{4.8}$$

where U is the flow velocity [$m\,s^{-1}$], t_e the time [s] to reach the equilibrium scour depth and D the pier diameter [m].

The **pier shape** F has a significant influence on the scour depth, which is described in Section 3.4.2. Neill (1978) as well as Müller and Wagner (2005) found that the pier shape does not affect the scour depth in the field as much as in the laboratory.

The influence of the **angle of attack** α has been intensively studied during the last decades. When using a single circular pier, this effect has no influence on the scour process (Section 3.4.3).

The **geometric standard deviation** σ of the sediment characterizes the uniformity of the sediment (Section 3.4.9). In the review of scour research carried out by Ettema et al. (2011), the authors mention that the effects of sediment non-uniformity are mostly accounted for in the flow intensity factor U/U_{crit}.

$$\sigma = \sqrt{\frac{d_{84}}{d_{16}}} \qquad [1] \tag{4.9}$$

4.2 Reduction of important parameters for the experiments

The determination of the relationship of all parameters of the scour process is virtually impossible. For this reason, Equation 4.3 can be simplified by excluding already known factors or variables with little impact.

The focus of this work is the substitution of natural sediment in hydraulic models with lightweight material, and to investigate the influence of ρ' on the scour process. On behalf of the relative density ρ', the sedimentological diameter D^* and the densimetric Froude number Fr_d were chosen, both containing in particular the sediment density.

For this reason the experiments were carried out **without** scaling the geometry. This means that the bridge pier D, as well as the water depth h (as two of the major parameters that influence the scour depth) were kept constant during the experiments, and only the sediment was changed. Therefore, the important parameter h/D in Equation 4.3 can be ignored in the following experiments.

Because of the different densities and grain sizes, the critical flow velocity U_{crit} for each material is different and was determined in the preliminary experiments (Section 5.3). With this information it was possible to set up the flume discharge so that the flow intensity was of the same value in all of the experiments ($U/U_{crit} = 1$). Therefore, the important parameter U/U_{crit} in Equation 4.3 can be removed.

In every experiment the same cylindric pier was used, meaning that the pier shape F, as well as the pier alignment α and the diameter D, can all be ignored. In addition, only uniform

sediment ($\sigma \leq 1.3$) was used in the experiments, in order to exclude effects of the grain size distribution.

The flow Reynolds number $\mathrm{Re}_{\mathrm{flow}}$ (Equation 4.10) is the ratio of inertial forces to viscous forces. Consequently, it quantifies the relative importance of these two types of forces for given flow conditions. The flow Reynolds number distinguishes the flow as either turbulent $\mathrm{Re}_{\mathrm{flow}} > 2300$ or laminar $\mathrm{Re}_{\mathrm{flow}} < 2300$ flows (Sigloch, 2008).

$$Re_{flow} = \frac{U\ R}{\nu} \tag{4.10}$$

where U [$\mathrm{m\,s^{-1}}$] is the mean velocity, R [m] the hydraulic radius and ν [$\mathrm{m^2\,s^{-1}}$] the kinematic viscosity. The flow condition for all of the experiments is assumed to be turbulent with the flow Reynolds number $\mathrm{Re}_{\mathrm{flow}}$ between 7800 to 46 000.

The drag coefficient of an obstacle depends on the Reynolds number of the obstacle, therefore depending directly on both the flow velocity and the obstacle diameter. The Wieselsberger diagram (Figure 4.2) shows that, for the experiments carried out in this thesis, the drag coefficient is fairly similar for pier Reynolds numbers between 10^3 to 10^4. The influence of the pier Reynolds number $\mathrm{Re}_{\mathrm{pier}}$ is consequently disregarded in the following experiments.

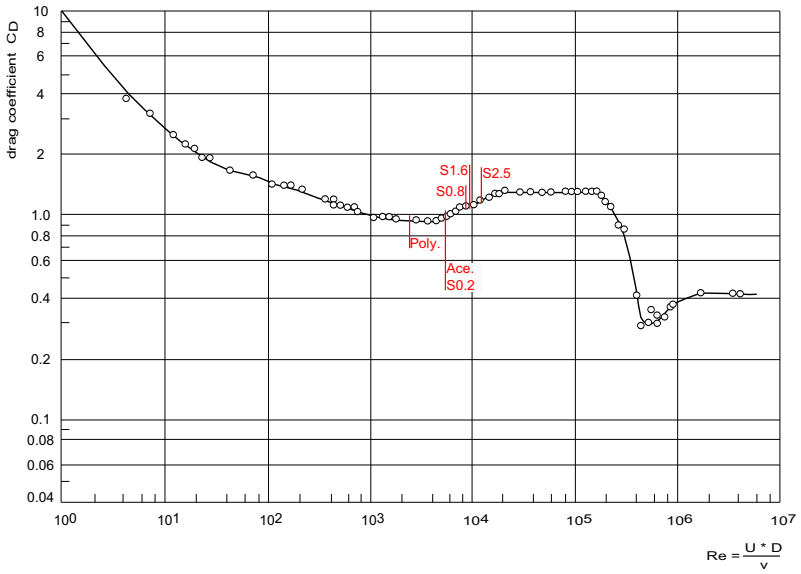

Figure 4.2: Drag coefficient of a circular cylinder versus pier Reynolds number due to Wieselsberger (Schlichting et al., 2006).

4.3 Result of the parameter reduction

Taking into account the results of the literature review (Section 3.5) and the dimensional analysis, the aim of the experiments is focused on the following parameters (Equation 4.11).

$$\frac{d_s}{D} = f\left(D*, Fr_d, \frac{D}{d_{50}}, t*\right) \tag{4.11}$$

With regard to the substitution of natural sediments by artificial lightweight material, the influence of the relative sediment density ρ' on the pier scour process is of central importance for this work. This is particularly the case in terms of the scour depth d_s and the time t* which is needed to reach the equilibrium scour depth. Instead of the relative density ρ', the sedimentological diameter D* and Fr_d were chosen, which both include the relative density.

The review of the sedimentological diameter D* as a transfer criterion for lightweight material (see Section 3.1 or the work carried out by Ettmer (2004)) leads inevitably to a change in the sediment coarseness D/d_{50}. As far as the author knows, there is no information on this parameter in combination with the use of lightweight materials, and, for this reason, this parameter is included in the following experiments.

Due to the change in the sediment density ρ the approach flow velocity U for the various materials is different as well, so as to keep the flow intensity constant ($U/U_{crit} = 1$). The densimetric Froude number Fr_d describes the relation of the impact forces of the approach flow to the resistant forces of the grain among's buoyancy. The parameter thus contains both the approach flow velocity U, as well as the relative sediment density ρ' and the grain size d_{50}. Therefore, Fr_d is tested in the following experiments regarding the influence on the scour depth development.

It must be noted that, practically, it is not possible to check the influence of all of the parameters given in Equation 4.11. Overall, m^n-tests are essential in adequately determining the influence of each parameter (m = number of experiments, n = number of variables) (Aberle and Mertens, 2006). Assuming that 6 tests are sufficient to determine the influence of a single parameter, $6^4 = 1296$ tests would be necessary to achieve an adequate solution for this current case.

Thus, in the following work, exemplary experiments are chosen to describe the general effect of the parameters.

5 Experiments

The following chapter describes the experiments that are carried out during this work. Initially, the laboratory equipment and the measuring technique are described. Afterwards, a description and characterization of the sediments, and a review of the characteristic parameters is given. This is followed by an explanation of the experimental procedure. The chapter concludes with a brief description of some additional tests carried out in a larger channel at the University of Applied Sciences Magdeburg-Stendal.

The aim of the laboratory tests was to measure the local scour depth development around bridge piers for different sediments. The fundamental differences between the tests were the sediment size and density, while the experimental set up was geometrically the same for all of the experiments. Clark et al. (1982) found that, in the case of a lighter sediment, a distortion of the relative roughness of the flow is permissible.

5.1 Test facility

5.1.1 The flume

The experiments were carried out in a 8.0 m long, 0.3 m wide and 0.6 m deep horizontal, non-tilting flume with smooth side walls. In order to keep the amount of sediment low, which was needed for the sediment layer inside the flume, a false floor with a 0.12 m deep and 1.2 m long recess, starting 4.5 m downstream of the inlet was created. The recess was filled up and the whole flume was covered with movable bed material resulting in a 0.03 m thick layer of movable sediment along the total flume length. A single cylindrical pier with a diameter of D = 0.03 m was embedded vertically in the center of the recess area. The blockage area due to the pier was 10 %, which is expected to have no influence on the scour process (Chiew and Ettema, 2003). The pier was positioned 5.0 m downstream of the intake. Using a high level tank ensured a constant water supply, and the discharge was measured with an inductive flow meter (IDM) at the intake pipe of the flume. The water level was adjusted by the control gate at the end of the flume (Figure 5.1), to keep the water depth h directly in front of the pier constant for every experiment. Due to the fact that pier scour models belong to the so called 'short models', it was not necessary to generate uniform flow conditions (Dorer, 1984).

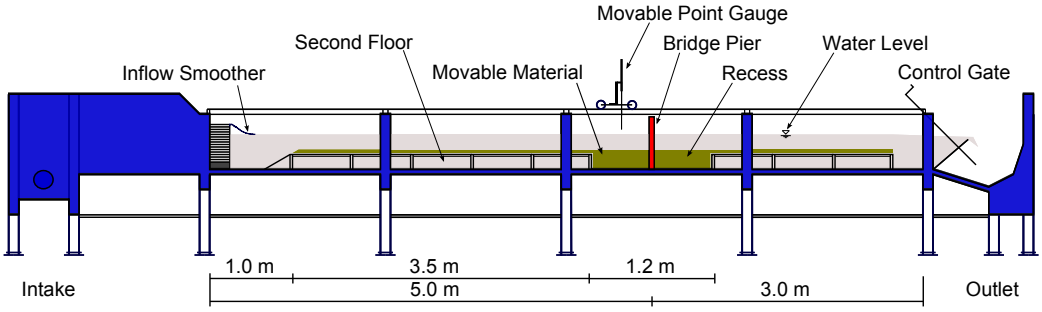

Figure 5.1: Illustration of the flume used in the laboratory of the Leichtweiß-Institut für Wasserbau at the Technische Universität Braunschweig.

5.1.2 Measurement technique

Flow velocity

During the experiments the discharge Q_{flume} into the flume was measured with an inductive discharge measurement device (IDM) at the flume's intake pipe. The velocity in the vicinity of the pier was determined by applying the continuity equation.

$$Q = U \times A \qquad [\mathrm{m}^3/\mathrm{s}] \tag{5.1}$$

Water depth

The water depth h was measured with a point gauge in front of the pier in the undisturbed approach flow and adjusted by a control gate at the end of the flume. Throughout the experiments the water depth in front of the pier was 0.1 m for all tested sediments, to keep constant the ratio of water depth to pier diameter (h/D).

Due to the fact that local pier scour can generally be associated with so called short models, it was not necessary to consider the sediment roughness and the energy line slope (Novák, 2010).

Scour depth

The scour depth development was measured with a point gauge without stopping the discharge after predefined time steps. The point gauge was mounted on a carriage and could be moved along the length and width of the entire flume, so that the maximum scour depths and geometrical measurements could be recorded. Figure 5.2 shows the lateral and longitudinal section in which the scour depth was measured. During the experiment visual observations, as well as test experiments without measurements, showed that there was no remarkable influence on the scour process due to the point gauge measurements. Particularly when

the experimental time was increased, the influence of the point gauge on the flow-sediment interaction decreased.

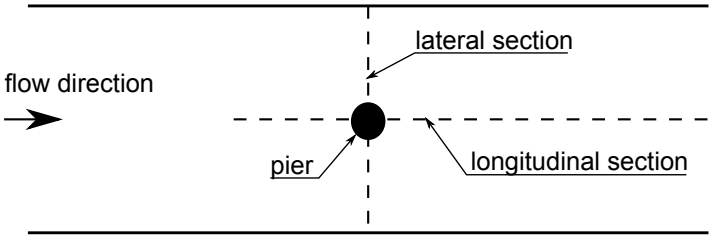

Figure 5.2: Measurement section around the pier.

For selected experiments, the entire scour surface was measured in a grid of 2 x 2 cm, beginning 14 cm upstream of the pier and ending 30 cm downstream, in order to compare the scour geometry for the various used sediments.

5.1.3 Accuracy of measurement

Considering the focus of this work, the accuracy of the used measurement technology is satisfactory. Fluctuations in discharge and in water level can be disregarded due to the relatively high uncertainties in determining the critical velocity of the sediment. The flow indicated by the IDM fits very well with the calculated flow rates.

The measurement results taken from the point gauge (accuracy of $\pm$ 0.10 mm) for the scour depth measurement are reliable and easy to handle.

5.2 Characterization of bed material properties

The main experiments were carried out with six different materials, which are presented in Figure 5.3. These materials differ substantially in grain-size and density. The lightweight material consisted of Acetal with $\rho_s = 1390\,\mathrm{kg\,m^{-3}}$ and Polystyrene with $\rho_s = 1040\,\mathrm{kg\,m^{-3}}$. The plastic granulates were characterized by uniform shapes (Figure 5.3 and 5.5) with a grain-size of 2.60 mm and 2.70 mm, respectively. The Acetal has an elliptic grain shape while the Polystyrene is cylindrical. Moreover, four natural sediments ($\rho_s = 2650\,\mathrm{kg\,m^{-3}}$) with varied grain-sizes were used. Fine sand, referred to as Sand0.2, with a grain-size of d_{50} = 0.21 mm, sand, referred to as Sand0.8, with a grain-size of $d_{50} = 0.82$ mm, coarse sand, referred to as Sand1.6, with $d_{50} = 1.6$ mm, and fine gravel, referred to as Sand2.5 with a grain-size of $d_{50} = 2.5$ mm.

Figure 5.3: Experimental material (starting from upper left): Sand2.5, Sand1.6, Sand0.8, Sand0.2, Acetal, Polystyrene.

The **sieve curve distribution** is characterized by the standard deviation σ for the sediments, and can be calculated by Equation 5.2.

$$\sigma = \sqrt{\frac{d_{84}}{d_{16}}} \qquad [1] \tag{5.2}$$

If $\sigma \leq 1.3$, the material can be treated like uniform, and armoring effects do not occur. Figure 5.4 shows the uniform grain-size distribution of the three types of sand. Due to the industrial fabrication, Acetal and Polystyrene are practical uniform ($\sigma \approx 1.0$). The fine gravel (Sand2.5) was separated from a sediment mixture of 1.0 mm to 3.0 mm using a 2.0 mm sieve and can also be assumed to be uniform.

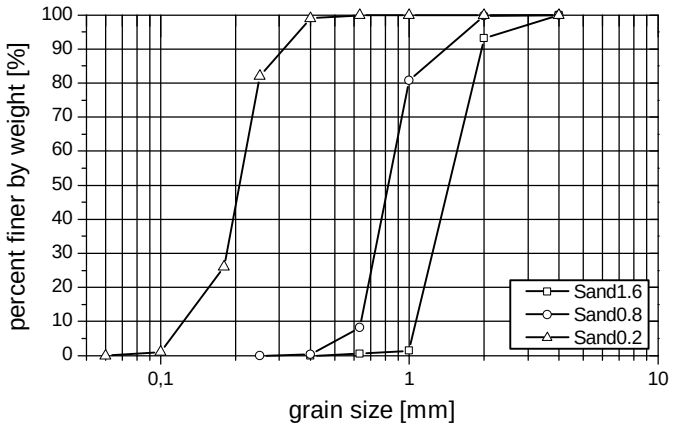

Figure 5.4: Sieve curves of the used materials.

At the first glance the shape of the artificial grains seem to be very different to the natural sediments. Therefore the so-called **form factor** FF for the artificial material was determined. The form factor characterizes the shape of a single grain and can be calculated by Equation

5.3. It is commonly recommended that, in the absence of any data, a form factor between 0.6 and 0.7 can be assumed for natural sediments (ASCE, 1962; Zanke, 1982a; Garde and Ranga Raju, 2000).

$$FF = \frac{c}{\sqrt{a \times b}} \qquad [1] \tag{5.3}$$

where a = long axis of the single grain [mm], b = medium axis of the single grain [mm] and c = short axis of the single grain [mm]. Table C.1 (Appendix C) comprises the results of the form factor determination for Acetal (FF = 0.71) and Polystyrene (FF = 0.75).

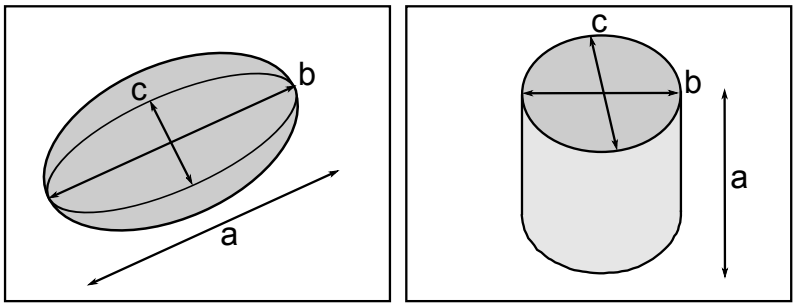

Figure 5.5: Sketch of the artificial sediments (left hand side Acetal, right hand side Polystyrene).

Van Rijn (1993) noted that the Θ_{crit} parameter is not that affected by the grain shape, when the nominal diameter (diameter that yields the same volume) is used as the characteristic parameter. Furthermore, Wang and Dittrich (1999) found that the particle shape does not have a great influence on the initiation of movement of the individual grains.

The **sedimentological diameter** D* is a characteristic dimensionless parameter that can be calculated by Equation 4.5 (Section 4.1). This parameter is independent of the hydraulic boundary conditions and includes only material properties. The materials Sand0.8 and Polystyrene, as well as Sand1.6 and Acetal, were selected in a similar way to D*. Sand0.2 and Sand2.5 were used to enlarge the range of this parameter, in order to identify correlations between D* and the scour depth development.

5.3 Determination of the material properties

Before starting the experiments with the selected materials, several tests and calculations were carried out to determine and verify the critical velocities U_{crit} and the material densities ρ. The following section comments on the main test and ends with a compilation of the material characteristics.

5.3.1 Critical mean velocity U_{crit}

The critical mean velocities U_{crit} for Sand0.8, Sand1.6, Polystyrene and Acetal were determined by the experiments executed by Ettmer (2004) in a 11 m long and 0.3 m wide flume, which is similar to the flume used in this work. Within the framework of this work, these values were compared to different equations that can be found in the literature. Due to the fact that the beginning of motion is not exactly assignable, the experimental results give approximately equivalent results. Bearing in mind that the mean velocity taken out of Ettmer defined the beginning of motion as the point in which only a 'few' sediment particles start moving the results fit well with each other. Therefore, the critical velocities estimated by Ettmer (2004) are reliable and thus used for the experiments.

In order to calculate the critical velocity in non cohesive material, seven existing equations to determine U_{crit} (see Appendix B) are compared to the measured values carried out by Ettmer (2004) (Table 5.1). While the equations from Neill, Zanke, Zhang and Hager include the material density, Laursen (in Richardson and Davis (2001)), van Rijn and Müller assume that the relative density ρ' is 1.65. All equations are based on the flow depth and the median diameter of the sediment particles. Zanke also included the viscosity of the water.

Most of the approaches are valid for coarse material $d_{50} \geq 0.002$ m and, therefore are not specifically applicable for the used material. In the absence of appropriate equations, the results should give a guideline for the values taken from the physical experiments.

The best results in comparison to the measured values are calculated using the equations of Neill (1967) and Zanke (1978) and, for the sand material, also the equation recommended by van Rijn (1993). Due to the absence of specific experiments executed in order to determine the critical velocity U_{crit} for Sand0.2 and Sand2.5, the Neill-Equation (Equation 5.4) was used as its results agreed with the the U_{crit}-values carried out by Ettmer (2004).

$$U_{\text{crit}} = \sqrt{2.5 \left(\frac{d}{h}\right)^{-0.2} \frac{\rho_s - \rho}{\rho} \, g \, d} \tag{5.4}$$

Table 5.1: Calculated critical flow velocities in comparison with measured values.

	Sand0.8		Sand1.6		Polystyrene		Acetal	
	U_{crit}	Δ U	U_{crit}	Δ U	U_{crit}	Δ U	U_{crit}	Δ U
Neill (1967)	0.29	0.00	0.38	0.06	0.07	0.00	0.23	0.04
Zanke (1978)	0.30	0.01	0.40	0.08	0.08	0.00	0.25	0.06
Zhang (1981)	0.31	0.02	0.39	0.07	0.08	0.00	0.23	0.03
Müller and Jones (1999)*	0.43	0.14	0.39	0.07				
van Rijn (1993)*	0.28	-0.01	0.37	0.05				
Richardson and Davis (2001)*	0.39	0.10	0.49	0.17				
Hager and Oliveto (2002)	0.35	0.06	0.47	0.15	0.08	0.00	0.25	0.06
Ettmer (2004)**	0.29		0.32		0.08		0.19	

*Equations only valid for natural sediments with $\rho' = 1.65$

**Measurements carried out by Ettmer (2004)

For both sediments, Equation 5.4 calculated the reliable values. Thus, the critical flow velocity for the Sand0.2 is $0.19\,\mathrm{m\,s^{-1}}$ and for the Sand2.5 $0.46\,\mathrm{m\,s^{-1}}$. The behavior of the sediments (moving or not moving) was controlled visually during the trial runs of each experiment.

5.3.2 Material density

The density of the sediments, especially for the lightweight materials, were determined with own pycnometer measurements (Figure 5.6) and compared to the data found in literature (Table 5.2).

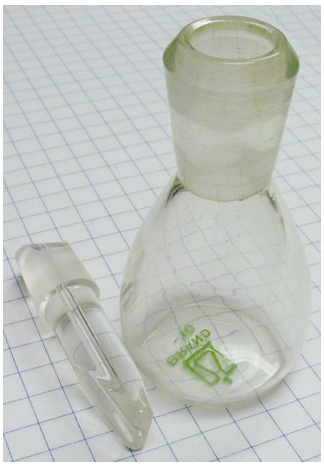

Figure 5.6: An empty glass pycnometer and stopper.

The measuring principle is based on the displacement of a defined fluid (density and temperature) located in the vessel. First, the sediment (m_0) and the fluid-filled vessel (m_1) has to be weighed, then the sediment and the fluid are put together into the vessel (m_2), and finally the overall weight has to be measured. For detailed results of these experiments see Table C.2 (Appendix C).

Using the weight differences data, the density of the sediment (ρ_s) can be calculated with the following equation:

$$\rho_s = \left(\frac{m_0}{m_0 + m_1 - m_2} \right) \rho_f \qquad [\mathrm{kg\,m^{-3}}] \tag{5.5}$$

The average of four measurements (P_1 to P_4) for each material was calculated and compared with the literature data. The results show a good correlation to the literature data, but slightly underestimate the density. This was partly due to the small air bubbles that stuck to the individual grains of the sample.

Table 5.2: Measured sediment densities in comparison to literature data.

	Sand [$\mathrm{g\,cm^{-3}}$]	Polystyrene [$\mathrm{g\,cm^{-3}}$]	Acetal [$\mathrm{g\,cm^{-3}}$]
measured values	2.61	1.04	1.34
Ettmer (2004)	2.65	1.04	1.39

5.4 Summary table of sediment properties

The tested materials are different in respect to their densities and grain-sizes, but the sedimentological diameter D* of Sand1.6 and Acetal, and of Sand0.8 and Polystyrene, respectively, is fairly similar. This is an important aspect to test the assumption that D* includes the relevant sediment properties and therefore can be used as a scaling parameter for model sediments (Section 3.1). The material properties of the tested materials are summarized in Table 5.3.

Table 5.3: Material properties of the material used in the experiments.

		Samd2.5	Sand1.6	Acetal	Sand0.8	Polystyrene	Sand0.2
d_{ch}	[mm]	2.50	1.60	2.60	0.82	2.74	0.21
ρ_s	[kg m^{-3}]	2650	2650	1390	2650	1040	2650
D*	[1]	60	40	40	20	20	5
FF	[1]	0.70	0.70	0.71	0.70	0.75	0.70
σ	[1]	–	1.29	–	1.30	–	1.25
U_{crit}	[m s^{-1}]	0.46	0.32	0.19	0.29	0.08	0.19

5.5 Experimental procedure

In order to find out the influence of the material density on the scour depth development, various experiments were carried out using the aforementioned sediments. To secure the reproducibility each experiment had to be repeated several times. The entire set of experiments are shown in Table 5.4. The procedure of each experiment was as follows:

1. The material was filled into the flume horizontally with a thickness of approximately 14 cm inside the material recess and 3.0 cm above the second floor, so that the bed roughness was the same over the entire flume length. No additional compacting or consolidation was accomplished. The height of the sediment bed was arranged onto the same level.

2. The pier was adjusted vertically in the centerline of the flume 5 m downstream of the inflow.

3. The water was filled up very slowly into the flume up to a depth of 10 cm. During this process any movement of the loose bed material especially around the pier was avoided.

4. The discharge was increased to the desired sediment specific value, while the water depth h in front of the pier was kept constant by calibrating the control gate at the end of the flume.

5. The experiment started with the first movement of material around the pier.

6. The scour depth was measured with the point gauge in the longitudinal section and the cross section at different points in time (15 min, 30 min, 60 min, 120 min, 240 min, 480 min, 1440 min and 14 400 min).

A total of six test series were conducted, in which only the sediment properties and therefore the associated approach flow U were essentially different. All series were conducted under clear-water conditions with a flow intensity of $U/U_{crit} \approx 1$ in order to generate the maximum scour depth. This means that the flow velocity U in each experiment was similar to the sediment-specific threshold velocity U_{crit}. All geometric variables, except the grain size, were kept constant. The different series were repeated several times under the same boundary conditions to get a representative scour depth development for each sediment.

A list of the experiments carried out is summarized in Table 5.4.

Table 5.4: Program of the experiments carried out in the laboratory of the Leichtweiß-Institut für Wasserbau at the Technische Universität Braunschweig.

name (material)	ρ [kg/m^3]	U/U_{crit} [1]	h [m]	D [m]	U_{crit} [m/s]	d_{50} [mm]	$Fr_{d,crit}$ [1]	t_{max} [min]
Sand0.2* (sand)	2650	1.0	0.1	0.03	0.19	0.2	3.34	14400
Sand0.8* (sand)	2650	1.0	0.1	0.03	0.28	0.8	2.53	14400
Sand1.6* (sand)	2650	1.0	0.1	0.03	0.32	1.6	1.99	14400
Sand2.5* (gravel)	2650	1.0	0.1	0.03	0.46	2.5	2.29	14400
Acetal* (acetal)	1390	1.0	0.1	0.03	0.19	2.6	1.91	14400
Poly.* (polystyrene)	1040	1.0	0.1	0.03	0.08	2.7	2.40	14400

*experiments with surface information

5.6 Additional experiments in a wider flume

Additional experiments were carried out in a larger flume at the University of Applied Sciences Magdeburg-Stendal. The experiments were executed in order to investigate the influence of the blockage area (W/D), the water depth h and the pier diameter D for lightweight material.

The flume length is 17.5 m, the depth 0.6 m and the flume width 0.60 m. The discharge through the flume was measured with an IDM and additionally with a Thomson weir. A control weir at the end of the flume set the water level h in front of the pier. The movable bed material was Polystyrene which was similar to the one used in Braunschweig (uniform material, a grain diameter of 2.0 mm and a material density of $\rho_s = 1070\,\mathrm{kg\,m^{-3}}$). The sedimentological diameter D* was calculated as 18. The threshold velocity U_{crit} for the beginning of motion for the tested material was $0.09\,\mathrm{m\,s^{-1}}$.

Three round piers were installed simultaneously in the centerline of the flume with different diameters beginning at 8.2 m downstream of the flume inflow. Starting with the small pier with a diameter of 2.5 cm, the medium pier of 5.0 cm and the large pier of 7.0 cm. The horizontal distance between the small and medium pier was 1.2 m and between the medium and large pier 1.8 m. A measuring tape was applied to the upstream face of the pier in order to measure the scour depth.

The blockage area of all the piers was less than 12 % and the sediment coarseness (D/d_{50}) for all materials was different due to the various pier sizes. The water depth h during the experiment was kept constant at 34 cm. According to the literature the influence of the water depth on the scour process can be neglected. The experimental boundary conditions are summarized in Table 5.5.

Table 5.5: Experimental boundary conditions of the large flume at the University of Applied Sciences Magdeburg-Stendal.

D	[cm]	2.5	5.0	7.0
d_{50}	[mm]	2.0	2.0	2.0
ρ_s	[kg m^{-3}]	1070	1070	1070
D*	[1]	18	18	18
σ	[1]	1.19	1.19	1.19
h	[m]	0.33	0.33	0.33
U_{crit}	[m s^{-1}]	0.09	0.09	0.09
D/d_{50}	[1]	12.5	25	35
blockage area D/W	[%]	4.2	8.3	11.6
h/D	[1]	13.2	6.6	4.7
Re_{pier}	[1]	2250	4500	6300

6 Results

In the following chapter the results of the experiments are described and discussed. A key aim of this work is to determine the influence of the sediment density on the scour process. The main geometric boundary conditions (channel width, flow depth, pier diameter) stayed constant for all of the experiments. In addition, the sediment-specific flow intensity was identical in each experiment ($U/U_{crit} \simeq 1$). Nevertheless, as a result of the different grain sizes and densities, the hydraulic conditions between the experiments did vary.

6.1 Main experiment setup and results

In total, six different sediments were tested focusing on the behavior of the artificial sediments Acetal and Polystyrene. The hydraulic conditions and parameters for the different test series are summarized in Table 6.1.

Table 6.1: Hydraulic conditions and parameters during the experiments.

		Sand2.5	Sand1.6	Acetal	Sand0.8	Polystyrene	Sand0.2
d_{50}	[m]	0.0025	0.0016	0.0026	0.0008	0.0027	0.0002
U	$[m\,s^{-1}]$	0.46	0.32	0.19	0.29	0.08	0.19
h	[m]	0.1	0.1	0.1	0.1	0.1	0.1
D	[m]	0.03	0.03	0.03	0.03	0.03	0.03
D/d_{50}	[1]	12.0	19.7	11.5	37.5	11.1	150.0
Fr	[1]	0.46	0.32	0.19	0.29	0.08	0.19
Fr_d	[1]	2.29	1.99	1.91	2.53	2.40	3.34
Re	[1]	46000	32000	19000	28800	7800	19000
Re_{pier}	[1]	13800	9690	5820	8640	2340	5820

6.1.1 Reproducibility of the experiments

An important aspect for physical hydraulic models is the reproducibility between the experimental runs. In general the experiments carried out for this thesis are reproducible, which, for example can be seen in Figure 6.1 for Sand1.6. The Sand1.6 experiment was repeated seven times. The amount of runs for the other tested materials was three times for Sand2.5, four times Sand0.2, seven times Acetal, eight times Polystyrene and eleven times Sand0.8.

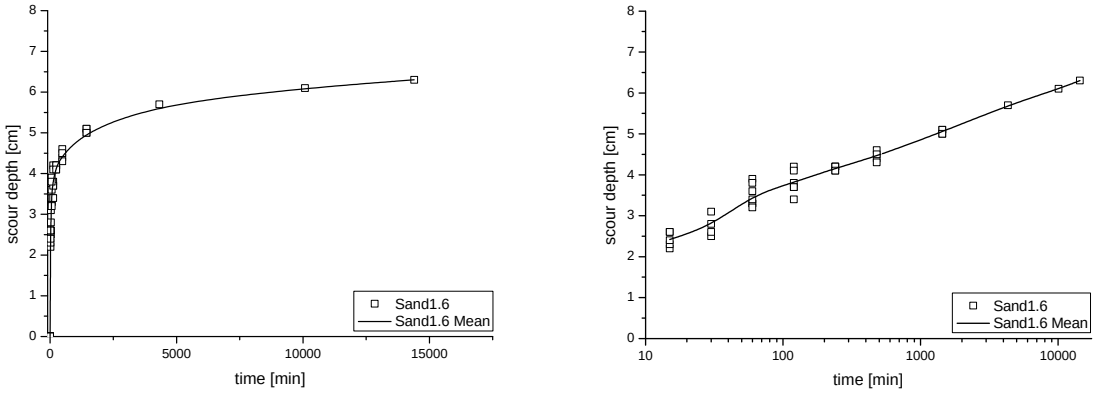

(a) linear time scale **(b)** logarithmic time scale

Figure 6.1: Sand1.6 experiments.

The arithmetic mean of the corresponding scour depth data for the used materials are plotted in Figure 6.2 and shown in Table 6.2.

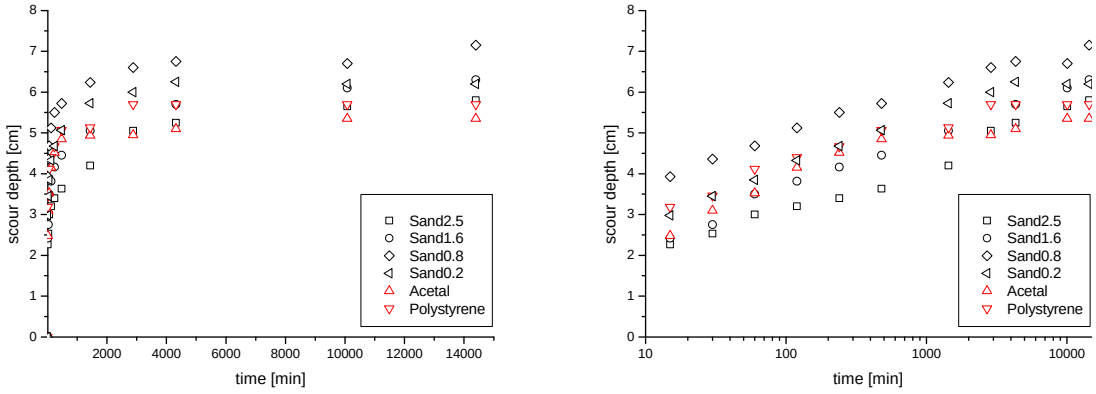

(a) linear time scale **(b)** logarithmic time scale

Figure 6.2: Scour depth results carried out in Braunschweig.

Table 6.2: Results of the different experiments (arithmetic mean) .

		Sand2.5 [cm]	Sand1.6 [cm]	Acetal [cm]	Sand0.8 [cm]	Polystyrene [cm]	Sand0.2 [cm]
15	[min]	2.27	2.42	2.48	3.93	3.18	2.98
30	[min]	2.53	2.75	3.10	4.36	3.46	3.45
60	[min]	3.00	3.50	3.53	4.68	4.12	3.85
120	[min]	3.20	3.82	4.15	5.12	4.40	4.33
240	[min]	3.40	4.16	4.52	5.50	4.67	4.68
480	[min]	3.63	4.45	4.85	5.72	5.07	5.07
1440	[min]	4.20	5.05	4.94	6.24	5.13	5.73
2880	[min]	5.05	–	4.95	6.60	5.70	6.00
4320	[min]	5.25	5.70	5.01	6.75	5.70	6.25
10080	[min]	5.65	6.10	5.35	6.70	5.70	6.20
14400	[min]	5.80	6.30	5.35	7.15	5.70	6.20

As an important result of this work, it is found that the uncertainties in the scour depth scatter for the same experimental set up seem to increase with decreasing material density. Exemplary Figure 6.1 (Sand1.6) and Figure 6.3 (Polystyrene) are shown. In both figures the great variance of scour depth for the same experiment can be seen, which makes a reliable estimation of the scour depth very difficult.

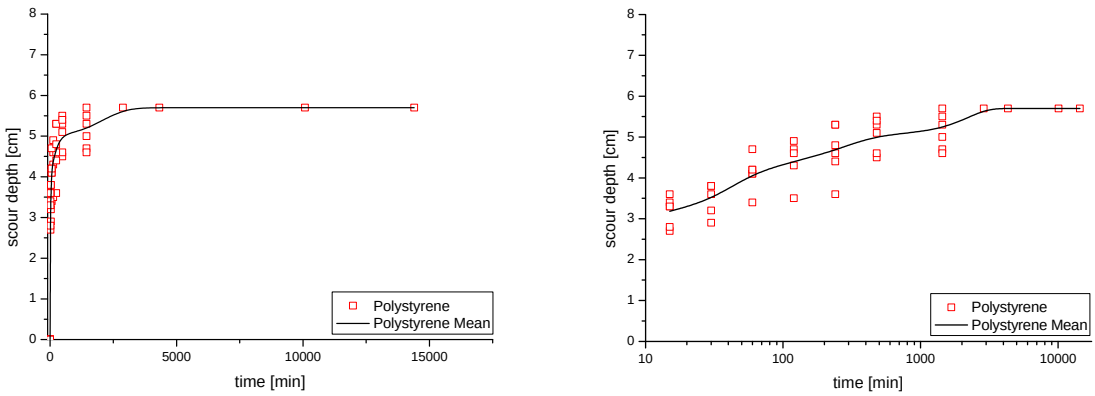

(a) linear time scale **(b)** logarithmic time scale

Figure 6.3: Polystyrene experiments.

An observation that may partly explain the significant spread of Polystyrene, is the formation of so-called clusters (Figure 6.4). A cluster is a conglomeration of single sediment grains which stick together and build up a stable compound that can, due to the individual grain size, substantially influence the scour depth. This phenomenon could be observed during the experiments with Polystyrene.

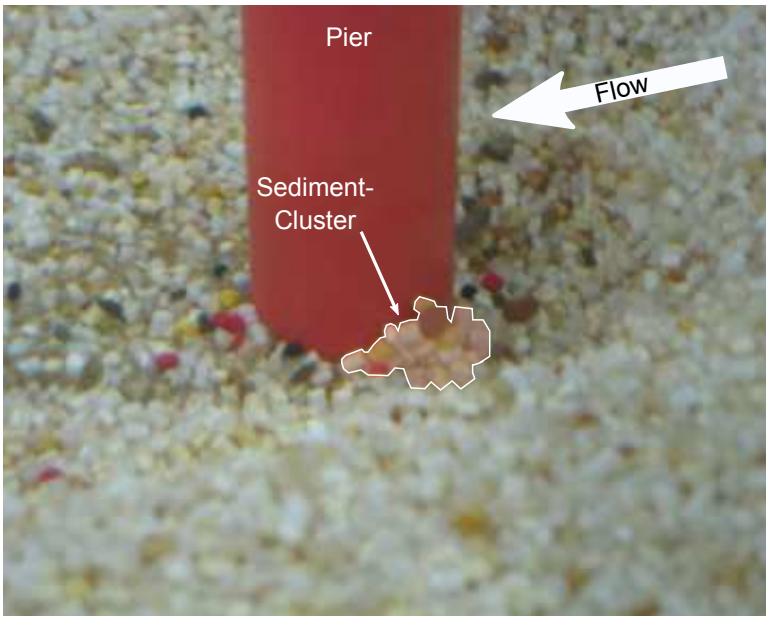

Figure 6.4: Sediment-Cluster during the experiments with Polystyrene.

6.1.2 General description of the experimental results

All experiments show the well known logarithmic evolution of the scour process with a rapid increase in scour depth at the beginning of the experiments. Moreover, the experiments show that, for natural sediments, the scour process is still continuing even after 14 400 min. This observation underlines the assumption that many scour experiments did not reach the maximum scour depth and therefore cannot be used for scour depth estimation (Section 3.4.11). This assumption is consistent with the experiments conducted in this work. Scour depths taken from experiments with an experimental time of less than 24 h are in many cases not sufficient, especially when looking for the maximum scour depth.

Furthermore, the data shows that the Sand0.8 reaches the maximum scour depth of 7.15 cm at the end of the experimental time (after 14 400 min). For Sand1.6, as well as for the Sand0.2, scour depths increase up to 6.3 cm and 6.2 cm respectively. For Sand2.5, a scour depth of 5.8 cm was registered. The logarithmic plots suggest that the equilibrium scour depth is not reached and that scour depths are still increasing (Figure 6.2).

The most important difference in results for the natural sediments is to be found in the scour depth after 14 400 min. It should be noted, however, that these differences develop mainly during the first 15 min. After this time, the scour rate per hour is quite similar.

The scour depth of the Polystyrene increases up to 5.7 cm after less than 2880 min, while the Acetal scour reaches a maximum depth of 5.6 cm after 10 080 min. In contrast to the sand experiments, the lightweight materials seem to reach their maximum scour depth long before the end of the experiments. Therefore it can be assumed that they both reach the equilibrium scour depth during the experimental time. The lightweight experiments consistently show similar scour depth developments in the first 480 min, which are also similar to the scour rate of the sands.

- Both materials (Polystyrene and Acetal) have a similar logarithmic scour development in the first 480 min.
- An equilibrium scour depth is reached after 2880 min for Polystyrene and 10 080 min for Acetal.
- The Polystyrene scour depth is slightly deeper than the Acetal scour.

6.2 Scour depth development as a function of different parameters

In the following section, the results of the experiments carried out in the context of this work are presented in relation to selected parameters. The parameters chosen in this case are particularly useful for the characterization of the sediment properties. The different symbols in the figures show the temporal development of the scour depth.

6.2.1 Sedimentological diameter D*

The sedimentological diameter D* as a scaling parameter for sediments is of major interest for this work, in particular because D* includes the sediment density. In this work two different natural sediments are compared with artificial lightweight granulates which have the same or a very similar sedimentological diameter D* (see Section 5.2). The scour depth for the different sediments are shown as a function of D* in Figure 6.5.

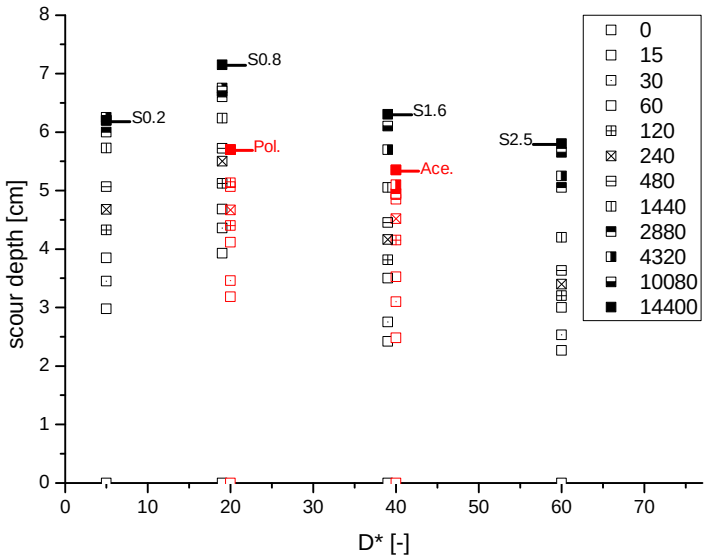

Figure 6.5: Scour depth development as a function of the sedimentological diameter D*.

The direct comparison of materials of same sedimentological diameter (D* = 20 and D* = 40) shows that there are significant discrepancies regarding the maximum scour depth. Interestingly, in both cases, the depths of the artificial sediments are lower than those of the natural sediments. The sedimentological diameter is therefore not suitable as a scaling parameter for the bed material in bridge pier models.

In addition to this finding, a decrease of the scour depth for both artificial and natural sediment is observed for an increasing D*. An exception is the Sand0.2 experiment, which has a smaller scour depth despite the low sedimentological diameter.

Influence of sediment density

The influence of the sediment density on the scour process is one of the central questions of this work. Although the relative sediment density ρ' is included in the sedimentological diameter D* and the densimetric Froude number Fr_d, at this point only the influence of the sediment density on the scour depth is described (Figure 6.6).

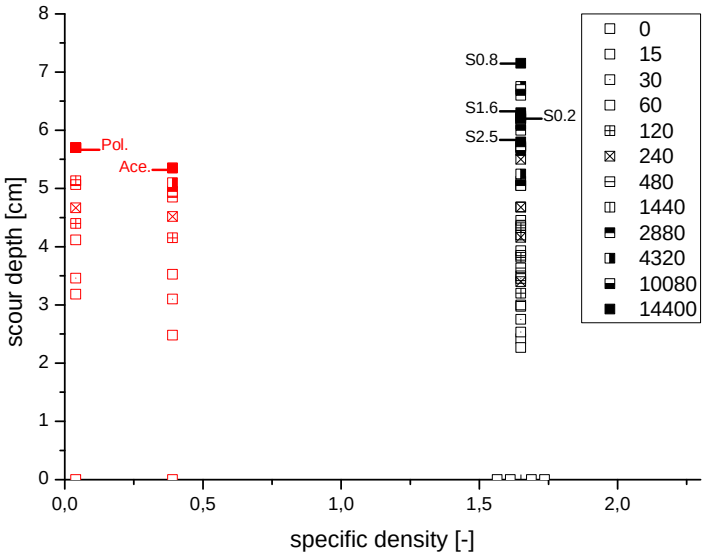

Figure 6.6: Scour depth development as a function of the specific sediment density ρ'.

In total, three different specific densities are used in the experiments (Polystyrene $\rho' = 0.04$, Acetal $\rho' = 0.39$, natural Sediments $\rho' = 1.65$). The densities of these materials vary strongly.

Comparing only the artificial sediments Acetal and Polystyrene, it can be said that the scour depth of Polystyrene is slightly, but not relevantly, deeper. However, there is a more interesting observable difference to be found in the temporal development of the scour depth. The Polystyrene scour reaches the equilibrium scour depth after 2880 min, whereas the full scour depth development of the Acetal takes more than 10 080 min.

The scour process of the natural sediments at 14 400 min is still going on and no equilibrium depth is reached.

6.2.2 Densimetric Froude number Fr_d

The densimetric Froude number Fr_d is the ratio of the impact forces of the water flow and the resistant forces of the grain among buoyancy. The parameter thus contains the approach flow velocity U, as well as the relative sediment density ρ' and the grain size d_{50}. Thus, it is an important parameter.

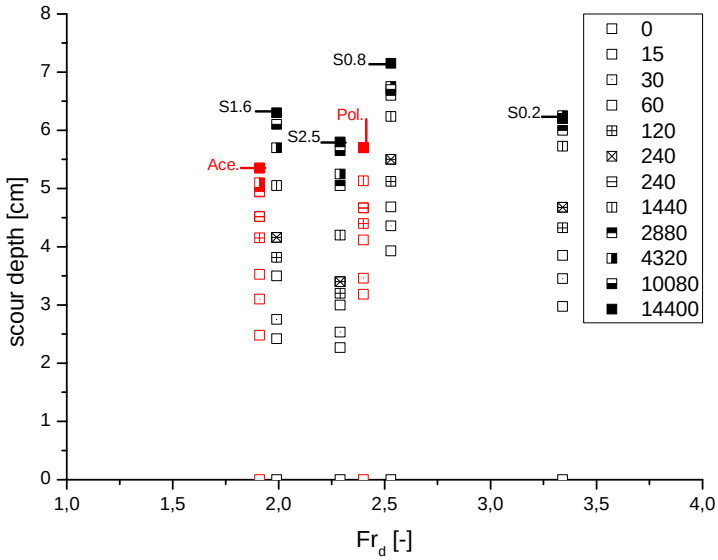

Figure 6.7: Influence of the densimetric Froude number on the maximum scour depth.

Analyzing the experimental results concerning their densimetric Froude number, it can be seen that there is no trend for the scour depth development with increasing Fr_d (Figure 6.7). Also, there is no consistent tendency for similar Fr_d. While Sand2.5 and Polystyrene have a similar Fr_d as well as similar scour depth, the scour depths for Acetal and Sand1.6, two materials that also share a similar densimetric Froude number, are actually very different. This in turn means that the densimetric Froude number is not a suitable scaling parameter.

Approach flow velocity U

To keep the flow intensity equal for all experiments ($U/U_{crit} = 1$), the approach flow velocity U was different depending on which material was used. Thus it was possible to investigate the influence of the approach flow velocity U in front of the pier. In particular, the scour depth development of two different sediments with nearly the same approach velocity U (Sand0.2 and Acetal) was of high interest. Furthermore, a focus was laid on the scour process of different sediments with a high variation of the approach flow velocities (e.g. Polystyrene and Sand2.5). Figure 6.8 shows the experimental results of the scour depth (at different time steps) as a function of the approach flow velocity U for the used sediments.

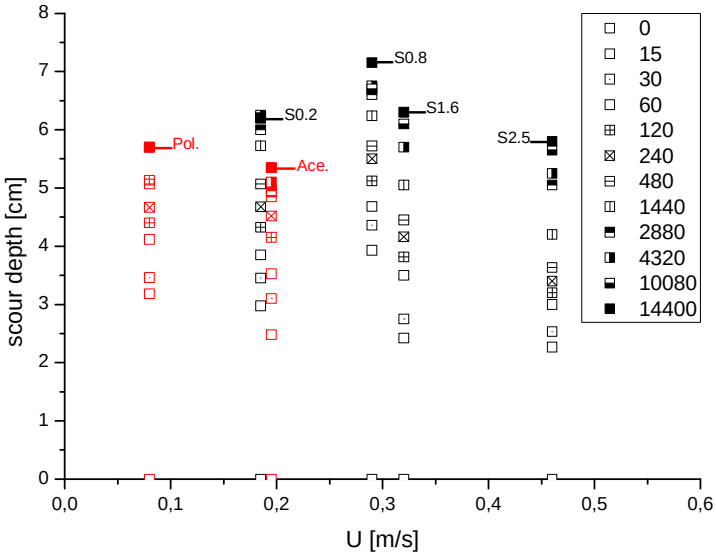

Figure 6.8: Scour depth development as a function of the approach flow velocity U.

The experiments with the same approach flow velocity U $\approx 0.19\,\mathrm{m\,s^{-1}}$ (Sand0.2 and Acetal) as well as the experiments with very different approach flow velocities (Polystyrene U $\approx 0.08\,\mathrm{m\,s^{-1}}$ and Sand1.5 U $\approx 0.46\,\mathrm{m\,s^{-1}}$) show, that the approach flow does not have a major effect on the maximum scour depth. Taking into account the fact that the same approach flow velocity interacts with the same bridge pier, it can be presumed that in case of equal U the vortex system has the same dimension. Under the hypothesis that the scour can be seen as a 'footprint' of the vortex system, one would then expect very similar scour geometry as well as scour depth in such cases. However, as the results show, these expectations are not met (Sand0.2 and Acetal). This means that sediment size, or in this case, density have to be responsible for the observed differences. The experiments carried out with Sand2.5 and Polystyrene have very different approach flow velocities but a similar scour depth. The maximum scour depth was reached in the Sand0.8 experiment with an approach flow velocity U $= 0.28\,\mathrm{m\,s^{-1}}$, which corresponds neither to the highest nor the lowest velocity.

A general consideration of the influence of the approach flow velocity U shows (Figure 6.8) that when keeping the ratio U/U_{crit} constant, an increase in approach velocity U does not necessarily lead to an increase in maximum scour depth.

6.2.3 Grain size

The grain size, or the ratio between pier width to sediment grain size (D/d_{50}), is one of the major scaling problems because of the scaling limit of sand. Some authors give the critical diameter d_{50} for sediment used in pier scour experiments as 0.5 mm (Clark et al., 1982), 0.8 mm (Unger, 2006) or 1.5 mm (Novák, 2010). This fact generally leads to a geometrical distortion of the hydraulic model because the relative sediment size is too big.

Figure 6.9 shows the experimental results of the scour depth (at different time steps) as a function of the the used sediments sizes d_{50}, d_{50} can be used in the present experiments analogously to D/d_{50}, as the same pier was used.

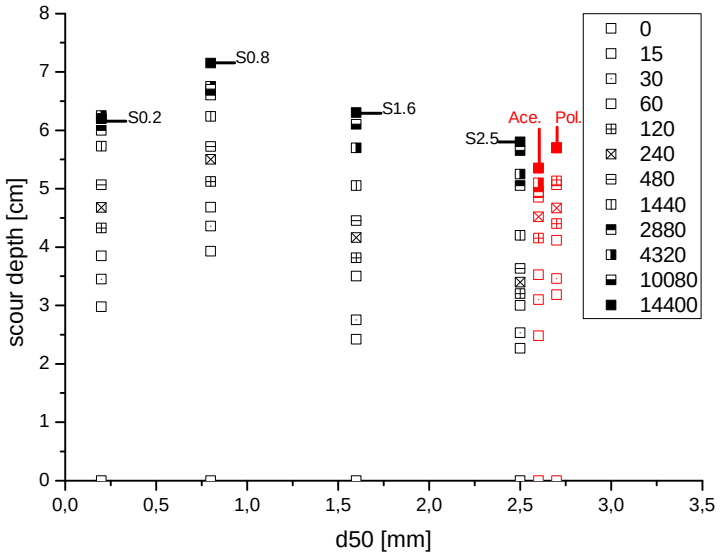

Figure 6.9: Scour depth development as a function of the sediment size d_{50}.

The experimental results, plotted in Figure 6.9, underline the importance of the sediment diameter for the scour process. Due to the fact that the pier diameter is equal in all experiments, these results are similar to those where the ratio D/d_{50} would be plotted on the abscissa instead of d_{50}.

For the natural sediment, the curve is similar to the one shown in Figure 6.5 (sedimentological diameter D*). The interesting difference from Figure 6.5 is the classification of artificial sediments in the curve. It can be seen that the maximum scour depth, especially of Sand2.5 ($d_{50} = 2.50$ mm) and Polystyrene ($d_{50} = 2.70$ mm), is more or less the same, and therefore more likely independent of the specific density ρ' and the absolute approach flow velocity U (if $U/U_{crit} \approx 1$).

6.2.4 Summary of the parameter study

The main findings from the results discussed above can now be summarized with the intent of improving future studies.

The **sedimentological diameter** D^* is no suitable scaling parameter for materials of different density in pier scour experiments, even though it contains, as key variables, both the relative sediment density ρ' and the grain size d_{50}. Theoretically, D^* gives good results for the initiation of sediment movement (Section 3.1) and can be used as a scaling parameter in scour models behind lock-gates (Ettmer, 2004). However, when evaluation experiments carried out using the same pier, the scour depths for sediments with the same sedimentological diameter are not similar. In both cases ($D^* = 20$; $D^* = 40$), the scour depths of the artificial sediments are smaller than those of the natural sediments.

The sediment density ρ for itself seems to have no significant influence on the maximum scour depth $d_{s,max}$, but definitely on the **time** t_e to reach the equilibrium scour depth d_{se}, the lighter the material, the faster the equilibrium scour depth is reached. The time to reach the equilibrium scour depth is particularly important because it can be assumed that in most experiments (carried out with natural sediments), the maximum depth has not been achieved within the experimental time. Therefore, the derived calculation approaches underestimate the scour depth. In the experiments conducted in this work no equilibrium scour for the natural sediments (Sand0.2, Sand0.8, Sand1.6 and Sand2.5) could be generated within an experimental time of 14 400 min.

The **densimetric Froude number** Fr_d describes the relation of the impact forces of the approach flow and the resistant forces of the grain among buoyancy. The parameter thus contains both the approach flow velocity U, as well as the relative sediment density ρ' and the grain size d_{50}. Nevertheless, the results show no dependence of this parameter.

Within the tests, it was also found that the approach flow velocity U does not have a major effect on the scour depth and time to achieve the equilibrium depth as long as $U/U_{crit} = 1$. This is particularly evident for the experiments carried out with Sand2.5 ($U = 0.46\,m\,s^{-1}$) and Polystyrene ($U = 0.08\,m\,s^{-1}$), which have very different approach flow velocities but a similar scour depth.

The **grain size** d_{50}, respectively the ratio D/d_{50}, seems to be the decisive parameter to achieve similar scour depth with natural sediment and lightweight material (Sand2.5, Acetal, Polystyrene), taking into account the experimental boundary conditions used here.

Turning to the question of whether natural sediments could be substituted with artificial lightweight material, two important findings are to be highlighted. First, the material density has significant influence on the time t_e to reach the equilibrium scour depth d_{se}, but not on the maximum scour depth itself. Secondly, if artificial granulate with a lower density is used instead of natural sediment, the grain size has to be similar in order to get similar scour depth.

6.3 Comparison of the measured and calculated scour depths

In Table 6.3, the results of different scour depth equation are compared for all tested materials. The used equations are valid for threshold conditions ($U/U_{crit} \leq 1$). In general, it can be said that none of the selected calculation approaches take the sediment density into account separately. It is therefore not surprising that the largest deviations between calculated and measured scour depths occur for Polystyrene (23 %), followed by Sand0.2 (16 %) and Sand0.8 (14 %). Because of the general application limits of the experimental material (especially the grain size), the results correspond very well with the expectations.

The best results with a mean deviation of 7 % are achieved with Sand1.6. Another striking finding is that the calculation approaches including the flow Froude number show great deviations from the actual measured scour depths.

In the following, the selected calculation approaches are briefly discussed with respect to their accuracy.

The approach used by **Laursen and Toch (1956)** includes only the pier width and flow depth. The total deviation for the measured scour depths, however, is only 9 %. Three scour depths are underestimated, two overestimated and one scour depth was determined exactly (Sand2.5). Except for the scour depth for Sand0.8 (- 19 %), the deviations between calculated and measured scour depths are below 10 %. In particular, the scour depths for Acetal (+ 9 %) and Polystyrene (+ 2 %) can be calculated very well.

The approach of **Shen et al. (1969)** estimates the scour depth by using the pier Reynolds number Re_{pier}. Thus, the result for scour depth depends mainly on the approach flow velocity U as well as on the pier width D. In comparison with the other approaches, the mean deviation for this method is the largest with 29 %. Except for Sand2.5 (+ 35 %) and Sand1.6 (exact), all scour depths are significantly underestimated. In particular, the scour depth for Polystyrene is underestimated to a degree of up to 53 %.

Breusers et al. (1977) employ an approach that includes not only the flow depth h and the pier diameter D, but also the ratio of the approach flow velocity U to the critical flow rate U_{crit}. This method thus indirectly takes into account the sediment characteristics. Overall, the calculated scour depths deviate from the average by about 7 %, with three over-estimated scour depths of up to 12 % (Acetal) and three under-estimations of up to 16 % (Sand0.8). The deviations of the calculated scour depth to the measured scour depth for the Polystyrene is only 5 % a relatively small number.

In addition to the ratio of the pier width D and approach flow depth h, the approach developed by **Jain (1981)** includes the flow Froude number, and thus, indirectly, the flow velocity U. Overall, the scour depth for five materials is underestimated up to 26 % (Polystyrene) and only the Sand2.5 scour is overestimated at a rate of 13 %. On average, the amount of deviation of the calculated scour depths to the measured scour depth is 13 %. The deviation

Table 6.3: Calculated equilibrium scour depth in [cm] for the experimental conditions for each sediment and their percentage deviation of the measured value.

		Sand2.5 D*≈60		Sand1.6 D*≈40		Acetal D*≈40		Sand0.8 D*≈20		Polystyrene D*≈20		Sand0.2 D*≈5	
Laursen and Toch	(1956)	5.8	0%	5.8	-8%	5.8	9%	5.8	-19%	5.8	2%	5.8	-6%
Shen	(1969)	7.8	35%	6.3	0%	4.5	-15%	5.9	-17%	2.7	53%	4.6	-27%
Breusers	(1977)	6.0	3%	6.0	-5%	6.0	12%	6.0	-16%	6.0	5%	6.0	-3%
Jain	(1981)	6.5	13%	6.0	-5%	5.2	-2%	5.8	-19%	4.2	-26%	5.2	-15%
CSU-Equation	(1988)	6.6	13%	5.6	-11%	4.5	-16%	5.4	-25%	3.1	-46%	4.5	-27%
Johnson	(1992)	5.3	-9%	4.6	-22%	4.4	-18%	4.5	-33%	3.7	-36%	4.4	-29%
Gao	(1993)	6.0	4%	6.2	-1%	6.0	13%	6.5	-8%	6.0	5%	7.2	16%
CSU-Equation	(1995)	7.2	25%	6.2	-2%	4.9	-8%	5.9	-17%	3.4	-40%	4.9	-20%
Melville	(1997)	5.9	1%	6.7	6%	5.8	8%	7.2	0%	5.7	0%	7.2	16%
May	(2002)	7.2	24%	7.2	14%	7.2	35%	7.2	0%	7.2	26%	7.2	16%
Sheppard	(2004)	5.3	-8%	6.3	0%	5.2	-2%	6.9	-3%	5.2	-10%	6.2	0%

of the calculated scour depth to the measured scour depth for the Acetal is very small, only 2 %.

Like Jain's approach, the **CSU-Equation (1988)** also contains the flow Froude number, the flow depth h and pier width D. The scour depths of five tested materials are underestimated on average by 25 % and only the scour depth for Sand2.5 is overestimated by 13 %. Overall, the calculated scour depths deviate from the measured scour depths by 23 %. The Polystyrene scour is underestimated by a staggering 46 %.

Johnsons' 1992 approach includes the flow Froude number, the pier width D and flow depth h. In contrast to the CSU-Equation (1988), all measured scour depths are underestimated with a mean deviation of 25 %.

The **Gao et al. (1999)** approach has a mean deviation from the measured scour depth of 8 % and the deviations between calculated and measured scour depths for four tested materials are below 10 %. Therefore, this approach can be classified as one of the well fitting equations. Two scour depths are underestimated (Sand1.6 by 1 % and Sand0.8 by 8 %) and four are overestimated by up to 16 % (Sand.0.2). The approach includes the ratio of the approach flow velocity U to the critical flow rate U_{crit} as well as the pier diameter D, the flow depth h and the sediment size d_{50}. In particular, the scour depths for Acetal (+ 13 %) and Polystyrene (+ 5 %) can be estimated very well.

The **CSU-Equation (1995)** includes two new K-factors but is otherwise identical to the CSU-Equation (1988). For clear-water scour without dunes, the calculated scour depth increases by 10 %. This means that, in comparison, the scour depths of five tested materials are underestimated on average by 17 % instead of 25 % and the scour depth for Sand2.5 is overestimated by 25 %. Overall, the calculated scour depths deviate from the measured scour depths by 19 %. The Polystyrene scour is underestimated by 40 %.

The formula of **Melville (1997)** overestimates four scour depths while two calculated depths exactly fit the results. Overall, the calculated scour depths deviate from the measured scour depths by 8 %. The deviation of the calculated scour depths from the measured scour depths is below 10 %, except for the scour depth of Sand0.2 (+ 16 %). In addition to including the ratio of pier diameter D to flow depth h and flow velocity U to the critical flow velocity U_{crit}, the Melville-Approach relates the ratio of pier width to sediment size D/d_{50}.

May et al. (2002) recommend an easy to use, factor based formula. The equation includes the pier shape and width, the flow depth, the velocity and the angle of attack. Five scour depths were overestimated with a mean deviation of 19 % and one measured scour depth is calculated exactly (Sand0.8). Overall, the calculated scour depths deviate from the measured scour depths by 23 %. In particular, the scour depths for Acetal (+ 35 %) and Polystyrene (+ 26 %) deviate remarkably.

Of the selected formulas to determine the maximum scour depth, the **Sheppard-Equation** has returned the best estimations for all tested sediments. Measurements and calculations yield the same values for Sand1.6 and Sand0.2. However, the remaining four materials were underestimated by about 6 % when compared to the measured scour depth. Overall, all results are within plus or minus 10 %, a result which is unique amongst all tested equations.

As the agreement between measured and calculated results for this approach is particularly good, the Sheppard-Equation is described in detail in the next section.

6.4 Sheppard approach

Even though there is a significant quantity of local scour data for circular piles reported in the literature, many of these data are not usable. For example, the duration of many experiments were not sufficient for the scour depth to reach (or even be extrapolated to) an equilibrium value. In other situations vital information about the flow, sediment and/or structure is missing. A thorough review of the literature resulted in 215 usable scour depth values from nine different sources for clear water scour conditions and 244 data points for live bed scour conditions. This data has been used in the development of Sheppard's local scour equations (Jones and Sheppard, 2000).

In particular, the appreciation of the influence of D/d_{50} on the scour process changed during the last decade. Before this time, it was the widespread opinion that the maximum scour depth for clear-water scour is unaffected by particle size as long as the value of D/d_{50} is larger than 25 (see for example Breusers and Raudkivi (1991)) or 50 (according to Melville and Chiew (1999)). However, Sheppard et al. (2004) found that the scour depth may decrease for increasing values of D/d_{50} beyond $D/d_{50} \sim 45$ as illustrated in Figure 6.10.

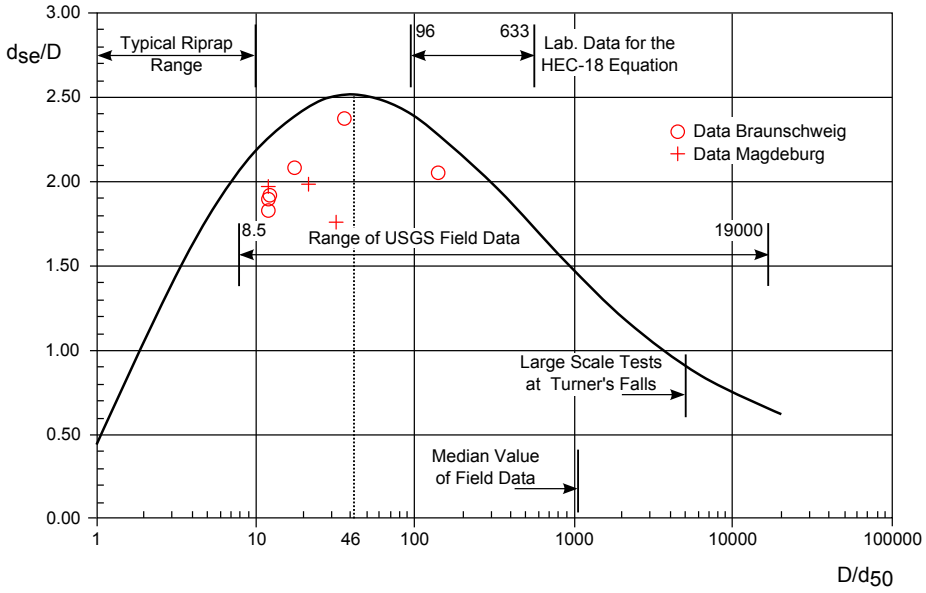

Figure 6.10: Equilibrium scour depth d_{se}/D as a function of D/d_{50} due to Jones and Sheppard (2000). The values of the experiments carried out in this work are added to this Figure.

The Sheppard-Equations consist of three functions (Equation 6.1), f_1 includes the structure-flow interaction (Equation 6.2), f_2 the flow-sediment interaction (Equation 6.3) and f_3 includes the structure-sediment interaction (Equation 6.4). The functions f_1,f_2 and f_3 lead to a reduction in scour depth, the maximum depth is thus 2.5 times pier width D.

$$\frac{d_{se}}{D} = 2.5\ f_1\ f_2\ f_3 \tag{6.1}$$

$$f_1 = \tanh\left[\left(\frac{h}{D}\right)^{0.4}\right] \tag{6.2}$$

$$f_2 = 1 - 1.75\left[\ln\left(\frac{U}{U_{crit}}\right)\right]^2 \tag{6.3}$$

$$f_3 = \frac{D/d}{0.4(D/d)^{1.2} + 10.6(D/d)^{-0.13}} \tag{6.4}$$

In Figure 6.11 the measured scour depths are plotted as a function of the equilibrium scour depth calculated with the Sheppard approach. The filled dots mark the measured scour depth after 14 400 min, the half-open dots the measured scour depth after 1440 min, 480 min and 240 min. The measured maximum scour depths agree well with the calculated depths, even for the artificial material (Table 6.4). This finding suggests that the key factors are quite well accounted for in Equation 6.1. The main remaining difference in between the experiments is the time that is needed to reach this value. It is noticeable that the scour process for the lightweight material is significantly shorter than the scour process for the Sands.

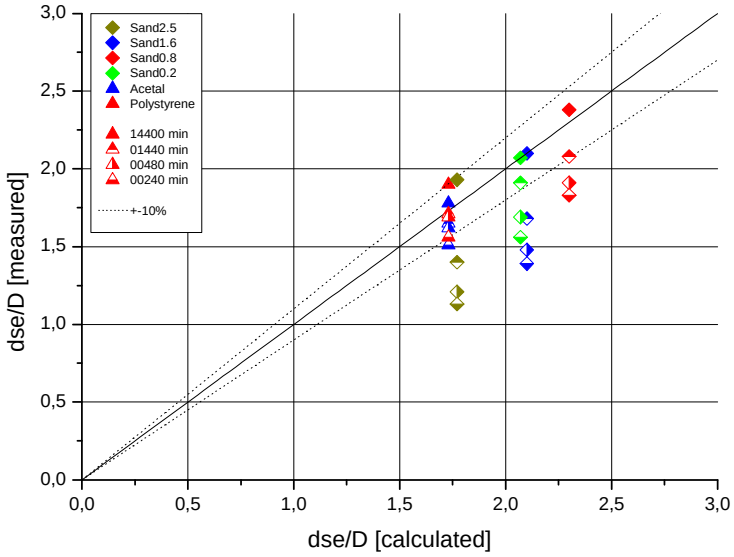

Figure 6.11: Comparison of the own experimental data with calculated results using the Sheppard-Equation.

Table 6.4: Comparison of the calculated and measured results for the given sediments using the Sheppard-Equation.

	Braunschweig					
	Sand2.5	Sand1.6	Sand0.8	Sand0.2	Acetal	Polysty.
measured scour depth [cm]	5.80	6.30	7.15	6.20	5.35	5.70
calculated scour depth [cm]	5.30	6.30	6.90	6.20	5.20	5.20

6.5 Time development

In this section, the experimental time of the scour experiments are compared with the function given by Melville and Chiew (1999) for the time t_e which is needed to reach the equilibrium scour depth (see Equation 3.44). The results are summarized in Table 6.5.

Table 6.5: Calculated time for equilibrium scour depth t_e in comparison to the experimental time.

	Braunschweig					
	Sand2.5	Sand1.6	Sand0.8	Sand0.2	Acetal	Polystyrene
experimental time [min]	14 400	14 400	14 400	14 400	14 400	14 400
calculated time [min]	2352	3381	3864	5694	5694	13 523
	Magdeburg					
	Pier2.5	Pier5.0	Pier7.0			
experimental time [min]	600	600	600			
calculated time [min]	9662	19 325	30 816			

The results in Table 6.5 show clearly that, according to the Melville-Equation, the experimental time of the experiments carried out in Braunschweig should have been sufficient to reach the equilibrium scour depth. However, results also show that the Equation 3.44 developed by Melville and Chiew (1999) seems not to be applicable for lightweight material (LWM) and natural sediments in hydraulic models. The experiments carried out by the author show that the equilibrium scour depth will be reached earlier for LWM and later for natural sediments. The results calculated with the approach developed by Melville and Chiew (1999) were found not to be valid for the experiments carried out in the thesis.

6.6 Vortex system

The vortex system, especially the main horseshoe vortex, has an essential impact on the scour geometry and depth and depends mainly on the hydraulic impact and the pier geometry. Research by Unger (2006) found that the influence of the sediment on the vortex system is negligible.

Unger (2006) gives an approach to calculate the time to develop the main horseshoe vortex (Equation 3.18) as well as an approach to calculate the vortex dimension (Equation 3.15). Both calculated results (time and vortex diameter) are shown in Table 6.6. As mentioned before, the scour geometry can be seen as the footprint of the main vortex and therefore insights on the vortex systems are gained by comparing the scour geometry of the experiments.

Table 6.6: Calculated time to develop the horseshoe vortex and calculated diameter of the horseshoe vortex according to Unger (2006).

		Sand2.5	Sand1.6	Acetal	Sand0.8	Polystyrene	Sand0.2
time	[sec]	0.94	1.83	1.94	5.19	5.71	41.52
diameter*	[cm]	2.4	1.9	1.9	2.6	2.4	3.8
diameter**	[cm]	2.8	2.2	2.2	3.1	2.9	4.5

* after 1440 min ** after 14 400 min

Concerning the time to develop the main horseshoe vortex, the results clearly show that the horseshoe vortex for all experiments is created immediately after the start of the experiments. The only exception is Sand0.2 (41.52 sec), but without the expected major impact on the final result due to the experimental time of 14 400 min. The reason for this may be that the material is outside the given limits for the used equation.

6.6.1 Scour geometry

A pier has a significant influence on the bed level surface and this influence can extend far downstream from the pier. When holding on the assumption that the scour geometry is a kind of footprint of the vortex system, it makes sense to describe the scour geometry especially in the near field of the pier, at least as long as the measurement technique is not able to scan the whole geometry and vortex system during the running experiments. Furthermore, the important maximum scour depth occurs close to the pier and is mostly at the upstream face of the pier. The bed level elevation for the cross and longitudinal section for each material after 14 400 min is shown in Figures 6.12.

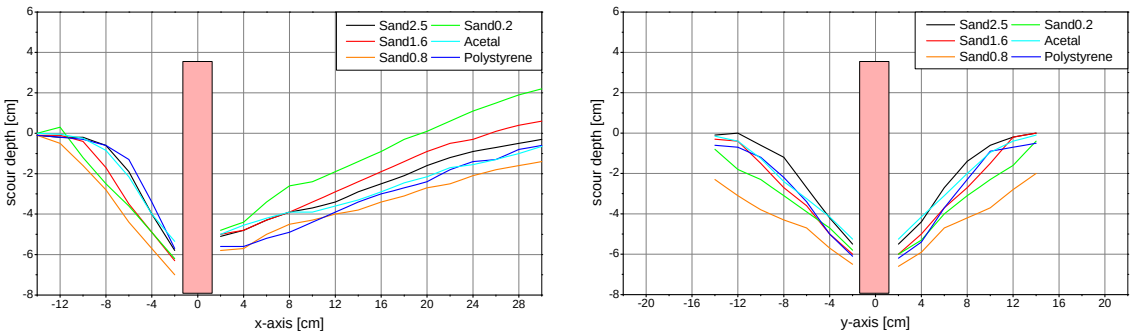

Figure 6.12: Maximum scour for all materials after 14 400 min.

The scour geometry of the different tested materials has different characteristics, which are described in more detail in the following illustrations.

Sand0.2

Sand0.2 is the material with the finest grain tested in this work and close to the size when cohesive forces occur. Several authors advise against using such a sediment in hydraulic models (Clark et al., 1982; Unger, 2006; Novák, 2010). Figure 6.13 shows the surface of the Sand0.2 scour after 14 400 min, the top-view including the counter-lines and the cross-section information for the x-axis and y-axis to illustrate the scour depth development. The following points characterize the scour geometry for the Sand0.2 after 14 400 min:

- the scour is symmetric and rounded and starts $\approx$ 12 cm upstream the pier
- the scour depth in front of the pier is significantly deeper than downstream of the pier; $\Delta = 1.4$ cm (difference between the scour depth upstream and downstream the pier)
- the transition between erosion and deposition downstream the pier after 14 400 min is at 20 cm

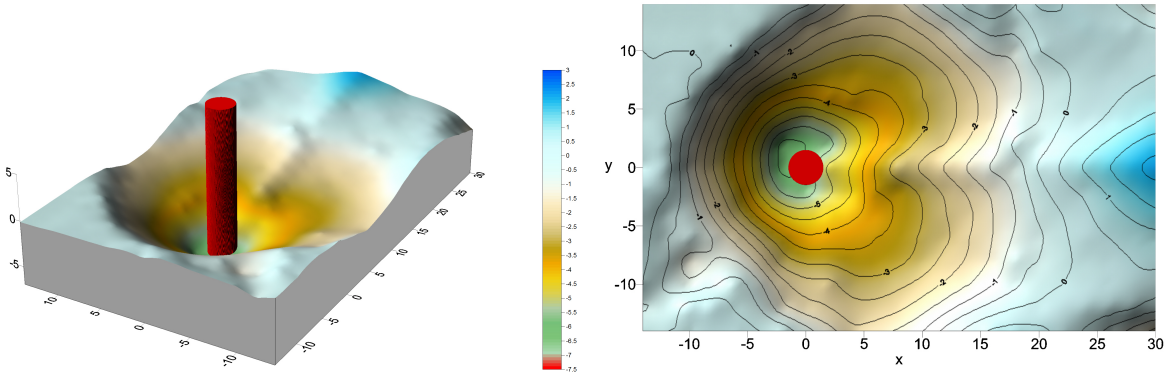

(a) surface **(b)** top-view counter line

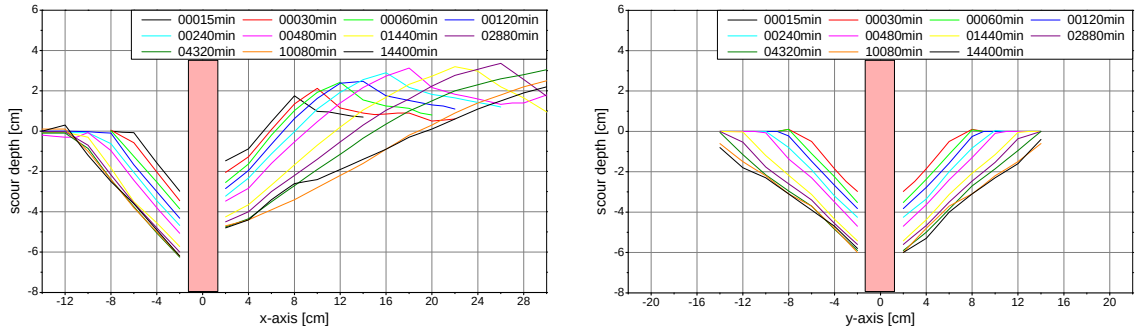

Figure 6.13: Scour geometry after 14 400 min and cross-section development of Sand0.2 .

- the highest measured deposit point was obtained after 2880 min with 3.4 cm
- after 4320 min the width of the scour reaches the flume width

Sand0.8

Sand0.8 produces the maximum scour depth and is, due to its sediment size, the recommended limit of applicability in physical hydraulic models. Figure 6.14 shows the surface of the Sand0.8 scour after 14 400 min, the top-view including the counter-lines and the cross-section information for the x-axis and y-axis to illustrate the scour depth development.

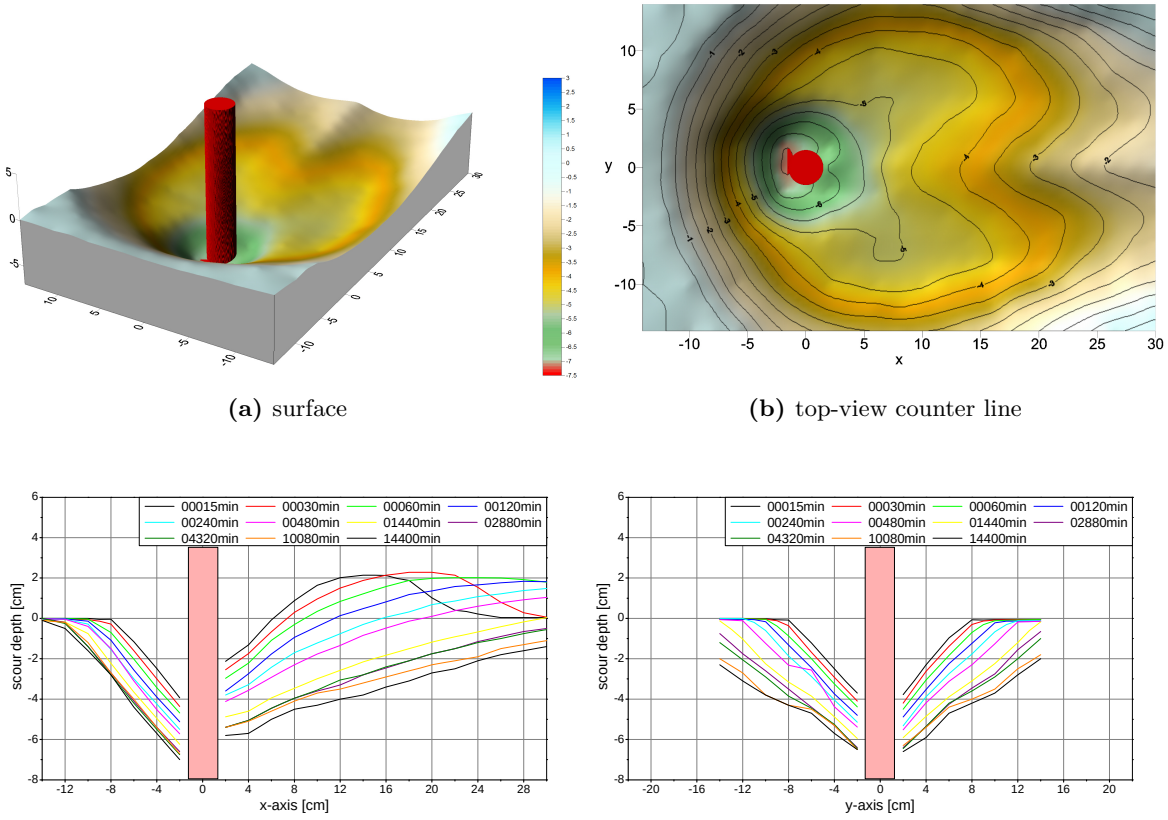

(a) surface **(b)** top-view counter line

Figure 6.14: Scour geometry after 14 400 min and cross-section development of Sand0.8 .

The following points characterize the scour geometry for Sand0.8 after 14 400 min:

- the scour is symmetrical and rounded and starts ≈ 12 cm upstream of the pier
- the scour depth in front of the pier is significantly deeper than downstream of the pier $\Delta = 1.2$ cm
- the transition between erosion and deposition downstream of the pier after 1440 min is at 30 cm
- the highest measured deposit point was obtained after 30 min with 2.3 cm
- after 1440 min the width of the scour reaches the flume width

Sand1.6

Figure 6.15 shows the surface of the Sand1.6 scour after 14 400 min. The top-view includes the counter-lines and the cross-section information for the x-axis and y-axis to illustrate the scour depth development.

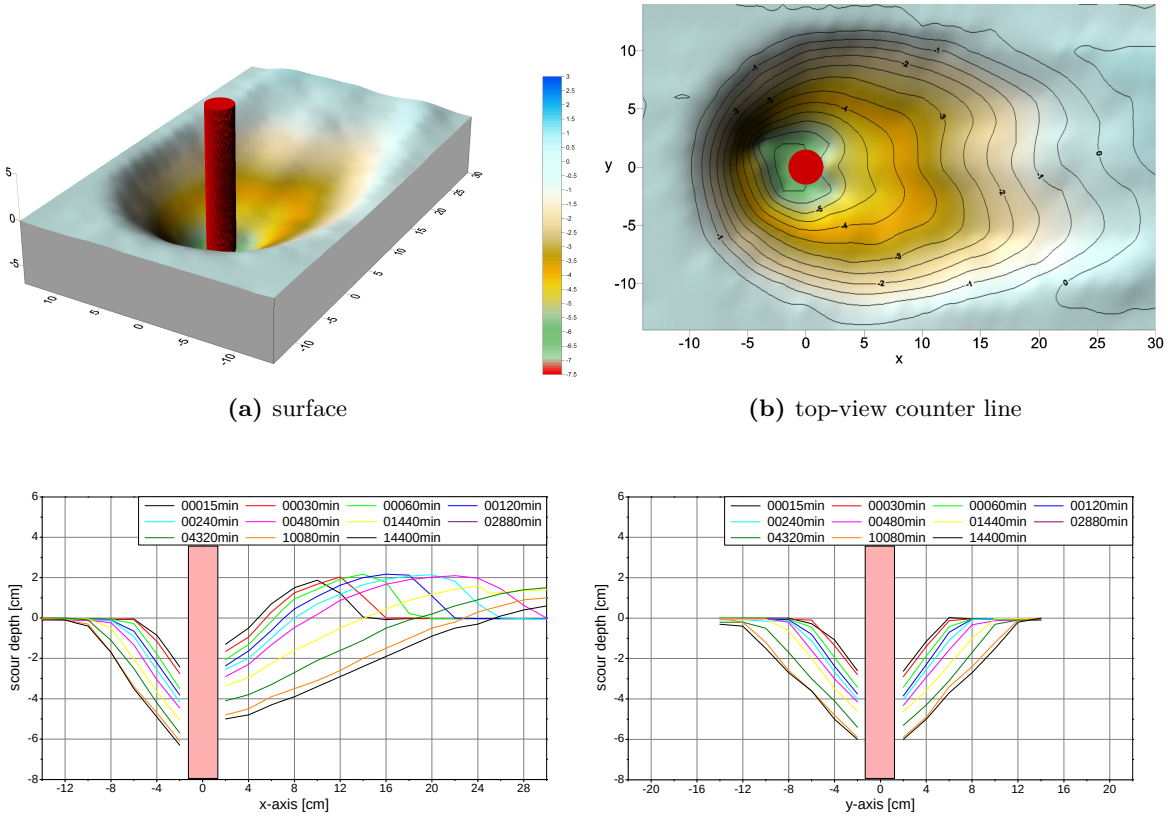

(a) surface **(b)** top-view counter line

Figure 6.15: Scour geometry after 14 400 min and cross-section development of Sand1.6 .

The following points characterize the scour geometry for Sand1.6 after 14 400 min:

- the scour is symmetrical and elongated and starts ≈ 10 cm upstream the pier
- the scour depth in front of the pier is significantly deeper than downstream of the pier $\Delta = 1.3$ cm
- the transition between erosion and deposition downstream the of pier after 14 400 min is at 25 cm
- the highest measured deposit point was obtained after 120 min with 2.2 cm
- after 14 400 min the total width of the scour in the pier cross-section is ≈ 24 cm (including the 3.0 cm pier)

Sand2.5

Figure 6.16 shows the surface of the Sand2.5 scour after 14 400 min. The top-view includes the counter-lines and the cross-section information for the x-axis and y-axis to illustrate the scour depth development.

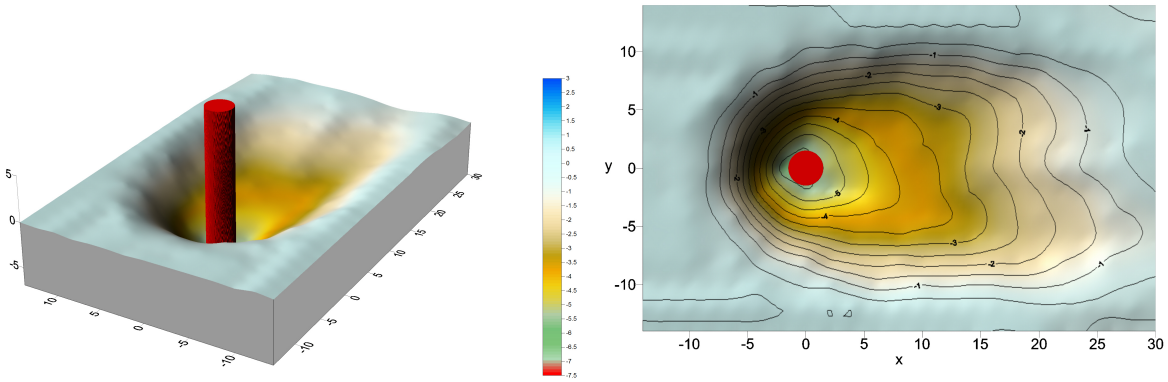

(a) surface **(b)** top-view counter line

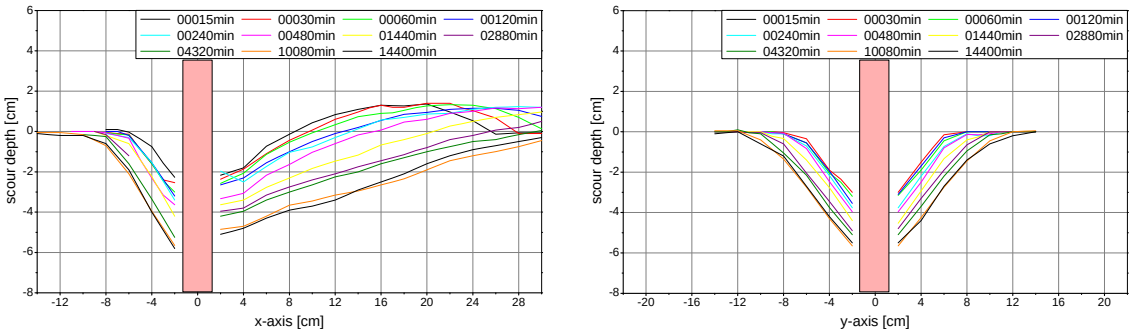

Figure 6.16: Scour geometry after 14 400 min and cross-section development of Sand2.5 .

The following points characterize the scour geometry for Sand2.5 after 14 400 min:

- the scour is symmetrical and elongated and starts ≈ 8 cm upstream of the pier
- the scour depth in front of the pier is deeper than downstream of the pier $\Delta = 0.7$ cm
- the transition between erosion and deposition downstream the pier after 14 400 min is at 30 cm
- the highest measured deposit point was obtained after 30 min with 1.4 cm
- after 14 400 min the total width of the scour in the pier cross-section is ≈ 20 cm (including the 3.0 cm pier)

Acetal

Figure 6.17 shows the surface of the Acetal scour after 14 400 min, the top-view includes the counter-lines and the cross-section information for the x-axis and y-axis to illustrate the scour depth development.

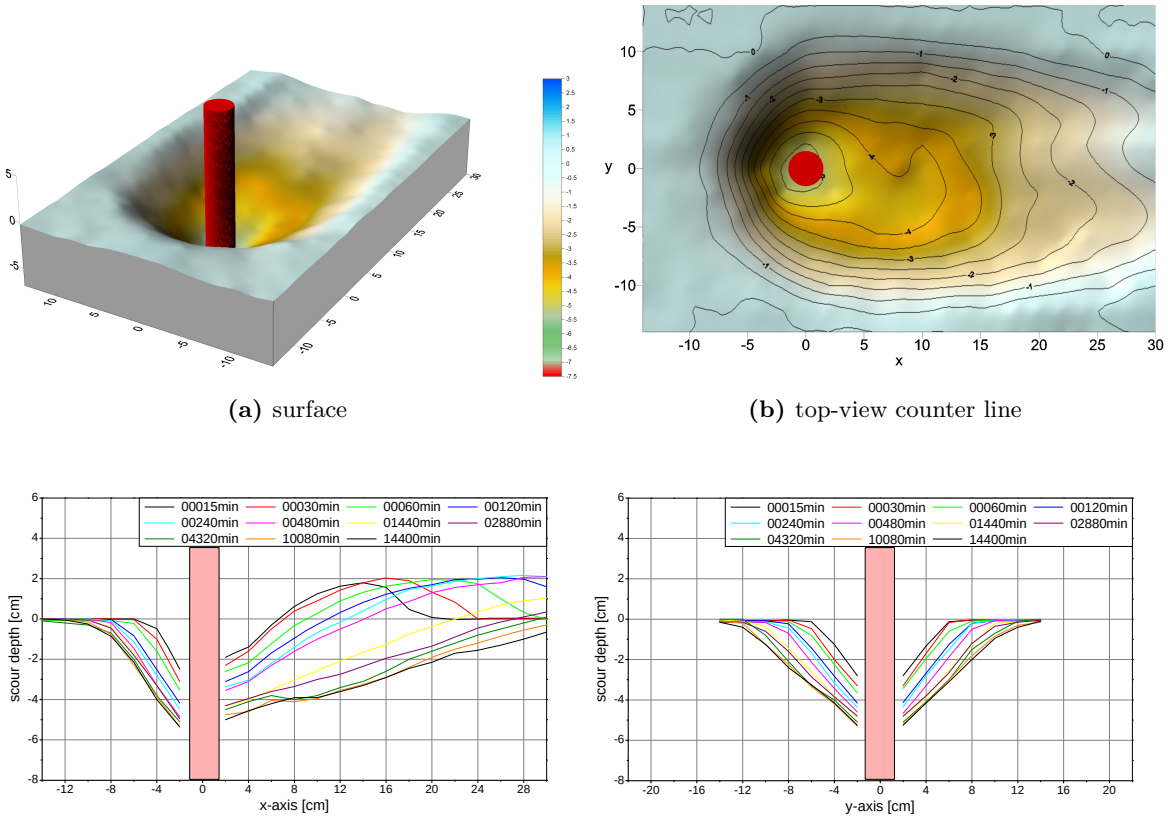

(a) surface **(b)** top-view counter line

Figure 6.17: Scour geometry after 14 400 min and cross-section development of Acetal .

The following points characterize the scour geometry for Acetal after 14 400 min:

- the scour is symmetrical and elongated and starts ≈ 8 cm upstream of the pier
- the scour depth in front of the pier is only 0.3 cm deeper than downstream of the pier
- the transition between erosion and deposition downstream of the pier after 4320 min is at 29 cm
- the highest measured deposit point was obtained after 240 min with 2.2 cm
- after 14 400 min the total width of the scour in the pier cross-section is ≈ 24 cm (including the 3.0 cm pier)

Polystyrene

Figure 6.18 shows the surface of the Polystyrene scour after 14 400 min. The top-view includes the counter-lines and the cross-section information for the x-axis and y-axis to illustrate the scour depth development.

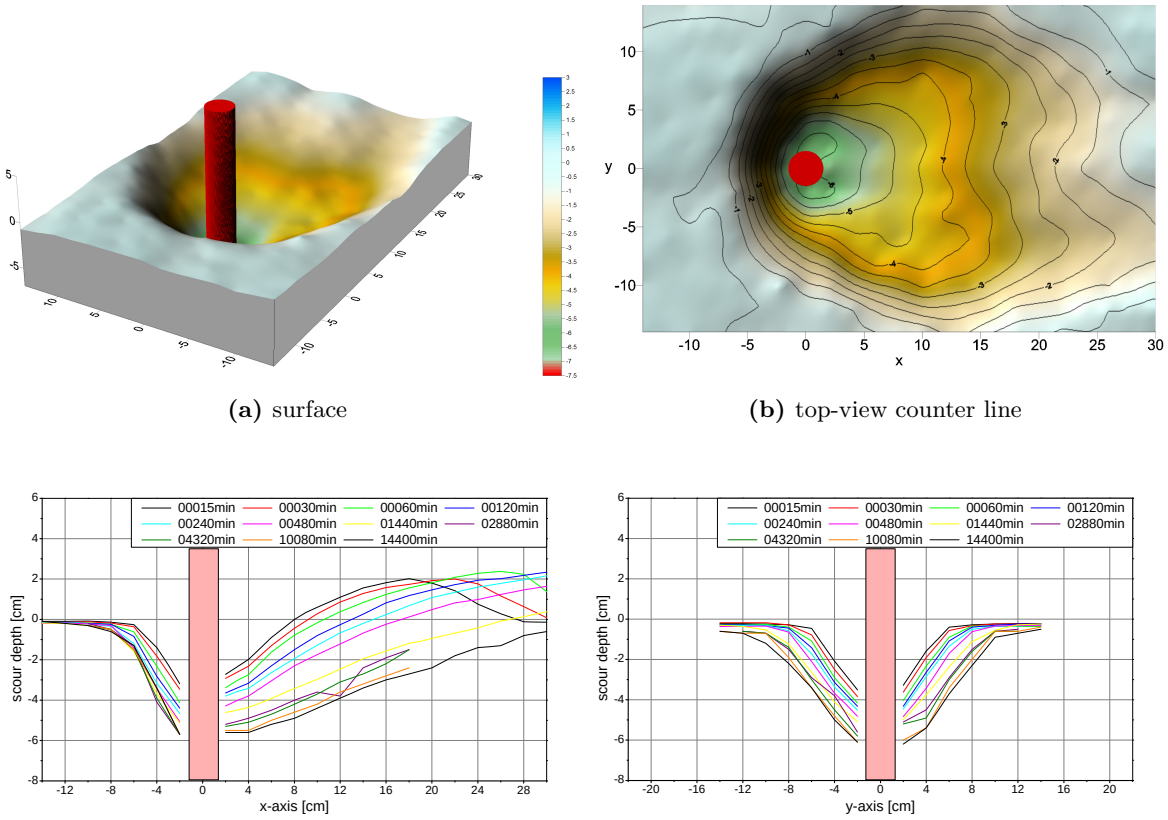

(a) surface **(b)** top-view counter line

Figure 6.18: Scour geometry after 14 400 min and cross-section development of Polystyrene.

The following points characterize the scour geometry for Polystyrene after 14 400 min:

- the scour is symmetrical and rounded and starts ≈ 8 cm upstream of the pier
- the scour depth in front and downstream of the pier is similar
- the transition between erosion and deposition downstream of the pier after 1440 min is at 27 cm
- the highest measured deposit point was obtained after 60 min with 2.4 cm
- after 14 400 min the total width of the scour in the pier cross-section is ≈ 20 cm (including the 3.0 cm pier)

6.6.2 Results of the scour geometry

Two significant differences are observed. First, there are different angles of repose for the upstream part of the scour. Sand0.2 has the lowest slope angle of roughly 32°, Sand1.6 has an upstream slope angle of 36°, Acetal of 36° and Polystyrene of 46°. Here, Polystyrene shows a very different result in comparison to the other materials. As a consequence, the scour extensions in front of the pier and at the pier sides are slighter for lightweight material.

The second observation made is that the scour with lightweight material forms a horizontal layer around the pier, which results nearly in the same scour depth downstream and upstream of the pier. This observation is in accordance with the observation for lightweight material described by Raudkivi (1998). In contrast, the maximum scour depth for the sand materials is located in front of the pier while downstream of the pier the scour depth is significantly smaller. This effect can be observed during the entire experimental time.

The main results of the geometric scour description are summarized in Table 6.7.

- All materials have different angle of slopes for the upstream scour, Polystyrene scour has the steepest slope with round about 46°.
- The scour extension differs depending on the materials employed, and is determined by sediment size and density.
- The bed is lowered at the rear of the pier for lightweight material.

Table 6.7: Summary of key results from the geometric view.

	Sand2.5	Sand1.6	Sand0.8	Sand0.2	Acetal	Polysty.
shape	r	r	el	r	el	r
upstream [cm]	8.0	10.0	12.0	12.0	8.0	8.0
upstream angle [°]	40.9	36.4	33.0	31.8	36.9	46.0
side angle [°]	31.5	30.1	26.2*	26.2**	25.9	33.5
downstream angle[°]	9.7	11.3	8.9	14.0	8.8	10.9
width [cm]	20.0	24.0	30*	30**	24.0	20.0
intersection [cm]	30.0	25.0	30*	20.0	29/**	27*
delta [cm]	0.7	1.3	1.2	1.4	0.3	0.1
hight [cm] (min)	1.4 (30)	2.2 (120)	2.3 (30)	3.4 (2880)	2.2 (240)	2.4 (60)

* after 1440 min; ** after 4320 min; r=rounded; el=elongated; hight=dune hight

Possible reasons for the differences in scour geometry between sand and lightweight material

Two main differences concerning the scour geometry between sand and lightweight material are mentioned in the previous section. Possible reasons for these observations are:

- The steep upstream angle of the lightweight scour may be caused by two major factors: first of all, by the artificial grain form, and second of all by the low specific weight under buoyancy. The energy dissipation of the turbulence is relatively high due to the high porosity of the sediment (grain size and shape). Hence, the upstream slope of the scour is more stable and less grain slides occur. The scour slope consequently occurs at a steeper angle.

- The lowered bed at the rear of the pier seems to appear as a typical phenomena of lightweight material and may occur due to a different transportation mechanism. The influence of the wake vortices at the downstream part of the pier seems to play an important role in this process. It is this vortex system that may be responsible for lifting single grains out of the sediment bed more easily, in order to carry them from the scour.

6.7 Results of the additional experiments

The results of the experiments carried out at the University of Applied Sciences Magdeburg-Stendal are shown in Figure 6.19. The experiments were carried out to investigate the influence of the blockage area (W/D), the water depth h and the pier diameter D.

Two experimental runs were carried out to control the reproducibility of the experiments. In each case, the scour depth was measured in front of the pier. It can be seen that the scour depth development in front of each pier is similar for both experimental runs. In addition, the absolute scour depth d_s increases with increasing pier diameter D. After 600 min the scour depth was 4.9 cm for the 2.5 cm pier, 9.8 cm for the 5.0 cm pier and 11.6 cm for the 7.0 cm pier.

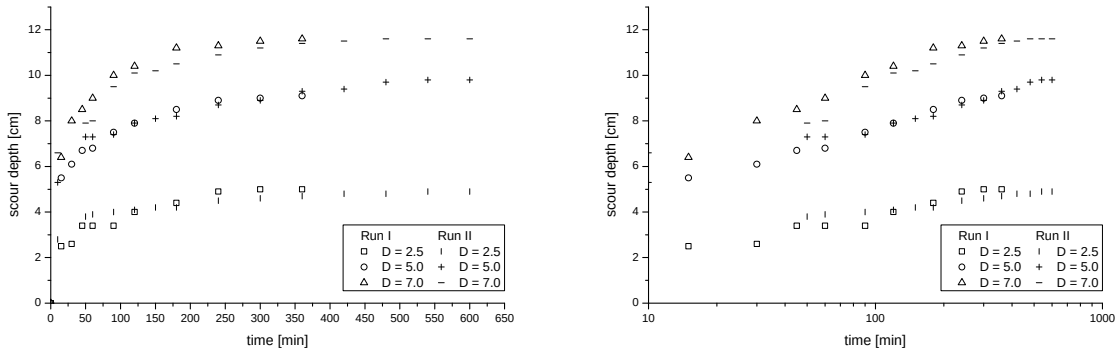

(a) linear time scale

(b) logarithmic time scale

Figure 6.19: Scour depth development for different pier width with Polystyrene d_{50}= 2.0 mm, and $U/U_{crit} \approx 1$.

The curves in Figure 6.19 indicate that in case of the small pier (D = 2.5 cm) the experimental time (t = 600 min) seems to be sufficient to reach the equilibrium scour depth d_{se}. The measured scour depth (d_s = 4.9 cm) is consistent with the calculated equilibrium scour depth (d_{se} = 4.8 cm) using the Sheppard-Approach (Section 6.4). In contrast, both piers with the larger diameters do not reach the calculated equilibrium scour depth (Table 6.8).

The gap between measured and calculated (equilibrium) scour depth increases with increasing pier diameter D. Thus, the experiments underline the important effect of pier diameter on the absolute scour depth and the associated time t* that is needed to achieve the equilibrium scour.

Table 6.8: Comparison of the calculated and measured results (after t = 600 min) for the given piers using the Sheppard-Equation.

	Magdeburg		
	Pier2.5*	Pier5.0*	Pier7.0*
measured scour depth [cm]	4.90	9.80	11.6
calculated scour depth [cm]	4.80	11.6	16.6

* Polystyrene d_{50}= 2.0 mm

In addition to this, Figure 6.20 compares the scour depth development of two similar bridge pier diameters in similar artificial sediments which each other. A comparison of the experimental results made in the small flume (Technische Universität Braunschweig, D = 3.0 cm) with the ones made in the wide flume (University of Applied Sciences Magdeburg-Stendal, D = 2.5 cm) shows a good agreement.

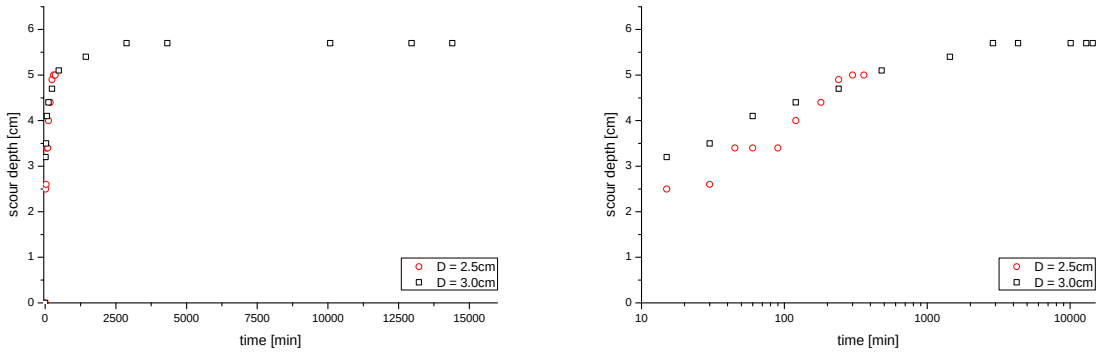

(a) linear time scale **(b)** logarithmic time scale

Figure 6.20: Comparison of the scour depth development experiments carried out in Braunschweig with those carried out in Magdeburg for similar pier diameter.

Concerning the blockage or constriction effect as well as the water depth h, which both have influence on the maximum scour depth (Section 3.4.4 and Section 3.4.5), Figure 6.20 shows that the assumption for the experiments carried out in Braunschweig were correct and the blockage effect as well as the influence of the water depth are negligible for the small flume experiments (Section 4.2). Both effects lead neither to an increase nor to an decrease of the scour depth.

7 Summary and outlook

Due to the large number of bridge damages caused by scour, an abundance of studies have been carried out related to the scouring process. Most of these studies focused on the estimation of equilibrium and/or maximum scour depth and time evolution of the scour. However, there are a number of issues still remaining unsolved.

Nearly all existing approaches have been developed on the basis of physical models carried out in the laboratory using well defined and often simplified boundary conditions. For the use of lightweight material as a substitute for natural sediment in pier scour experiments, no systematic studies are available. Thus, lightweight material has been used in pier scour models without specifying and testing the transferability of results obtained in this way.

The effects of the sediment density on the scour process was investigated in this work using hydraulic physical model tests. The study focused essentially on the effects of density on the pier scour process and the possibility of natural sediment substitution by artificial sediments. The general limitations of this study are:

- rectangular and linear flume geometry
- uniform bed roughness
- water as fluid
- water depth h = 0.1 m
- clear-water conditions, $U/U_{crit} \approx 1$
- mean sediment diameter d_{50} = 0.2 mm to 2.7 mm
- sedimentological diameter D* = 5, 20, 40, 60
- sediment uniformity $\sigma \leq 1.3$
- cylindric pier with diameter D = 3 cm
- sediment coarseness D/d_{50} = 12-150
- blockage ratio D/W = 0.1

7.1 Summary of the results

Within the work extensive laboratory tests have been performed concerning the influence of uniform artificial lightweight material on the scour process for a single round pier. In particular the parameters D* and Fr_d, which both include the relative density ρ' were tested concerning their applicability as transmission parameters for model sediment. Due to the particular importance of the time t_e and the sediment coarseness D/d_{50} on the scour process, both parameters were included in the analysis.

At this point it is important to note again that the experimental boundary conditions were geometrically identical between the experiments, the only difference being the sediments that were used. All experiments were performed with the same flow intensity ($U/U_{crit} = 1$).

In general, pier scour with lightweight material has the same characteristic temporal development like scour in natural sediments. This means that at the beginning the scour increases very quickly and then slowly approaches the equilibrium scour depth. It seems to be possible to reach similar scour depths in front of the pier between natural and artificial lightweight material if the grain size for both sediments is similar. The results of this thesis are especially important for complex pier structure scour in hydraulic models.

The results of this thesis can be summarized as follows:

- Concerning the time t_e which is needed to reach the equilibrium scour depth d_{se}, pier scour with lightweight material seems to reach the equilibrium scour depth much faster than with natural sediment. The lighter the material the faster the scour depth development. This fact is a very important point and advantage especially in case of complex pier structures. The experiments show clearly that even for small pier diameter ($D = 3.0\,cm$) the time t_e needed to reach equilibrium scour depth with natural sediments is more than 14 400 min or 10 days.

  In case of the experiments carried out in this work the Polystyrene ($\rho = 1040\,kg\,m^{-3}$) scour reaches the maximum (equilibrium) scour depth after 2880 min, the Acetal ($\rho = 1380\,kg\,m^{-3}$) scour after 10 080 min while the Sand2.5 ($\rho = 2650\,kg\,m^{-3}$) scour experiment was finished after 14 400 min without identifying the equilibrium scour depth.

  In the experiments carried out in Magdeburg ($\rho = 1070\,kg\,m^{-3}$, $d_{50} = 2.0\,mm$) the equilibrium scour depth for the small pier ($D = 2.5\,cm$ was even reached after less than 600 min.

  Taking into account that large model tests are often preferable to small model tests, it is important to note that the time to reach the equilibrium scour depth increases with increasing pier size. Thus the use of LWM, especially in large models, can be useful to achieve equilibrium scour depth within a given experimental time.

- Within this work the possibility of applying the sedimentological diameter D* as a scaling parameter for sediments in hydraulic bridge pier models was tested. To do so, the material pairs of Sand0.8 and Polystyrene (D* = 20) and Sand1.6 and Acetal (D* = 40) were selected for comparison, as their respective sedimentological diameter are similar. However, in the experiments, it was not possible to generate similar scour depth and the scour depth for the same D* varied widely. Thus, it can be stated that D* is, contrary to previous assumption, not a suitable scaling factor for sediments in bridge pier models.

  The analysis of the scour depth d_s in dependency of the relative particle density ρ' also show no clear relationship between scour depth and sediment density.

- The densimetric Froude number Fr_d describes the relation of the impact forces of the approach flow and the resistant forces of the grain among buoyancy. The parameter thus contains both the approach flow velocity U, as well as the relative sediment density ρ' and the grain size d_{50}. Analyzing the experimental results concerning their densimetric Froude number, it can be seen that there is no trend for the scour depth development with increasing or decreasing Fr_d. Therefore, the densimetric Froude number Fr_d is not a suitable scaling parameter for sediments in bridge pier models.

  During these tests, it was also found that the approach flow velocity U does not have a major effect on the scour depth and time to achieve the equilibrium depth as long as $U/U_{crit} = 1$. This is particularly evident for the experiments carried out with Sand2.5 ($U = 0.46\,m\,s^{-1}$) and Polystyrene ($U = 0.08\,m\,s^{-1}$), which have very different approach flow velocities but a similar scour depth.

- The grain size d_{50} seems to be the decisive parameter to achieve similar scour depth with natural sediment and lightweight material (Sand2.5, Acetal, Polystyrene). Taking into account the experimental boundary conditions used here, the ratio D/d_{50} is responsible for the achievable scour depth, with the proviso that the same pier diameter is used.

  As the pier size D has direct influence on the absolute scour depth and thus the time t_e, simply maintaining the D/d_{50} ratio does not always guarantee similar scour depth.

- Notwithstanding the consideration of the maximum scour depth, the geometry of lightweight scour differs from those with natural sediment in the fact that for them, the scour depth upstream and downstream the pier is equal. In addition, pier scours in lightweight material (especially Polystyrene) have a smaller upstream scour extension due to a steeper sediment angle of response.

  Overall, the handling of LWM in physical hydraulic models is more complicated than that of natural sediment and takes some practice.

For the substitution of natural sediments with artificial lightweight material under the given boundary conditions, the findings can finally be summarized in two main points. First, the material density has significant influence on the time t_e to reach the equilibrium scour depth, but not on the maximum scour depth d_{se}. Secondly, if artificial granulate with a lower density is used in a bridge pier model instead of natural sediment, the grain size d_{50} must be similar to achieve a similar scour depth.

7.2 Outlook

The present study on the influence of density cannot be considered to be complete. Despite the great progress in the scour depth research, the present work shows that the exact effects and mechanisms of the scour depth development especially for lightweight sediments are still not sufficiently clear. Therefore, research in the application of lightweight material in physical hydraulic models is still of great interest. Results from this research may also prove very useful for further scour research.

- In particular, the fact that today it is possible to order specific particle sizes and densities makes a detailed investigation of the density and grain size possible. Similary, it is possible to investigate sediment mixtures with lightweight material to study the influence of the non-uniformity.

- It seems that one of the main advantages of lightweight material is its a faster scour depth development, which takes considerably less time than that of natural sediments, thus the experimental time to reach the equilibrium scour depth can be greatly reduced. However, to capture the precise scale effects based on the material density, a large number of further systematic experiments are required, especially for different pier geometries.

- A further interesting advantage of lightweight material as model sediment is the possibility to study the scour behavior for very large U/U_{crit} conditions. When using natural sediments in the laboratory, such conditions are often not investigated, because the maximum flow rates that can be generated in the laboratory are not sufficient for this purpose.

- With the help of new measurement techniques, for example PIV, the vortex systems around the pier as well as the aproach flow development should be investigated for lightweight material. The influence of the approach flow development as a function of different sediment roughness on the scour process seems to be highly relevant. The knowledge about this effect should be improved through additional experiments.

Bibliography

Aberle, J. and Mertens, W. (2006). Anwendung und Bedeutung der Dimensionsanalyse im experimentellen Wasserbau. Mitteilungen des Leichtweiss-Instituts für Wasserbau (155), Braunschweig.

Alston, S., Berthelot, C., Cihak, M., Danzanvilliers, P., Healy, J., Jensen, H. N., Melsom, I., Diaz Morales, E., and Morisugi, H. (2004). *Méthodes d'évaluation économique des projets routiers dans les pays membres de l'AIPCR*. PIARC.

Annandale, G. W. (1994). Guidlines for the hydraulic design and maintenance of river crossings: Volume VI: Risk analysis of river crossing failure. Commitee of State Road Authorities.

Annandale, G. W., Melville, B. W., and Chiew, Y.-M. (2002). *Fallstudien zur Kolkbildung*. Mitteilungsblatt der Bundesanstalt für Wasserbau. Bundesanstalt für Wasserbau.

Apaydin, M. (2010). *A study on risk assessment of scour vulnerable bridges*. PhD thesis, Middle East Technical University.

ASCE (1962). Sediment transportation mechanics: Introduction and properties of sediment. *Journal of the Hydraulics Division*, 88(HY 4).

Baker, R. E. (1986). Local scour at bridge piers in non-uniform sediment. University of Auckland Department of Civil Engineering.

Ballio, F., Radice, A., and Dey, S. (2010). Temporal scales for live-bed scour at abutments. *Journal of Hydraulic Engineering*, 136(7):395–402.

Bonnefille, R. (1963). Essais de synthese des lois de debut d'entrainment des sediment sous l'action d'un courant en regime uniform. Bull. du CREC, No. 5, Chatou.

Breusers, H. N., Nicollet, G., and Shen, H. W. (1977). Local scour around cylindrical piers. *Journal of Hydraulic Research*, 15(3):211–252.

Breusers, H. N. and Raudkivi, A. J. (1991). *Scouring*, volume 2 of *Hydraulic structures design manual*. Balkema, Rotterdam.

Buckingham, E. (1914). On physically similar systems; illustration of the use of dimensional equations. *Physical Review*, 4(4):345–376.

Buffington, J. M. (1999). The legend of a. f. shields. *Journal of Hydraulic Engineering*, 125(4):376–387.

Chabert, J. and Engeldinger, P. (1956). Etude des affouillements autour des piles des ponts. *Laboratoire d'Hydraulique*.

Chang, F. F. M. (1973). A statistical summary of the cause and cost of bridge failures. Federal Highway Administration, Report No. FHWA-RD-75-87.

Chiew, Y.-M. (1995). Mechanics of riprap failure at bridge piers. *Journal of Hydraulic Engineering*, 121(9):635–643.

Chiew, Y.-M. and Ettema, R. (2003). Similitude in laboratory pier-scour studies. In Ganoulis, J., Prinos, P., Maksimovic, C., and Kaleris, V., editors, *Urban and Rural Water Systems for sustainable Development*, volume II of *Proc. XXX IAHR Congress*, pages 269–276, Thessaloniki and Greece.

Clark, A., Novák, P., and Russel, K. (1982). Modelling of local scour with particular reference to offshore structures. In *Papers presented at the International Conference on the Hydraulic Modelling of Civil Engineering Structures*, pages 411–423, Cranfield and Bedford and England. BHRA Fluid Engineering.

Dargahi, B. (1989). The turbulent flow field around a circular cylinder. *Experiments in Fluids*, 8(1-2):1–12.

Dey, S. and Papanicolaou, A. (2008). Sediment threshold under stream flow: A state-of-the-art review. *KSCE Journal of Civil Engineering*, 12(1):45–60.

Dey, S. and Raikar, R. V. (2007a). Characteristics of horseshoe vortex in developing scour holes at piers. *Journal of Hydraulic Engineering*, 133(4):399–413.

Dey, S. and Raikar, R. V. (2007b). Clear-water scour at piers in sand beds with an armor layer of gravels. *Journal of Hydraulic Engineering*, 133(6):703–711.

Dietz, J. W. (1969). *Kolkbildung in feinen oder leichten Sohlmaterialien bei strömendem Abfluß*. Universität, Karlsruhe.

Dietz, J. W. (1972). Systematische Modellversuche über die Pfeilerkolkbildung. Mitteilungsblatt der Bundesanstalt für Wasserbau (31), Karlsruhe.

Dittrich, A., Rosport, M., and Badde, O. (1992). *Untersuchungen zum Stabilitätsverhalten von Gerinnesohlen*, volume 182 of *Mitteilungen des Institut für Wasserbau und Kulturtechnik, Versuchsanstalt für Wasserbau "Theodor-Rehbock-Laboratorium"*. Institut für Wasserbau und Kulturtechnik, Karlsruhe.

Dorer, H. (1984). Ähnlichkeit bei Flussbaulichen Modellen. Mitteilungsblatt der Bundesanstalt für Wasserbau.

Ettema, R. (1976). Influence of bed material gradation on local scour. University of Auckland Department of Civil Engineering, Report 124.

Ettema, R. (1980). Scour at bridge piers. University of Auckland Department of Civil Engineering, Report 216.

Ettema, R., Constantinescu, G., and Melville, B. (2011). Evaluation of Bridge Scour Research: Pier Scour Processes and Predictions. NCHRP Web-Only Document.

Ettema, R., Mostafa, E. A., Melville, B. W., and Yassin, A. A. (1998). Local scour at skewed piers. *Journal of Hydraulic Engineering*, 124(7):756–759.

Ettmer, B. (2004). *Untersuchungen zu Kolkvorgängen hinter dem unterströmten Schütz*, volume 1. Papierflieger, Clausthal-Zellerfeld.

Eustis, E. L. (1936). Studies of lightweight materials with special reference to their movement and use as model bed material. War Department Mississippi River Commission.

Florida Department of Transportation (2005). Florida bridge scour manual.

Franzetti, S., Larcan, E., and Mignosa, P. (1982). Influence of test duration on the evaluation of ultimate scour around circular piers. In *Papers presented at the International Conference on the Hydraulic Modelling of Civil Engineering Structures*, Cranfield and Bedford and England. BHRA Fluid Engineering.

Gao, D., Posada, L., and Nordin, C. F. (1999). Pier scour equation used in china. In Richardson, E. V. and Lagasse, P. F., editors, *Stream stability and scour at highway bridges*, pages 217–222. The Society, Reston and Va.

García, M. H., editor (2008). *Sedimentation engineering: Processes, measurements, modeling, and practice*, volume 110 of *ASCE manuals and reports on engineering practice*. American Society of Civil Engineers, Reston and Va.

Garde, R. J. and Ranga Raju, K. G. (2000). *Mechanics of sediment transportation and alluvial stream problems*. New Age International, New Delhi, 3rd ed. edition.

Ghorbani, B. (2008). A field study of scour at bridge piers in flood plain rivers. *Turkish Journal of Engineering and Environmental Sciences*, 32:189–199.

Grimaldi, C., Gaudio, R., Calomino, F., and Cardoso, A. H. (2009). Countermeasures against local scouring at bridge piers: Slot and combined system of slot and bed sill. *Journal of Hydraulic Engineering*, 135(5):425–431.

Hager, W. H. and Oliveto, G. (2002). Shields' entrainment criterion in bridge hydraulics. *Journal of Hydraulic Engineering*, 128(5):538–542.

Hentschel, B. (2007). Hydraulische Flussmodelle mit beweglicher Sohle. Mitteilungsblatt der Bundesanstalt für Wasserbau (90).

Hoffmans, G. J. C. M. and Verheij, H. J. (1997). *Scour manual*, volume 96-120 of *P-DWW*. Balkema, Rotterdam.

Hughes, S. A. (1993). *Physical models and laboratory techniques in coastal engineering*, volume 7 of *Advanced series on ocean engineering*. World Scientific, Singapore.

ISDR (2009). UNISDR Terminology on Disaster Risk Reduction. United Nations International Strategy for Disaster Reduction, Geneva.

Jain, S. C. (1981). Maximum clear-water scour around circular piers. *Journal of the Hydraulics Division*, 107(HY5).

Johnson, P. A. (1992). Reliability-based pier scour engineering. *Journal of Hydraulic Engineering*, 118(10):1344–1358.

Jones, J. S. and Sheppard, D. M. (2000). Scour at wide bridge piers. In Hotchkiss, R. H. and Glade, M., editors, *Proceedings of Joint Conference on Water Resource Engineering and Water Resources Planning and Management 2000*, volume 104. ASCE.

Kobus, H. (1974). Anwendung der dimensionsanalyse in der experimentellen forschung des bauingenieurwesens. *Die Bautechnik*, 51(3):88–94.

Kwak, K. S. (2001). Prediction of scour depth versus time for bridge piers in the case of multi-flood and multi-layer soil system. *KSCE Journal of Civil Engineering*, 5(1):67–74.

Lança, R., Fael, C., and Cardoso, A. H. (2010). Assessing equilibrium clear-water scour around single cylindrical piers. In Dittrich, A., Koll, K. A. J., and Geisenhainer, P., editors, *River flow 2010*, Karlsruhe. Bundesanst. für Wasserbau.

Lança, R., Fael, C., and Cardoso, A. H. (2011). Effect of relative sediment size on clear-water equilibrium scour depth at single cylindrical piers. In Valentine, E. M. and Apelt, C. J.,

editors, *Proceedings of the 34th World Congress of the International Association for Hydro-Environment Research and Engineering*, pages 3582–3589, Barton and A.C.T. Engineers Australia.

Laursen, E. and Toch, A. (1956). Scour around bridge piers and abutments. Iowa Highway Research Board Bulletin (4).

Lee, S. O. and Sturm, T. W. (2009). Effect of sediment size scaling on physical modeling of bridge pier scour. *Journal of Hydraulic Engineering*, 135(10):793–802.

Link, O. (2006). *Untersuchung der Kolkung an einem schlanken zylindrischen Pfeiler in sandigem Boden*. Inst. für Wasserbau und Wasserwirtschaft, Darmstadt, 136 edition.

Maibach, M., Schreyer, C., Sutter, D., van Essen, H., Boon, B., Smokers, R., Schroten, A., Doll, C., Pawlowska, B., and Bak, M. (2007). Handbook on estimation of external cost in the transport sector.

May, R. W. P., Ackers, J. C., and Kirby, A. M. (2002). *Manual on scour at bridges and other hydraulic structures*. CIRIA, London.

Melville, B. W. (1997). Pier and abutment scour: Integrated approach. *Journal of Hydraulic Engineering*, 123(2):125–136.

Melville, B. W. and Chiew, Y.-M. (1999). Time scale for local scour at bridge piers. *Journal of Hydraulic Engineering*, 125(1):59–65.

Melville, B. W. and Coleman, S. E. (2000). *Bridge scour*. Water Resources Publ., Highlands Ranch and Colo.

Melville, B. W. and Sutherland, A. J. (1988). Design method for local scour at bridge piers. *Journal of Hydraulic Engineering*, 114(10):1210–1226.

Merz, B. (2006). *Hochwasserrisiken: Grenzen und Möglichkeiten der Risikoabschätzung ; mit 33 Tabellen*. Schweizerbart, Stuttgart.

Merz, B. (2007). RIMAX: Risikomanagement extremer Hochwasserereignisse. 2. Erweiterte Auflage, GeoForschungsZentrum Potsdam.

Mia, F. and Nago, H. (2003). Design method of time-dependent local scour at circular bridge pier. *Journal of Hydraulic Engineering*, 129(6):420–427.

Mia, F. and Nago, H. (2004). Closure to "design method of time-dependent local scour at circular bridge pier" by md. faruque mia and hiroshi nago. *Journal of Hydraulic Engineering*, 130(12):1213.

Molinas, A. (2003). Bridge scour in nonuniform sediment mixtures and in cohesive materials: Synthesis Report. Federal Highway Administration, FHWA-RD-03-083.

Müller, D. S. and Jones, J. S. (1999). Evaluation of recent field and laboratory research on scour at bridge piers in coarse bed materials. In Richardson, E. V. and Lagasse, P. F., editors, *Stream stability and scour at highway bridges*, pages 298–310. The Society, Reston and Va.

Müller, D. S. and Wagner, C. R. (2005). Field observations and evaluations of streambed scour at bridges. Federal Highway Administration.

Neill, C. R. (1967). Mean velocity criterion for scour of coarse uniform bed material. In Water Resources Publications, editor, *Proceedings of the XII IAHR Congress*, volume 3 of *12th Congress - Fort Collins*, pages 46–54. Littleton and Colorado.

Neill, C. R. (1978). Local scour around piers. *Journal of Hydraulic Research*, 16(3):259–262.

Nicollet, G. and Ramette, M. (1971). Affouillements au voisinage de piles des ponts cylindriques circulaires. In IAHR, editor, *Fourteenth Congress of the International Association for Hydraulic Research*, volume 3, pages 315–322, Paris. Societe Hydrotechnique de France.

N.N. (2004). Dokumentation des Hochwassers vom August 2002 im Einzugsgebiet der Elbe. Internationale Kommission zum Schutz der Elbe, Magdeburg.

Novák, P. (2010). *Hydraulic modelling - an introduction: Principles, methods, and applications*. Spon, London.

Oertel, H., Böhle, M., and Dohrmann, U. (2009). *Strömungsmechanik: Grundlagen - Grundgleichungen - Lösungsmethoden - Softwarebeispiele*. Strömungsmechanik. Vieweg+Teubner Verlag / GWV Fachverlage GmbH Wiesbaden, Wiesbaden, 5 edition.

Oliveto, G. and Hager, W. H. (2002). Temporal evolution of clear-water pier and abutment scour. *Journal of Hydraulic Engineering*, 128(9):811.

Oliveto, G. and Hager, W. H. (2005). Further results to time-dependent local scour at bridge elements. *Journal of Hydraulic Engineering*, 131(2):97.

Ong, M. C., Lim, S. Y., Yu, G., and Tan, S. K. (2004). Abutment scour using lightweight bed material. In Chiew, Y.-M., editor, *2nd International Conference on Scour and Erosion*, pages 187–198. Nanyang Technological University.

Pearson, D., Stein, S., and Jones, J. S. (2002). HYRISK Methodology and User Guide. Federal Highway Administration, FHWA-RD-02-XXX.

Pliefke, T., Sperbeck, S., Peil, U., and Budelmann, H. (2007). A standardized methodology for managing disaster risk – An attempt to remove ambiguity. Proceedings of the 5th International Probabilistic Workshop, Ghent, Belgium.

Radice, A., Porta, G., and Franzetti, S. (2009). Analysis of the time-averaged properties of sediment motion in a local scour process. *Water Resources Research*, 45(3).

Raikar, R. V. and Dey, S. (2009). Maximum scour depth at piers in armor-beds. *KSCE Journal of Civil Engineering*, 13(2):137–142.

Raudkivi, A. J. (1998). *Loose boundary hydraulics*. Balkema, Rotterdam, 4. edition.

Reichelt, A. and Richter, S. (2003). Hochwasserschäden im vorlandbereich der elbebrücke riesa - maßnahmen zu deren beseitigung. In *13. Dresdner Brückenbausymposium*, pages 175–187.

Rhodes, J. and Trent, R. (1993). Economics of floods, scour, and bridge failures. In Shen, H. W., Su, S. T., and Wen, F., editors, *Hydraulic engineering '93*, pages 928–933, New York and NY. American Society of Civil Engineers.

Richardson, E. V., Briaud, J.-L., and Buchanan, S. J. (2002). Praktische Berechnungen zu Kolken an Brücken in den USA: United States Practice for Bridge Scour Analysis. Mitteilungsblatt der Bundesanstalt für Wasserbau (85).

Richardson, E. V. and Davis, S. R. (1995). Evaluating Scour At Bridges. Hydraulic Engineering Circular (18), Federal Highway Administration.

Richardson, E. V. and Davis, S. R. (2001). Evaluating Scour At Bridges: Fourth Edition. Hydraulic Engineering Circular (18), Federal Highway Administration.

Richardson, E. V., Simons, D. B., and Lagasse, P. F. (2001). *River Engineering for highway encroachments: Highways in the River Enviroment*. Hydraulic Design Series. Washington DC.

Richardson, J. R. and Richardson, E. V. (2008). Bridge scour evaluation. In García, M. H., editor, *Sedimentation engineering*, volume 110 of *ASCE manuals and reports on engineering practice*, pages 505–542. American Society of Civil Engineers, Reston and Va.

Saunders, R. D. (2004). *Seabed Scour Emanating from Submerged Three Dimensional Objects: Archaeological case studies*. PhD thesis, University of Southhampton, Southhampton.

Schlichting, H., Gersten, K., and Krause, E. (2006). *Grenzschicht-Theorie*. Springer, Berlin, 10., überarb edition.

Shen, H. W., Schneider, V. R., and Karaki, S. (1969). Local scour around bridge piers. *Journal of the Hydraulics Division*, 95(HY 6):1919–1940.

Sheppard, D. M., Odeh, M., and Glasser, T. (2004). Large scale clear-water local pier scour experiments. *Journal of Hydraulic Engineering*, 130(10):957–963.

Shields, A. (1936). *Anwendung der Ähnlichkeitsmechanik und der Turbulenzforschung auf die Geschiebebewegung*, volume 26 of *Mitteilungen der Preußischen Versuchsanstalt für Wasserbau und Schiffbau*. Berlin.

Shirole, A. and Holt, R. (1991). Planning for a comprehensive bridge safety assurance program. In *Third Bridge Engineering Conference*, volume Volume 1 of *Transportation research record*, pages 39–50, Washington and D.C. Transportation Research Board National Research Council.

Sigloch, H. (2008). *Technische Fluidmechanik: Mit 40 Tabellen, sowie 114 gelösten Berechnungsbeispielen*. Springer-11774 /Dig. Serial]. Springer-Verlag, Berlin and Heidelberg, 6., neu bearb. aufl. edition.

Simarro, G., Fael, C. M. S., and Cardoso, A. H. (2011). Estimating equilibrium scour depth at cylindrical piers in experimental studies. *Journal of Hydraulic Engineering*, 137(9):1089.

Simarro, G., Teixeira, L., and Cardoso, A. H. (2007). Flow intensity parameter in pier scour experiments. *Journal of Hydraulic Engineering*, 133(11):1261–1264.

Stein, S. and Sedmera, K. (2006). Risk-Based Management Guidelines for Scour at Bridges with unknown Foundations.

Sumer, B. M. and Fredsøe, J. (2006). *Hydrodynamics around cylindrical structures*, volume 26 of *Advanced series on ocean engineering*. World Scientific, Singapore, revised ed. edition.

Unger, J. (2006). *Strömungscharakteristika um kreiszylindrische Brückenpfeiler: Anwendung von Particle Image Velocimetry in der Kolkhydraulik*. Versuchsanst. für Wasserbau Hydrologie und Glaziologie, Zürich, 197 edition.

van Rijn, L. C. (1984). Sediment transport: Part i: Bed load transport. *Journal of Hydraulic Engineering*, 110(10):1431–1456.

van Rijn, L. C. (1993). *Principles of sediment transport in rivers, estuaries and costal seas*. Aqua Publications, Amsterdam u.a.

van Rijn, L. C. (2007). Unified view of sediment transport by currents and waves: I: Initiation of motion, bed roughness, and bed-load transport. *Journal of Hydraulic Engineering*, 133(6):649–667.

Wang, Z.-Y. and Dittrich, A. (1999). Effect of shape on incipient motion of sediment particles. *International Journal of Sediment Research*, 14(2):179–186.

Whitehouse, R. (1998). *Scour at marine structures: A manual for practical applications*. Thomas Telford, London.

Yalin, M. S. (1971). *Theory of hydraulic models*. Macmillan civil engineering hydraulics. Macmillan, London.

Yalin, M. S. (1972). *Mechanics Of Sediment Transport*. Pergamon Press, Oxford, first edition.

Yanmaz, A. M. and Köse, Ö. (2007). Surface characteristics of scouring at bridge elements. *Turkish Journal of Engineering and Environmental Sciences*, 31:127–134.

Yu, G., Tan, S. K., Lim, S. Y., and Ong M.-C. (2003). Evaluation of the formulae of bridge pier scour depth using data of lightweight bed material. In Ganoulis, J., Prinos, P., Maksimovic, C., and Kaleris, V., editors, *Urban and Rural Water Systems for sustainable Development*, Proc. XXX IAHR Congress, pages 277–283, Thessaloniki and Greece.

Zanke, U. (1978). Zusammenhñge zwischen Strömung und Sedimenttransport. Teil 1 Berechnung des Sedimenttransportes - allgemeiner Fall. Mitteilungen des Franzius-Instituts für Wasserbau und Küsteningenieurwesen der Technischen Universität Hannover.

Zanke, U. (1982a). *Grundlagen der Sedimentbewegung: Mit 188 Abbildungen und 13 Tabellen*. Hochschultext. Springer-Verlag, Berlin.

Zanke, U. (1982b). Kolke am Pfeiler in richtungskonstanter Strömung und unter Welleneinfluss. Mitteilungen des Franzius-Instituts für Wasserbau und Küsteningenieurwesen der Universität Hannover.

A Risk management

To describe the procedure, in the following tables (Table A.1) English units are used instead of the metric system by reasons of literature availability. For detailed information about the data source in these tables see Pearson et al. (2002); Stein and Sedmera (2006).

Table A.1: Occupancy per vehicle mile by daily trip purpose (Stein and Sedmera, 2006).

trip purpose	mean
all personal vehicle trips	1.63
work	1.14
work-related	1.22
family/personal	1.81
church/school	1.76
social/recreational	2.05
other	2.02

Table A.2: Cost of bridge construction (Stein and Sedmera, 2006).

bridge superstructure type, demolition	dollar/ft^2
reinforced concrete flat slab; simple span	50–65
reinforced concrete flat slab; continuous span	60–80
steel deck/girder; simple span	62–75
steel deck/girder; continuous span	70–90
pre-stressed concrete deck/girder; simple span	50–70
pre-stressed concrete deck/girder; continuous span	65–110
post-tensioned, cast-in-place,	
concrete box girder cast on scaffolding; span length $\leq$ 240 ft	75–110
steel box deck/girders	
span range from 150 to 280 ft	76–120
for curvature add a 15 % premium segmental	
concrete box girders; span range from 150 to 280 ft	80–110
movable bridges; bascule spans and piers	900–1500
demolition of existing bridges	
typical	9–15
bascule spans and piers	63

Table A.3: Vehicle cost per mile (Stein and Sedmera, 2006).

cost category	automobiles	trucks
total per mile	\$ 0.45	\$ 1.80
drivers cost	–	\$ 0.50
total vehicle cost per mile	\$ 0.45	\$ 1.30

Table A.4: Mean values of time costs in the USA according to Stein and Sedmera (2006).

	\$ per hour
mean wage	\$ 17.06
value of time	\$ 6.99

Table A.5: Assumed number of lives lost in bridge failure (Stein and Sedmera, 2006).

average daily traffic (ADT)					number of lives lost
		ADT	$<$	100	0
100	$\leq$	ADT	$<$	500	1
500	$\leq$	ADT	$<$	1000	2
1000	$\leq$	ADT	$<$	5000	2
5000	$\leq$	ADT*			5
5000	$\leq$	ADT**			10

* not an interstate or arterial

** interstate or arterial

Table A.6: Estimates of the values of travel time (Stein and Sedmera, 2006).

travel purpose	automobiles		trucks	
	small	medium	4-tire	6-tire
business travel				
value per person	$ 21.20	$ 21.20	$ 21.20	$ 18.10
average vehicle occupancy	1.43	1.43	1.43	1.05
total business	$ 31.55	$ 31.96	$ 32.47	$ 22.01
personal travel				
value per person	$ 10.60	$ 10.60	$ 10.60	
average vehicle occupancy	1.67	1.67	1.67	
total business	$ 17.70	$ 17.70	$ 17.70	

B Critical velocity equations

Many equations for the critical depth-average velocity can be found in literature, most are given for coarse gravel and stone material ($d_{50} \geq 0.002\,\mathrm{m}$).

Neill (1967) proposes a conservative design curve with the equation

$$U_{crit} = \sqrt{2.5 \left(\frac{d}{h}\right)^{-0.2} \frac{\rho_s - \rho}{\rho}\, g\, d}$$

Zanke (1978) gives the following equation

$$U_{crit} = \frac{U}{U_s}\left(2.0\sqrt{\frac{\rho_s - \rho}{\rho}\, g\, d} + 10.5\frac{\nu}{d}\right)$$

with

$$\frac{U}{U_s} = 1 + 0.4\tanh(3.09 \times 10^{-4} \times H^*)$$

$$H^* = \left(\frac{g}{\nu^2}\right)^{\frac{1}{3}} (h_0 - h')$$

Zhang (1981) gives the following equation, taken from Gao et al. (1999)

$$U_{crit} = \left(\frac{h}{d}\right)^{0.14} \sqrt{17.6\, \frac{\rho_s - \rho}{\rho}\, d + 0.000000605 \left(\frac{10 + h}{d}\right)}$$

Van Rijn (1993) gives the following equation to estimate the depth-average critical velocity, which is explicitly valid for sand particles in the range of 0.0005 to 0.002 m with $d_{90} = 2d_{50}$.

$$U_{crit} = 8.50\, d_{50}^{0.6}\, \log\left(\frac{12h}{3d_{90}}\right)$$

Müller and Jones (1999) define the critical velocity for incipient motion using a variable Shield's parameter as follows

$$U_{crit} = 31.34\, \theta^{\frac{1}{2}}\, h^{\frac{1}{6}}\, d^{\frac{1}{3}}$$

$$\theta = \beta_1\, d^{\beta_2}$$

with:

			β_1	β_2
	d	$\geq 2.0\,\mathrm{mm}$	0.047	0
$2.0\,\mathrm{mm} >$	d	$> 0.9\,\mathrm{mm}$	0.0765	0.175
$0.9\,\mathrm{mm} \geq$	d		0.003	-0.384

Richardson and Davis (2001) recommend the following equation for SI-Units and material density of $\rho = 2650\ \mathrm{kg\,m^{-3}}$

$$U_{crit} = 6.19\, h^{\frac{1}{6}}\, d^{\frac{1}{3}}$$

Hager and Oliveto (2002) calculate the critical flow velocity as follows

$$U_{crit} = 2.33 D^{*-\frac{1}{4}} \left(\frac{R}{d_{50}}\right)^{\frac{1}{6}} \sqrt{\rho\prime g d_{50}} \qquad \text{for} \quad D^* \leq 10$$

$$U_{crit} = 1.08 D^{*\frac{1}{12}} \left(\frac{R}{d_{50}}\right)^{\frac{1}{6}} \sqrt{\rho\prime g d_{50}} \qquad \text{for} \quad 10 \leq D^* \leq 150$$

$$U_{crit} = 1.65 \left(\frac{R}{d_{50}}\right)^{\frac{1}{6}} \sqrt{\rho\prime g d_{50}} \qquad \text{for} \quad D^* \geq 150$$

C Results of the material properties

Results of the material investigations for the form factor FF, in which a = longest axis, b = mean axis and c = shortest axis.

Table C.1: Calculation of the form factor for the material which is used in the preliminary experiments.

	Acetal			Polystyrene		
	a	b	c	a	b	c
Measurement	[mm]	[mm]	[mm]	[mm]	[mm]	[mm]
1	3.25	2.35	1.80	3.30	2.50	2.45
2	3.15	2.60	2.20	2.50	2.50	1.85
3	2.95	2.45	1.95	3.30	2.50	2.25
4	3.20	2.65	2.15	2.80	3.00	2.00
5	3.50	2.10	1.85	2.70	3.00	2.00
6	2.95	2.75	2.15	3.10	3.10	2.25
7	3.30	2.50	2.45	2.75	3.20	2.45
8	2.55	2.45	2.00	2.60	2.95	2.15
9	3.05	3.00	2.35	2.55	3.45	2.45
10	3.00	2.85	1.70	3.00	2.55	2.00
11	3.15	2.70	1.05	3.10	3.05	2.25
12	3.50	2.65	2.20	2.65	3.15	2.15
13	3.35	2.80	2.40	2.75	3.20	2.45
14	3.10	2.80	2.10	2.70	2.50	1.90
15	3.35	2.50	2.35	3.15	2.35	1.80
Mean	3.17	2.60	2.05	2.88	2.86	2.16
FF		0.71			0.75	

Results of the density measurements carried out with a pycnometer.

Table C.2: Results of the density measurements.

	Acetal			
	P_1	P_2	P_3	P_4
mass of the body; m_0 [g]	5.040	5.144	5.062	5.016
mass of fluid-filled vessel; m_1 [g]	144.74	144.736	144.733	144.733
mass of vessel filled with water and body; m_3 [g]	146.043	146.034	146.013	146.005
water density (18 °C) [g cm^{-3}]	0.998 403			
material density [g cm^{-3}]	1.3465	1.3354	1.3363	1.3376
mean density [g cm^{-3}]	1.34			

	Polystyrene			
	P_1	P_2	P_3	P_4
mass of the body; m_0 [g]	6.042	5.998	6.036	6.060
mass of fluid-filled vessel; m_1 [g]	144.734	144.737	144.737	144.738
mass of vessel filled with water and body; m_3 [g]	144.969	144.97	144.937	144.948
water density (18 °C) [g cm^{-3}]	0.998 403			
material density [g cm^{-3}]	1.0388	1.0388	1.0326	1.0342
mean density [g cm^{-3}]	1.04			

	Sand			
	P_1	P_2	P_3	P_4
mass of the body; m_0 [g]	12.608	13.447	19.557	13.991
mass of fluid-filled vessel; m_1 [g]	144.733	144.734	144.732	144.728
mass of vessel filled with water and body; m_3 [g]	152.509	153.053	156.804	153.38
water density (18 °C) [g cm^{-3}]	0.998 403			
material density [g cm^{-3}]	2.605	2.6181	2.6087	2.6163
mean density [g cm^{-3}]	2.61			

D Experimental boundary conditions

Table D.1 summarizes the boundary condition for the different experiments which were carried out at the Technische Universität Braunschweig.

Table D.1: Experimental boundary conditions.

	unit	Sand1.6	Acetal	Sand0.8	Polysty.	Sand2.5	Sand0.2
water depth	[m]	0.1					
pier width	[m]	0.03					
pier form	[1]	circular					
gravity	[m/s^2]	9.81					
kinematic viscosity	[m^2/s]	10^{-6}					
flow condition	[1]	$U = U_{crit}$					
sediment size	[m]	0.0016	0.0026	0.0008	0.0027	0.0025	0.0002
uniformity	[1]	1.29	–	1.3	–	–	1.25
relative density	[1]	1.65	0.38	1.65	0.04	1.65	1.65
critical velocity	[m/s]	0.32	0.19	0.29	0.08	0.46	0.19

E Full experimental data set

Table E.1: Results of the experiments for Sand1.6 carried out at the Technische Universität Braunschweig.

Sand1.6	**0**	**15**	**30**	**60**	**120**	**240**	**480**	**1440**	**2880**	**4320**	**10080**	**14400**
E6-I	0	2.2	2.5	3.3	3.8	4.1	4.4					
E6-II	0	2.3	2.8	3.3	3.7	4.2	4.3					
E6-III	0	2.4	2.6	3.4	4.2	4.2	4.6	5.0				
E6-IV	0	2.6	3.1	3.9	4.1	4.2	4.5					
E6-V	0			3.6	3.7	4.1		5.1				
E6-VI	0			3.2	3.4			5.1				
E6-VII	0	2.6		3.8				5.0		5.7	6.1	6.3
E6-Mean	0	2.42	2.75	3.5	3.82	4.16	4.45	5.05		5.7	6.1	6.3

Table E.2: Results of the experiments for Acetal carried out at the Technische Universität Braunschweig.

Acetal	**0**	**15**	**30**	**60**	**120**	**240**	**480**	**1440**	**2880**	**4320**	**10080**	**14400**
F6-I	0	2.0	2.6	3.1	3.5	4.1	4.7					
F6-II	0	2.8	3.5	4.1	4.3	4.6	4.8	5.0				
F6-III	0	2.4	3.2	3.9	4.1	4.2	4.8					
F6-IV	0				4.2	4.6		4.8				
F6-V	0				4.4	5.0	5.1	5.4				
F6-VI	0	2.3		3.0				4.8	5.0		5.6	5.6
F6-VII	0	2.9			4.4	4.6		4.7	4.9	5.1	5.1	5.1
F6-Mean	0	2.48	3.1	3.53	4.15	4.52	4.85	4.94	4.95	5.1	5.35	5.35

Table E.3: Results of the experiments for Polystyrene carried out at the Technische Universität Braunschweig.

Polystyrene		**15**	**30**	**60**	**120**	**240**	**480**	**1440**	**2880**	**4320**	**10080**	**14400**
G6-II	0	3.3	3.6	4.1	4.3	4.4	4.6	4.7				
G6-III	0	3.4	3.8	4.2	4.7	5.3	5.5	5.5				
G6-IV	0	2.8	3.2	4.1	4.6	4.6	5.3	5.3				
G6-V	0	3.3	3.8	4.7	4.9	5.3	5.4					
G6-VI	0							5.7	5.7	5.7	5.7	5.7
G6-VII	0							4.6				
G6-VIII	0	3.6		4.2		4.8	5.1	5.0				
G6-Mean	0	3.18	3.46	4.12	4.4	4.67	5.07	5.13	5.7	5.7	5.7	5.7

Table E.4: Results of the experiments for Sand0.8 carried out at the Technische Universität Braunschweig.

Sand0.8		**15**	**30**	**60**	**120**	**240**	**480**	**1440**	**2880**	**4320**	**10080**	**14400**
H6-I	0	3.6	4	4.4	4.7	5.1	5.3					
H6-II	0	4	4.4	4.8	5.4	5.7	5.9	6.1				
H6-III	0	3.8	4.3	4.5	5.2	5.4	5.6					
H6-IV	0	4.2	4.5	4.7	5.1	5.6	5.9					
H6-V	0	4.2	4.6	5	5.2	5.7	5.9	6.3				
H6-VI	0							6.5				
H6-VII	0							6.1				
H6-VIII	0							6.3				
H6-IX	0							6.3				
H6-X	0	3.9		4.7				6.2	6.9	6.9		7.3
H6-XI	0	3.8						6.1	6.3	6.6	6.7	7
H6-Mean	0	3.93	4.36	4.68	5.12	5.5	5.72	6.238	6.6	6.75	6.7	7.15

Table E.5: Results of the experiments for Sand0.2 carried out at the Technische Universität Braunschweig.

Sand0.2		**15**	**30**	**60**	**120**	**240**	**480**	**1440**	**2880**	**4320**	**10080**	**14400**
I6-I	0	3	3.6	3.9	4.4	4.8		6				
I6-II	0	2.9	3.4	3.7	4.3	4.7	5.2	5.6	6			
I6-III	0	2.9	3.3	3.9	4.2	4.4	4.7	5.5	5.8	6	6.2	6.2
I6-IV	0	3.1	3.5	3.9	4.4	4.8	5.3	5.8	6.2	6.5		
I6-Mean	0	2.98	3.45	3.85	4.33	4.68	5.07	5.725	6	6.25	6.2	6.2

Table E.6: Results of the experiments for Sand2.5 carried out at the Technische Universität Braunschweig.

Sand2.5		**15**	**30**	**60**	**120**	**240**	**480**	**1440**	**2880**	**4320**	**10080**	**14400**
J6-I	0	3.1	3.2	3.3	3.5	3.8	4	4.7	5.1	5.4	5.7	5.8
J6-II	0	2.0	2.0	2.8	2.9	3.2	3.2	3.8				
J6-III	0	1.7	2.4	2.9		3.2	3.7	4.1	5.0	5.1	5.6	
J6-Mean	0	2.27	2.53	3	3.2	3.4	3.63	4.2	5.05	5.25	5.65	5.8

Table E.7: Results of the experiments for Polystyrene carried out at the Universität Magdeburg-Stendal.

	pier diameter [m]					
	0.025		0.05		0.07	
	Run I	Run II	Run I	Run II	Run I	Run II
0	0	0	0	0	0	0
15	2.5	2.8	5.5	5.3	6.4	6.60
30	2.6		6.1		8	
45	3.4		6.7		8.5	
50		3.8		7.3		7.9
60	3.4	3.9	6.8	7.3	9	8
90	3.4	4	7.5	7.4	10	9.5
120	4	4.1	7.9	7.9	10.4	10.1
150		4.2		8.1		10.2
180	4.4	4.2	8.5	8.2	11.2	10.5
240	4.9	4.5	8.9	8.7	11.3	10.9
300	5	4.6	9	8.9	11.5	11.2
360	5	4.7	9.1	9.3	11.6	11.4
420		4.8		9.4		11.5
480		4.8		9.7		11.6
540		4.9		9.8		11.6
600		4.9		9.8		11.6